

https://dspace.org/

Development of a nanoparticle in-film-matrix for enhanced antiretroviral drug absorption in the female genital tract

Takalani, Funanani

2025
University of the Witwatersrand, Johannesburg
https://hdl.handle.net/10539/48407
Takalani, Funanani . (2025). Development of a nanoparticle in-film-matrix for enhanced antiretroviral drug absorption in the female genital tract [PhD thesis, University of the Witwatersrand, Johannesburg]. https://hdl.handle.net/10539/48407

Downloaded from a DSpace repository. https://dspace.org/

DEVELOPMENT OF A NANOPARTICLE-IN-FILM MATRIX FOR ENHANCED ANTIRETROVIRAL DRUG ABSORPTION IN THE FEMALE GENITAL TRACT

Funanani Takalani

A thesis submitted to the Faculty of Health Sciences, University of the Witwatersrand, in fulfilment of the requirements for the degree of Doctor of Philosophy

Supervisor:

Professor Yahya Essop Choonara

Wits Advanced Drug Delivery Platform Research Unit, Department of Pharmacy and Pharmacology, University of the Witwatersrand, Johannesburg, South Africa

Co-Supervisor:

Professor Pradeep Kumar

Wits Advanced Drug Delivery Platform Research Unit, Department of Pharmacy and Pharmacology, University of the Witwatersrand, Johannesburg, South Africa

Johannesburg, 2025

DECLARATION

I, Funanani Takalani, hereby declare that the research presented in this thesis is my original work. It is being submitted for the degree of Doctor of Philosophy in the Faculty of Health Sciences, University of the Witwatersrand, Johannesburg, South Africa. This thesis has not been previously submitted for any degree or examination at this university or any other.



Signature

29th of April 2025

RESEARCH OUTPUTS

LIST OF PUBLICATIONS

1. Takalani F., Kumar P., Kondiah P.P.D., Choonara Y.E and Pillay V (2020) Lipid-drug conjugates and associated carrier strategies for enhanced antiretroviral drug delivery. Pharmaceutical Development and Technology, 25:3, 267-280. Available online at the following website: DOI: https://doi.org/10.1080/10837450.2019.1694037

2. Takalani F., Kumar P., Kondiah P.P.D and Choonara Y.E (2024) Co-emulsified Alginate-Eudragit Nanoparticles: Potential Carriers for Localized and Time-defined Release of Tenofovir in the Female Genital Tract. AAPS Pharm Sci Tech, 25:15, 1-17. Available online at the following website: DOI: https://doi.org/10.1208/s12249-023-02723-4.

RESEARCH FUNDING

This work was funded by the National Research Foundation (NRF) South African Research Chairs Initiative (SARChI) Grant and the South African Medical Research Council (SAMRC); Bongani Mayosi National Health Scholarship (BM-NHSP), Research Capacity Development (RCD).

ABSTRACT

This study explored strategies for lipid–drug conjugation and delivery systems for enhancing antiretroviral (ARV) drug efficacy. Lipid–drug conjugates (LDCs) have the potential to enhance oral bioavailability, lipophilicity, toxicity, and drug adsorption. So, linking ARV drugs with lipids produces LDCs, which alters the pharmacokinetic properties of ARV drugs, resulting in improved effectiveness. Although LDCs may be administered without a delivery carrier, they are typically integrated into suitable delivery systems such as lipid nanoparticles, polymeric nanoparticles, micelles, liposomes, emulsions, and carbon nanotubes. Herein explored the possibility of Eudragit S100 (ES100), a methylmethacrylate-methacrylic acid copolymer, and sodium alginate as nanocarriers for a lipidic ARV prodrug [tenofovir disoproxil fumarate (TDF)] in the female genital tract (FGT). Vaginal $CD4^+$ T cells constitute the primary significant target for successful establishment of HIV infection.

Oral pre-exposure prophylaxis (PrEP) has been successful as a prevention tool for individuals at high risk of getting HIV-1. However, the challenges with this medication include strict user compliance, a decrease in condom use, bone and renal toxicity, and the development of antiviral resistance. To circumvent these drawbacks, topical delivery systems for PrEP have been proposed. Within these delivery systems, intra vaginal films possess a greater likelihood of enhancing drug delivery due to quick dissolving nature, small size for administration and lack of need for an applicator. Nanoparticle-based drug delivery systems, on the other hand, have the potential to deliver drugs that are poorly water-soluble, like most ARVs. Hence, in this research, TDF-loaded alginate-ES100 nanoparticles were developed, and subsequently incorporated into a hydroxypropyl methylcellulose (HPMC) film.

Alginate, alginate-ES100 nanoparticles, and HPMC films were prepared using the ionic gelation, emulsion/gelation complexation method, and the casting method, respectively. Nanocarriers were tested using morphological, physicochemical, *in vitro* drug release, and cytotoxicity analyses. The presence of spherical and uniformly distributed nanoparticles was revealed in SEM and TEM nanoparticle images, whereas SEM images for films showed significant degrees of porosity and compactness. The FTIR spectrum showed that alginate and calcium chloride interacted due to ionic bonds linking divalent calcium ions and the -COO- of alginate groups. Alginate and ES100 interacted via the ester C=O amide stretching, resulting in the formation of a novel and potent anhydride bond. HPMC was also adhered to this anhydride bond.

The results obtained from the XRD revealed sharp, clear peaks, which are associated with the high purity of the systems. The DSC results, on the other hand, suggest that there is a thermodynamic compatibility between sodium alginate, ES100, and the TDF drug, as evidenced by the endothermic and exothermic peaks observed. Moreover, the results of the DSC confirmed that the TDF-loaded nanoparticles were successfully incorporated into the HPMC polymer. Under experimental design and optimization, overall size distribution results ranged from 134.9 to 228.0 nm, while zeta potential results showed stable nanoparticles (−17.8 to −38.4 MV). The optimal nanoparticle formulation exhibited a maximum cumulative *in vitro* release of 72% (pH 4.2) for a duration of 96 hours, whereas the 2.5% film released the highest amount (54%) of the TDF drug for a duration of 96 hours.

In vitro cytotoxicity tests revealed the safety of TDF-loaded nanoparticles on vaginal epithelial cells at concentrations of 0.025 mg/mL, 0.5 mg/mL, and 1 mg/mL for 72 h. Lastly, histopathology analysis showed mild to moderate changes when the film delivery system containing 60 mg of the TDF drug was inserted for four days in pigs. When taken together, the *in vitro* findings indicate that alginate-ES100 nanoparticles possess the capability to preserve and sustain the release of the TDF drug in the FGT. On the contrary, *in vivo* studies suggest the possibility of developing a low-dose, non-toxic microbicide that can be administered for a prolonged period in the vagina for HIV patients.

DEDICATION

This thesis is dedicated to my parents, Mr. and Mrs. Takalani, my uncle, Mr. Rembuluwani Takalani, and my big sister, Mrs. Phathutshedzo Ramovha. These people provided me with invaluable support from the commencement of my Ph.D. journey to its conclusion. I am pleased to acknowledge that they have been consistent sources of support throughout every stage of my Ph.D. Without their assistance, I would not have been able to complete my dissertation. They exerted tremendous efforts to assist me in obtaining this degree. Hence, I'm incredibly appreciative and humbled by the love they showed me throughout this journey. Additionally, I would like to express my special gratitude to my husband, Advocate Zama Russel Chauke, for believing in me and supporting my dream. This has been one of the most challenging experiences of my life. At times, I felt like giving up or not worthy or qualified enough to obtain this degree, but it was the support of my family that kept me going. I never lacked financial or emotional support because my family was always there for me.

When I revisit or reflect on this journey, I perceive the divine grace and mercy bestowed upon my life. There are numerous instances, challenges, or obstacles that could have prompted me to discontinue my registration or give up. However, God provided me with the courage to persevere and renewed my enthusiasm for science. My PhD completion could have taken longer than anticipated, however, it was all in God's plan, as what we commonly refer to as a delay is actually God's preparation. This doctoral degree not only enabled me to develop in the field of science, but it also shaped my character in ways that I had never imagined. Now, I am stronger and wiser than ever before. Hence, by the mere submission of this thesis, I am confident that one of the divine mandates for my life has been fulfilled. May God be praised!

ACKNOWLEDGEMENTS

I would like to express my gratitude to the late Professor Viness Pillay, my supervisor, for believing in me and granting me the opportunity to pursue my PhD at the Wits Advanced Drug Delivery Platform (WADDP) Research Unit. I would also like to acknowledge my supervisors, Professor Yahya Choonara and Professor Pradeep Kumar, for their unwavering support and guidance throughout my PhD journey.

I want to thank my colleagues from the WADDP research group for their support. The assistance and efforts they have devoted to this research are highly valued.

I would like to express my deepest gratitude to the Wits Research Animal Facility (WRAF) team for their help with my animal research.

Lastly, I would like to thank the NRF and SAMRC for funding this research.

ANIMAL ETHICS DECLARATION

I hereby confirm that the study entitled “Assessment of a nano-enclatherated bioadhesive system (TDF-loaded nanoparticles-in-films) in large white female pigs for prolonged release and minimal toxicity of the TDF drug for vaginal delivery” was approved by the Animal Research Ethics Committee (AREC) of the University of the Witwatersrand with ethics clearance number 23-07-002C (see appendix C).

TABLE OF CONTENTS

Declaration ii
Research Outputs iii
Research Funding iv
Abstract v
Dedication vii
Acknowledgements viii
Animal Ethics Declaration ix
List of Figures xv
List of Tables xviii
List of Equations xix
List of Abbreviations xxi

Chapter 1

Introduction and motivation for the development of nanoparticle-in-film matrix

1.1 Introduction 1
1.2 Rationale and motivation of the study 3
1.3 Aim and objectives 4
1.4 Novelty of the study 5
1.5 Overview of thesis 5
1.6 References 7

Chapter 2

Lipid-drug conjugates and associated carrier strategies for enhanced antiretroviral drug delivery

2.1 Introduction 11
2.2 Advantages and drawbacks of lipid–drug conjugates (LDCs) 12
2.3 Methods for processing LDCs into lipidic delivery systems 12
2.4 Characterization techniques for LDCs 13
2.5 ARV drugs and lipid synthesized conjugates 14
2.5.1 ARV lipidic prodrugs approved by the United States (US) and European Union (EU) food and drug administration (FDA) 14
2.5.1.1 Tenofovir disoproxil fumarate (TDF) 14
2.5.1.2 Tenofovir alafenamide (TAF) 15

2.5.2 ARV lipidic prodrugs in clinical trials and those still under assessment 16
2.5.2.1 Tenofovir (TFV) and hexadecyl-oxypropyl (HDP) [HDP-TFV] 16
2.5.2.2 Cidofovir (CDV) and 1-0-hexadecyl-oxypropyl (HDP) 17
2.5.2.3 Emtricitabine (FTC) and elvitegravir (ELG) with docosahexaenoic acid (DHA) 17
2.5.2.4 Ganciclovir (GCV) and acyl ester 18
2.5.2.5 Emtricitabine (FTC) and lamivudine (3TC) with fatty acyl ester derivatives 19
2.5.2.6 Zidovudine (AZT) and ether lipids 19
2.5.2.7 AZT and thioether lipid 19
2.5.2.8 AZT and synthetic phosphocholine lipid 19
2.5.2.9 AZT and ursodeoxycholic acid (UDCA) 20
2.5.2.10 Indinavir (IDV) with phosphatidylcholine and cholesterol lipid 20
2.6 Strategies for the delivery of LDCs 23
2.6.1 ARV drug-fatty acids conjugation 23
2.6.2 ARV drug–glycerides conjugation 23
2.6.3 ARV drug–steroids conjugation 24
2.6.4 ARV drug–phospholipids conjugation 24
2.7 Delivery systems for LDCs 24
2.7.1 Lipid and polymeric nanoparticles 25
2.7.2 Liposomes 26
2.7.3 Polymeric nanomicelles 26
2.7.4 Nanoemulsions 27
2.7.5 Carbon nanotubes 27
2.8 Nano-enabled particulate systems for LDCs 30
2.8.1 Myristoylated abacavir (ABC) in poloxamer nanoparticles 30
2.8.2 UDCA-AZT in solid lipid microparticles (SLMs) 30
2.8.3 Tenofovir disoproxil fumarate (TDF) with Compritol 888 ATO & oleic acid in NLCs 32
2.8.4 HDP-P-GCV (1-O-hexadecylpropanediol-3-phospho-ganciclovir) in liposome 32
2.8.5 AZT myristate (AZT-M) in liposomes 32
2.9 Concluding remarks 34
2.10 References 35

Chapter 3

Co-emulsified alginate-eudragit nanoparticles: potential carriers for localized and time-defined release of tenofovir in the female genital tract

3.1 Introduction 44
3.2 Materials and methods 45
3.2.1 Materials 45

3.2.2 Preparation of alginate and alginate-ES100 TDF-loaded nanoparticles 45
3.2.2.1 Alginate nanoparticles 45
3.2.2.2 Alginate-ES100 nanoparticles 47
3.3 Characterization of nanoparticles 48
3.3.1 Morphological analysis 48
3.3.2 Nanoparticles size, zeta potential, and polydispersity index (PDI) 48
3.3.3 Fourier transform infrared spectroscopy (FTIR) 48
3.3.4 X-ray diffraction (XRD) 48
3.3.5 Differential scanning calorimetry (DSC) 49
3.4 Determining the entrapment efficiency (EE%) and drug loading capacity (DL%) of nanoparticles 49
3.5 *In vitro* release of TDF-loaded nanoparticles 50
3.6 Development of the experimental design 50
3.6.1 Optimization using the desirability function 51
3.7 Cell culture and cytotoxicity studies 51
3.8 Results and discussion 52
3.8.1 Morphology of alginate nanoparticles as well as Alginate-ES100 nanoparticles 52
3.8.2 Nanoparticle size, polydispersity index (PDI), and zeta Potential 53
3.8.3 Fourier transform infrared spectroscopy 55
3.8.4 X-ray diffraction 57
3.8.5 Differential scanning calorimetry 59
3.9 Determination of EE% and DL% of nanoparticles 60
3.10 *In vitro* release of TDF-loaded nanoparticles 61
3.11 Experimental design analysis 63
3.11.1 Optimization using the desirability function 71
3.12 Cytotoxicity assessment of alginate-ES100 TDF-loaded nanoparticles 77
3.13 Clinical significance of the study 74
3.14 Concluding remarks 75
3.15 References 76

Chapter 4

Characterization, and *in-vitro* drug release studies of alginate-ES100 nanoparticles loaded with TDF within the film matrix

4.1 Introduction 85
4.2 Materials and methods 86
4.2.1 Materials 86

4.2.2 Preparation of alginate-eudragit nanoparticles 86
4.2.2.1 Alg-ES100 nanoparticles 86
4.2.2.2 Film preparation 86
4.2.3 Scanning electron microscope 87
4.2.4 *In vitro* drug release of TDF-loaded nanoparticles in films 87
4.2.5 Fourier transform infrared spectroscopy 87
4.2.6 Differential scanning calorimetry 87
4.3 Results and discussion 88
4.3.1 The scanning electron microscope images depicting the optimized Alginate-ES100 nanoparticles into HPMC films 88
4.3.2 *In vitro* drug release for alginate-ES100 nanoparticles in HPMC films 89
4.3.3 Fourier transform infrared spectroscopy of TDF-loaded alginate-ES100 nanoparticles in film 90
4.3.4 Differential scanning calorimetry of TDF-loaded alginate-ES100 nanoparticles in film 91
4.4 Concluding remarks 93
4.5 References 94

Chapter 5

***In vivo* assessment of TDF-loaded nanoparticles-in-films in large white female pigs**

5.1 Introduction 97
5.2 Materials and methods 98
5.2.1 Materials 98
5.2.2 Ethical approval for the use of animals in this study 98
5.2.3 Preparation of Alg-ES100 nanoparticles and films 98
5.2.4 Transportation and housing of the experimental animals 98
5.2.5 Experimental design 99
5.2.6 Insertion of a catheter into the jugular vein 99
5.2.7 Vaginal administration of films to large white female pigs 100
5.2.8 Vaginal tissue sample collection for histopathology assessment 100
5.3 Results and discussion 101
5.3.1 Histopathology analysis of porcine vaginal epithelia 101
5.4 Concluding remarks 104
5.5 References 105

Chapter 6

Conclusions and recommendations

6.1 Conclusions 107
6.2 Limitations of the study 108
6.3 Recommendations 108

Appendices

Appendix A: Abstract of a review paper that has been published from this dissertation 110
Appendix B: Abstract of a research paper that has been published from this dissertation 111
Appendix C: Animal ethics clearance certificate 112

LIST OF FIGURES

		Page
Figure 1.1:	An illustration of the drug embedded in nanoparticles and later incorporated into the film matrix	2
Figure 1.2:	A proposed mechanism of calcium alginate and eudragit S100 Interaction	4
Figure 2.1:	Chemical structures of ARV lipidic prodrugs approved by the FDA (TDF and TAF)	16
Figure 2.2:	Results showing improved antiretroviral activities of FTC and ELG conjugated with DHA in CD1 mice (Figure adapted with permission from Krovi et al. 2018)	18
Figure 2.3:	Results showing improved antiretroviral activities of FTC and ELG conjugated with DHA *in vitro* (Figure adapted with permission from Krovi et al. 2018)	18
Figure 2.4**:**	Chemical structures of lipid–drug conjugates	22
Figure 2.5:	*In vitro* release of UDCA-AZT from SLMs based on tristearin or stearic acid (Figure adapted with permission from Dalpiaz et al. 2014)	31
Figure 2.6:	Uptake of UDCA-AZT-loaded stearic acid SLMs detected in the CSF after nasal administration in the presence of chitosan (Figure adapted with permission from Dalpiaz et al. 2014)	31
Figure 2.7:	Plasma concentration profiles of AZT and AZT-M incorporated in liposomes (Figure adapted with permission from Jin et al. 2005)	33
Figure 3.1:	SEM images of the TDF drug loaded into alginate nanoparticles. Images taken at a scale of 500 nm	46
Figure 3.2:	Standard calibration curve confirming quantification of the TDF drug at a wavelength of 265 nm	49

Figure 3.3: A SEM image of alginate nanoparticles taken at a scale of 500 nm. Ratios 1:1.4, 1:2b, 1:1b, and 2:1b: SEM images of the TDF drug loaded into alginate-ES100 nanoparticles. Images were taken at a scale of 1 µm and 500 nm. Ratios 1:2a, 1:1a, and 2:1a: Transmission electron microscopy (TEM) images of the TDF drug loaded into alginate-ES100 nanoparticles. Images were taken at a scale of 500 nm (1:2a) and 200 nm (1:1a and 2:1a) 53

Figure 3.4: FTIR spectra of the TDF drug, ES100, alginate (Alg), unloaded (Alg-ES100), and TDF-loaded nanoparticles (Alg-TDF-ES100) 57

Figure 3.5: X-ray diffraction patterns of alginate, TDF drug, ES100, drug free (Alg-ES100), and TDF-loaded nanoparticles (Alg-TDF-ES100) 58

Figure 3.6: DSC thermograms of alginate, TDF drug, ES100, drug free (Alg-ES100), and TDF-loaded nanoparticles (Alg-TDF-ES100) 60

Figure 3.7: Entrapment efficiencies and drug loading capacities of the 15 formulations 61

Figure 3.8: Cumulative *in vitro* release of the experimental design formulations [a–e (F1–F15)] and the optimized formulations [f (1–3)] in simulated vaginal fluid (SVF) at pH 4.2. The release was sustained for up to 96 h 62

Figure 3.9: **a** Residual plots and **b** 3-D response surface plots for drug release, mean particle size, poly dispersity index, and zeta potential 68

Figure 3.10: Contour plots for drug release, mean particle size, poly dispersity index, and zeta potential 69

Figure 3.11: Pareto charts demonstrating the standardized effects of alginate, eudragit, calcium chloride and their interactions on drug release, mean particle size, poly dispersity index, and zeta potential 70

Figure 3.12: Main effects plots for drug release, mean particle size, poly dispersity index, and zeta potential 70

Figure 3.13: Interaction plots for drug release, mean particle size, poly dispersity index, and zeta potential 71

Figure 3.14: Cell viability for TDF-loaded nanoparticles, drug-free nanoparticles, and TDF at 24 h and 72 h 73
Figure 4.1: Scanning electron microscope of the optimized TDF-loaded nanoparticles in HPMC films at different concentrations (1%, 2.5 % and 3.5 %). Film images were taken at a scale of 400 nm whereas nanoparticles were taken at a scale of 1 µm 89
Figure 4.2: The cumulative *in vitro* release of TDF-loaded nanoparticles in HPMC film with concentrations of 1%, 2.5%, and 3.5% in simulated vaginal fluid (SVF) at pH 4.2. The release was sustained for up to 96 h 90
Figure 4.3: Fourier transform infrared spectra of TDF-loaded nanoparticles, HPMC, and TDF-loaded nanoparticles in film 91
Figure 4.4: Differential scanning Calorimetry thermograms of TDF-loaded nanoparticles, HPMC, and TDF-loaded nanoparticles in film 92
Figure 5.1: HPMC film solutions of 60 ml containing nanoparticle Powders loaded with 60 mg of the drug were dried on glass Petri dishes measuring 90 mm× 60 mm. subsequently, the dried films were folded and inserted into the vagina of the large white female pig 100
Figure 5.2: Histopathology images of the excised pig vaginal tissues showing; 1. normal vaginal tissue of a pig, 2. Focal vaginitis, 3. Focal ulcerative vaginitis, 4. Moderate neutrophil influx and 5. Muscular injury 103

LIST OF TABLES

		Page
Table 2.1:	Lipid synthesized ARV-conjugate delivery systems	21
Table 2.2:	Lipid-ARV prodrugs and nanoparticle synthesized-conjugate delivery systems	29
Table 2.3:	ARV drugs and nanoparticle synthesized-conjugate delivery Systems	33
Table 3.1:	Outline of the trial formulations that were used to test for the formation of alginate nanoparticles	46
Table 3.2:	Outline of the trial formulations for alginate-ES100 nanoparticles, prepared using F3 from table 3.1 as a standard for model formulation. All formulations were undertaken in triplicate	47
Table 3.3:	Upper and lower actual values for input critical factors	51
Table 3.4:	Desirability and predicted values for the optimized formulations	51
Table 3.5:	Box-Behnken Experimental Design: Formulation Variables and Responses of Alginate-ES100 Nanoparticles (All Analyses were Undertaken in Triplicate)	55
Table 3.6:	Model summary, analysis of variance and regression equation for drug release	64
Table 3.7:	Model summary, analysis of variance and regression equation for mean particle size	64
Table 3.8**:**	Model summary, analysis of variance and regression equation for PDI	65
Table 3.9:	Model summary, analysis of variance and regression equation for zeta potential	65
Table 5.1:	Histopathological observations of the vaginal sections excised from pigs 1-5	103

LIST OF EQUATIONS

Page

Equation 3.1: 49

$$EE\% = \frac{drug\ within\ nanoparticle}{Initial\ amount\ of\ drug}\ X100$$

Equation 3.2: 49

$$DL\% = \frac{amount\ of\ drug\ in\ nanoparticles}{amount\ of\ nanoparticle}\ X100$$

Equation 3.3: 50

$$Y = [Alginate].[Eudragit].[CaCl2].[Alginate] * [Alginate].\ [Eudragit] * [Eudragit].[CaCl2] * [CaCl2].[Alginate] * [Eudragit].[Alginate] * [CaCl2].\ [Eudragit] * [CaCl2]$$

Equation 3.4: 66

$$DR\ \% = -1{,}375\ -\ 0{,}0046\ [Alginate] + 0{,}02472\ [Eudragit] +\ 0{,}0545\ [CaCl2] + 0{,}000059\ [Alginate] * [Alginate] - 0{,}000070\ [Eudragit] * [Eudragit] - 0{,}001350\ [CaCl2] * [CaCl2] -\ 0{,}000047\ [Alginate] * [Eudragit]$$

Equation 3.5: 66

$$PS\ (nm) = 1532\ -\ 21{,}89\ [Alginate] - 2{,}48\ [Eudragit] +\ 2{,}48\ [CaCl2] + 0{,}0869\ [Alginate] * [Alginate] + 0{,}00491\ [Eudragit] * [Eudragit] + 0{,}01583\ [Alginate] * [Eudragit] - 0{,}0243\ [Eudragit] * [CaCl2]$$

Equation 3.6: 66

$$PDI = 2{,}463 - 0{,}03066\,[Alginate] - 0{,}00214\,[Eudragit] - 0{,}0484\,[CaCl2] + 0{,}000119\,[Alginate] * [Alginate] + 0{,}000006\,[Eudragit] * [Eudragit] + 0{,}001542\,[CaCl2] * [CaCl2] + 0{,}000027\,[Alginate] * [Eudragit] - 0{,}000094\,[Eudragit] * [CaCl2]$$

Equation 3.7: 67

$$ZP = -52 + 0{,}26\,[Alginate] - 0{,}591\,[Eudragit] + 5{,}03\,[CaCl2] - 0{,}00484\,[Alginate] * [Alginate] + 0{,}00097\,[Eudragit] * [Eudragit] - 0{,}089\,[CaCl2] * [CaCl2] + 0{,}00486\,[Alginate] * [Eudragit] - 0{,}0084\,[Eudragit] * [CaCl2]$$

LIST OF ABBREVIATIONS

Acquired immunodeficiency syndrome	AIDS
Adenosine triphosphate	ATP
Alginate-eudragit S100	Alg-ES100
Antiretrovirals	ARVs
Animal research ethics committee	AREC
Blood brain barrier	BBB
Box Behnken design	BBD
Central nervous system	CNS
Differential scanning calorimetry	DSC
Drug loading	DL
Drug release	DR
Entrapment efficiency	EE
Ether lipids	EL
Female genital tract	FGT
Food and drug administration	FDA
Fourier transformed infrared spectra	FTIR
Highly active drugs for antiretroviral therapy	HAART
Human immunodeficiency virus 1	HIV-1
Hydroxypropyl methylcellulose	HPMC
Injection-drug users	IDUs
Intra vaginal rings	IVR
Lipid–drug conjugates	LDCs
Nanostructured lipid carriers	NLCs
Particle size	PS
Phospholipase A_2	PLA_2
Post-exposure prophylaxes	PEP
Polydispersity Index	PDI
Poly (lactic-co-glycolic acid)	PLGA
Pre-exposure prophylaxes	PrEP
Protein kinase C	PKC
Response surface methodology	RSM
Scanning electron microscope	SEM
Simulated vaginal fluid	SVF
Solid lipid nanoparticles	SLNs

Sub-Saharan Africa	SSA
Standard operating procedures	SOPs
Tenofovir disoproxil fumarate	TDF
Transmission electron microscopy	TEM
Treatment as prevention	TasP
Triglycerides	TGs
United nations agency for international development	UNAIDS
Urso-deoxycholic acid	UDCA
Wits research animal facility	WRAF
X-ray diffraction	XRD
Zeta potential	ZP

CHAPTER 1

Introduction and motivation for the development of nanoparticle-in-film matrix

1.1 Introduction

In recent decades, the major source of the AIDS pandemic (HIV-1) has been widely spread and studied. The 2022 global statistics from the United Nations Agency for International Development (UNAIDS) show that 84.2 million people have contracted HIV since the outbreak, while 1.5 million people have just been infected (Mohamud et al., 2023). Although infection rates are high in almost every country, there has been great suffering in sub-Saharan Africa (SSA) caused by HIV-1 infection, of which half of these infections are women (Reis Machado et al., 2014; Corsi et al., 2016; Mohamud et al., 2023). The transmission of HIV-1 involves: (i) mother-child transmission, wherein infected maternal cells enter the circulation of the infant during pregnancy or birth. (ii) The sharing of needles or syringes contaminated with blood from an infected individual among injection-drug users (IDUs), and (iii) accidental contact with contaminated fluid or needle sticks in healthcare settings (Sharma et al., 2015).

Nonetheless, the most prevalent method by which HIV-1 can be transmitted is through sexual contact with an infected partner. During intercourse, the virus can enter the body through both male and female genital tracts, (Reis Machado et al., 2014; Sharma et al., 2015); but in this study, we focused only on the female genital tract (FGT) following reasons mentioned before. The mechanisms that HIV undergoes when it reaches the mucosa of the FGT are not well understood. However, HIV infects mainly $CD4^+$ T cells of the vagina, ectocervix and endocervix in the FGT. Therefore, for successful establishment of HIV infection, it appears that these cells are the major significant target (Carias et al., 2013; Reis Machado et al., 2014). So, from a pharmaceutical research perspective, we can develop nanomedicine to combat and prevent HIV/AIDS. Nanomedicine is a subfield of medicine that employs nanotechnology tools or applications to diagnose, treat, and prevent ailments (Boisseau & Loubaton, 2011).

The term “nanotechnology” pertains to the interaction of biological molecules at a nanoscale level, as nanomedicine operates on the same size scale as structures and biological molecules in living cells. Pre-exposure prophylaxes (PrEP), post-exposure prophylaxes (PEP) and treatment as prevention (TasP) are some current HIV prevention technologies (Keogh & Dodds, 2015). Oral PrEP has demonstrated success as a prevention platform for individuals who are at high risk of being infected with HIV-1. However, the obstacles associated with oral PrEP encompass strict user compliance, a decrease in condom utilization, bone and renal toxicity, and the development of antiviral resistance (Marrazzo et

al., 2015; Tyo et al., 2017). To overcome these limitations, topical PrEP delivery strategies have been devised. To date, antiviral gels, intra vaginal films, and intra vaginal rings (IVR) are available. Within these delivery technologies, IVR meets the “gold standard” of providing sustained release of multiple ARV's for up to three to four months (Tyo et al., 2017). However, even with this exciting technology (IVR), the issue of user adherence, especially among youth adults aged between 18–25 years, remains an ongoing challenge (Baeten et al., 2016). On the contrary, it has been shown that intra vaginal films have a higher chance of improving drug delivery, so this study focused on the development of drug loaded nanoparticles in films. Films are more acceptable to women due to quick dissolving nature, small size for administration and lack of need for an applicator (Srinivasan et al., 2016).

On the other hand, nanoparticle-based drug delivery systems have the potential to deliver drugs that are poorly water-soluble, like most ARVs. Nanoparticles encapsulate and prevent drugs from degradation. This allows for a sustained and controlled release (Takalani et al., 2020). As a result, incorporating ARV drug loaded nanoparticles into the film delivery system presents a great possibility to overcome challenges associated with HIV infections in the FGT. Nano-formulations can improve the pharmacokinetic profile as well as bioavailability of ARVs, giving them the opportunity to penetrate the female genital tract to eradicate the virus (Corsi et al., 2016). Figure 1.1 illustrates the film development process, where drugs are first loaded into nanoparticle carriers and then further incorporated into films. Other examples of carriers include micelles, liposomes, emulsions, and carbon nanotubes, which are elaborated upon in chapter two.

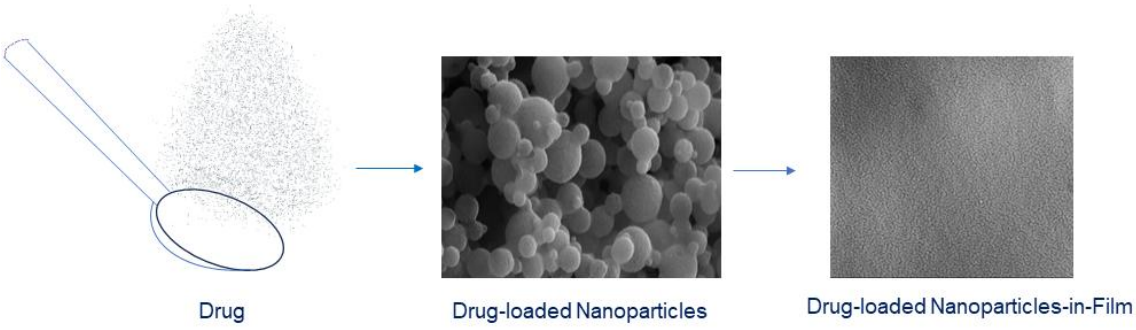


Figure 1.1: An illustration of the drug embedded in nanoparticles and later incorporated into the film matrix

1.2 Rationale and motivation of the study

Despite the establishment of HIV/AIDS treatment in the past and recent decades, the prevalence of the disease remains high and a serious concern worldwide (Shallangwa et al., 2023). To date, more than 30 highly active antiretroviral therapy (HAART) medications have been granted approval by the US-based Food and Drug Administration (FDA), with the aim of preventing and reducing the transmission of HIV-1 infection. However, it is expected that the number of people living with this infection will continue to increase. The first study to evaluate ARV drugs in the FGT reported that lamivudine, zidovudine, tenofovir, and emtricitabine were excellent PrEP/PEP candidates, while atazanavir and lopinavir could potentially serve as useful agents for these applications (Dumond et al., 2010; Tyo et al., 2017). Nonetheless, it has been reported that tenofovir disoproxil fumarate (TDF), a prodrug of tenofovir, exhibits a brief tolerance in HIV patients, whereas prolonged administration may result in renal and bone cytotoxicity (Foster et al., 2009). Consequently, patients become dissatisfied with the necessity of administering multiple daily doses to attain the desired therapeutic effect, particularly over a prolonged period.

This calls for the need to develop nanomedicine that can be administered topically to prolong the release of the TDF drug while reducing its toxicity levels. Considering this information, we found it intriguing to develop alginate-Eudragit S100 (Alg-ES100) nanoparticles for the extended release of the TDF drug in the FGT. An outline of the proposed mechanism for the interaction of these polymers is depicted in Figure 1.2, wherein calcium alginate interacts with ES100 via the C=O ester bond, resulting in the formation of a novel and potent anhydride bond. The preparation of alginate and alginate-ES100 nanoparticles was accomplished by employing the ionic gelation and emulsion/gelation complexation methods, respectively (Takalani et al., 2024). The emulsion/gelation complexation method was selected because it is the most common and recent manufacturing technique for alginate-based nanoparticle delivery systems (Choukaife et al., 2020).

The selection of alginate and ES100 polymers, on the other hand, was influenced by their acknowledged capabilities to prolong the release and their toxicological characteristics, as both have been reported to be non-toxic (Thakral et al., 2013; Joshy et al., 2017). Further properties of these polymers are described in chapter 3. In this research, the primary objective was to devise a sustained non-toxic TDF loaded nanoparticle formulation that could be subsequently incorporated into a film to treat and prevent HIV infection. The film was subjected to testing for histopathology assessment on large white female pigs to imitate humans. In this case, hydroxypropyl methylcellulose (HPMC) was utilized for film development due to its hydrophilic nature and mucoadhesive properties (Acarturk, 2009).

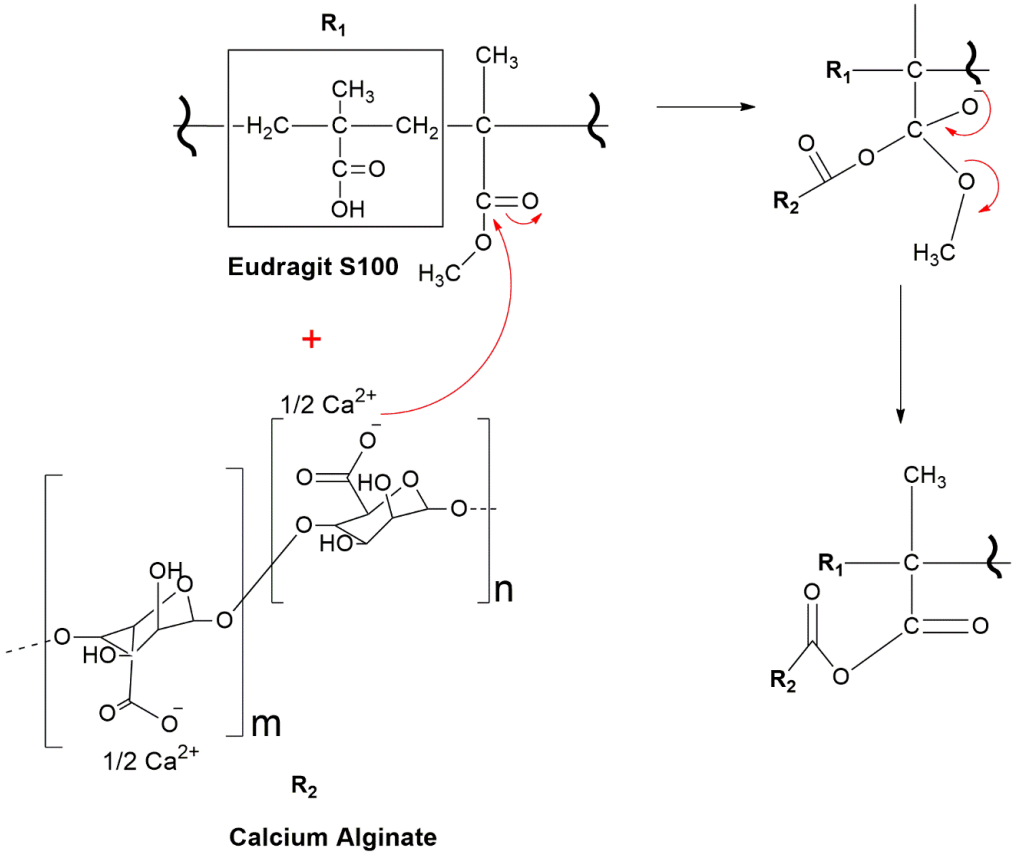


Figure 1.2: A proposed mechanism of calcium alginate and eudragit S100 interaction

1.3 Aim and objectives

The aim of this study was to develop a drug delivery system (TDF-loaded alginate-ES100 nanoparticles-in-film) to prolong the release and minimize toxicity levels of the TDF drug in the female genital tract to treat and prevent HIV/AIDS. This aim was achieved through the following objectives:

1. Synthesis or pre-formulation of alginate-ES100 nanoparticles containing the ARV drug (TDF).
2. Performing experimental design for optimization purposes of the developed nanoparticles formulations, followed by characterization of these formulations using various lab techniques such as SEM, TEM, FTIR, XRD, and DSC.
3. Determination of *in vitro* drug kinetics and cytotoxicity (VK2 cells) assessment of alginate-ES100 nanoparticles.
4. Development of HPMC vaginal films and incorporating the optimized nanoparticles powder sample into these films for further analysis.

5. Determination of physicochemical, morphological, and *in vitro* properties of TDF-loaded nanoparticles in films, as well as histopathological assessment of these films in large white female pigs.

1.4 Novelty of the study

The novelty aspect of this study involves:

1. A detailed report on LDCs and their associated carrier strategies for enhanced antiretroviral efficacy. This could prove to be advantageous in the development of novel therapeutics for HIV to overcome challenges associated with various biological barriers that hinder ARV bioavailability.

2. The successful production of TDF-loaded alginate-ES100 nanoparticles. This research has the potential to enrich the existing knowledge base by extending the release of the TDF drug and reducing its therapeutic dose.

3. The preparation of Alginate-ES100 nanoparticles, which was accomplished through a novel amalgamation of three distinct processes, namely the gelation process, followed by an emulsion process, and a subsequent gelation of alginate emulsion droplets with a covalent or ionic cross-linker.

4. The selection of alginate, ES100 and HPMC polymers aimed at minimizing toxicity in the FGT. These polymers have been reported as non-toxic and are suitable for use in the FGT; however, fewer studies have used them in the FGT.

5. The development of a film vaginal delivery system that could be used for a prolonged period by HIV-positive patients.

1.5 Overview of thesis

Chapter one of this dissertation outlines the historical context and rationale of the study. The purpose, objectives, and novelty of the study are thoroughly discussed.

Chapter two is a published literature review titled: “Lipid-drug conjugates and Associated Carrier Strategies for Enhanced Antiretroviral Drug Delivery.” In this chapter, comprehensive explanations are provided on the utilization of lipids and ARV drugs in conjunction to enhance antiretroviral efficacy. Furthermore, the various delivery carriers that can accommodate these

lipid-drug conjugates are thoroughly examined, including but not limited to lipid nanoparticles, polymeric nanoparticles, micelles, liposomes, emulsions, and carbon nanotubes.

Chapter three is a published research article entitled “Co-emulsified Alginate-Eudragit Nanoparticles: Potential Carriers for Localized and Time-defined Release of Tenofovir in the Female Genital Tract.” This chapter specifically focuses on the synthesis and characterization of alginate-ES100 nanoparticles as carriers for the TDF drug to evaluate their potential application in the female genital tract. The utilization of alginate nanoparticles turned out to be the most advantageous option, as it has been demonstrated to enhance the bioavailability of drugs. Together with ES100, they are both non-toxic and are recommended for controlled drug administration. Different techniques, including SEM, TEM, FTIR, XRD, and DSC, were used, followed by the execution of a cytotoxicity MTT assay for further analysis. Additionally, a Box Behnken Design (BBD) mathematical model was adopted with the Minitab software to optimize the developed alginate-ES100 nanoparticles for vaginal drug delivery. As critical parameters for drug delivery systems, cumulative drug release percent, mean particle size, PDI, and zeta potential were evaluated. Subsequently, residual plots, response surface and contour plots, Pareto charts, main effects and interaction plots were generated. The statistical validity of the models was established through the utilization of an analysis of variance (ANOVA) test, whereas regression analysis and coefficient of determination tests were employed to assess the suitability of the models. The optimal formulation was determined using the desirability function approach.

Chapter four describes the successful incorporation of the optimized alginate-ES100 nanoparticles into a HPMC film matrix for further characterization, and *in vitro* drug release studies. Herein, the films were analyzed using SEM, FTIR, DSC, and *in vitro* drug release techniques.

Chapter five outlines the successful administration of the film delivery system within the vagina of large female white pigs. Upon completion of the *in vivo* experiment, the pigs were euthanized, and their vaginal tissues were removed for further histopathological examination.

Chapter six provides conclusions, limitations, and recommendations pertaining to the developed delivery system for enhanced effectiveness in HIV patients.

1.6 References

Acarturk, F. (2009). Mucoadhesive vaginal drug delivery systems. Recent patents on drug delivery & formulation, 3(3), 193–205. https://doi.org/10.2174/187221109789105658

Baeten, J. M., Palanee-Phillips, T., Brown, E. R., Schwartz, K., Soto-Torres, L. E., Govender, V., Mgodi, N. M., Matovu Kiweewa, F., Nair, G., Mhlanga, F., Siva, S., Bekker, L.-G., Jeenarain, N., Gaffoor, Z., Martinson, F., Makanani, B., Pather, A., Naidoo, L., Husnik, M., … Hillier, S. (2016). Use of a vaginal ring containing dapivirine for HIV-1 prevention in women. N. Engl. J. Med, 375(22), 2121–2132. https://doi.org/10.1056/nejmoa1506110

Boisseau, P., & Loubaton, B. (2011). Nanomedicine, nanotechnology in medicine. C. R. Physique, 12(7), 620–636. https://doi.org/10.1016/j.crhy.2011.06.001

Carias, A. M., Mccoombe, S., Mcraven, M., Anderson, M., Galloway, N., Vandergrift, N., Fought, A. J., Lurain, J., Duplantis, M., Veazey, R. S., & Hope, T. J. (2013). Defining the interaction of HIV-1 with the mucosal barriers of the female reproductive tract. J. Virol, 87(21), 11388–11400. https://doi.org/10.1128/JVI.01377-13z

Choukaife, H., Doolaanea, A. A., & Alfatama, M. (2020). Alginate nanoformulation: influence of process and selected variables. In Pharm. 13(11). https://doi.org/10.3390/ph13110335

Corsi, F., Sorrentino, L., Mazzucchelli, S., Truffi, M., Capetti, A., Rizzardini, G., & Fiandra, L. (2016). Antiretroviral therapy through barriers: a prominent role for nanotechnology in HIV-1 eradication from sanctuaries. J. Pharm. Pharmacol, 4, 328–339. https://doi.org/10.17265/2328-2150/2016.07.007

Dumond, J. B., Yeh, R. F., Patterson, K. B., Corbett, A. H., Hwa, B., Rezk, N. L., Bridges, A. S., Stewart, P. W., Cohen, M. S., & Kashuba, D. M. (2010). Antiretroviral drug exposure in the female genital tract: implications for oral pre- and post-exposure prophylaxis. AIDS, 21(14), 1899–1907. https://doi.org/10.1097/QAD.0b013e328270385a.Antiretroviral

Foster, C., Lyall, H., Olmscheid, B., Pearce, G., Zhang, S., & Gibb, D. M. (2009). Tenofovir disoproxil fumarate in pregnancy and prevention of mother-to-child transmission of HIV-1: Is it time to move on from zidovudine? In HIV Med, 10(7), 397–406. https://doi.org/10.1111/j.1468-1293.2009.00709.x

Joshy, K. S., George, A., Jose, J., Kalarikkal, N., Pothen, L. A., & Thomas, S. (2017). Novel dendritic structure of alginate hybrid nanoparticles for effective anti-viral drug delivery. Int. J. Biol. Macromol, 103, 1265–1275. https://doi.org/10.1016/j.ijbiomac.2017.05.094

Keogh, P., & Dodds, C. (2015). Pharmaceutical HIV prevention technologies in the UK: six domains for social science research. AIDS Care, 27(6), 796–803. https://doi.org/10.1080/09540121.2014.989484

Marrazzo, J. M., Gita, R., Richardson, B. A., Gomez, K., Mgodi, N., Nair, G., Palanee, T., Nakabiito, C., Straten, A. van der, Noguchi, L., Hendrix, C. W., Dai, J. Y., Ganesh, S., Mkhize, B., Talijaard, M., Parikh, U. M., Piper, J., Mâsse, B., Grossman, C. VOICE Study Team. (2015). Tenofovir-based preexposure prophylaxis for HIV infection among African women. N. Engl. J. Med, 372(6), 506–518. https://doi.org/10.1056/NEJMoa1402269

Mohamud, L. A., Hassan, A. M., & Nasir, J. A. (2023). Determinants of HIV/Aids knowledge among females in somalia: findings from 2018 to 2019 SDHS Data. HIV AIDS (Auckl), 15, 435–444. https://doi.org/10.2147/HIV.S414290

Reis Machado, J., Da Silva, M. V., Cavellani, C. L., Antônia Dos Reis, M., Monteiro, M. L. G. D. R., Teixeira, V. D. P. A., & Rosa Miranda Corrêa, R. (2014). Mucosal immunity in the female genital tract, HIV/AIDS. Biomed Res. Int, 2014 (February 2016). https://doi.org/10.1155/2014/350195

Shallangwa, M. M., Musa, S. S., Iwenya, H. C., Manirambona, E., Lucero-Prisno, D. E., & Tukur, B. M. (2023). Assessment of COVID-19 vaccine hesitancy among people living with HIV/AIDS: a single-centered study. PAMJ-OH, 10. https://doi.org/10.11604/pamj-oh.2023.10.2.37945

Sharma, A., Kushawaha, S. K., Anghore, D., Pandit, V., & Sharma, D. R. (2015). HIV/AIDS overview - recent advancement made by WHO. IJPTP, 6(1), 1582–1590.

Srinivasan, P., Zhang, J., Martin, A., Kelley, K., McNicholl, J. M., Buckheit, R. W., Smith, J. M., & Ham, A. S. (2016). Safety and pharmacokinetics of quick-dissolving polymeric vaginal films delivering the antiretroviral IQP-0528 for preexposure prophylaxis. Antimicrob Agents Chemother, 60(7), 4140–4150. https://doi.org/10.1128/AAC.00082-16

Takalani, F., Kumar, P., Kondiah, P. P. D., & Choonara, Y. E. (2024). Co-emulsified alginate-eudragit nanoparticles: potential carriers for localized and time-defined release of tenofovir in the female genital tract. AAPS PharmSciTech, 25(1), 1–17. https://doi.org/10.1208/s12249-023-02723-4

Takalani, F., Kumar, P., Kondiah, P. P. D., Choonara, Y. E., & Pillay, V. (2020). Lipid–drug conjugates and associated carrier strategies for enhanced antiretroviral drug delivery. Pharm Dev Technol, 25(3), 267–280. https://doi.org/10.1080/10837450.2019.1694037

Thakral, S., Thakral, N. K., & Majumdar, D. K. (2013). Eudragit®: A technology evaluation. In Expert Opin. Drug Deliv, 10(1), 131–149. https://doi.org/10.1517/17425247.2013.736962

Tyo, K. M., Vuong, H. R., Malik, D. A., Sims, L. B., Alatassi, H., Duan, J., Watson, W. H., & Steinbach-Rankins, J. M. (2017). Multipurpose tenofovir disoproxil fumarate electrospun fibers for the prevention of HIV-1 and HSV-2 infections *in vitro*. Int. J. Pharm, 531(1), 118–133. https://doi.org/10.1016/j.ijpharm.2017.08.061

CHAPTER 2

Lipid-drug Conjugates and Associated Carrier Strategies for Enhanced Antiretroviral Drug Delivery

PHARMACEUTICAL DEVELOPMENT AND TECHNOLOGY
https://doi.org/10.1080/10837450.2019.1694037

Taylor & Francis
Taylor & Francis Group

REVIEW ARTICLE

Check for updates

Lipid–drug conjugates and associated carrier strategies for enhanced antiretroviral drug delivery

Funanani Takalani, Pradeep Kumar, Pierre P. D. Kondiah, Yahya E. Choonara and Viness Pillay

Wits Advanced Drug Delivery Platform Research Unit, Department of Pharmacy and Pharmacology, School of Therapeutic Sciences, Faculty of Health Sciences, University of the Witwatersrand, Johannesburg, South Africa

ABSTRACT

Mortality rate of patients infected with HIV-1 has been significantly reduced by using HAART. However, the virus to date has not been eradicated. Transmission of HIV-1 infection through sexual intercourse remains an ongoing challenge, with increased risk of infection occurring in women. Interestingly, ARV drugs can be chemically linked with lipids to produce lipid–drug conjugates (LDCs). This alters pharmacokinetic properties of ARV drugs and thereby resulting in improved effectiveness. Although LDCs can be administered without a delivery carrier, they are usually incorporated into suitable delivery systems such as lipid nanoparticles, polymeric nanoparticles, micelles, liposomes, emulsions, and carbon nanotubes. Given that LDCs have the potential to improve oral bioavailability, lipophilicity, toxicity, and drug targeting, it is of our great interest to review strategies of lipid–drug conjugation together with their delivery systems for enhanced antiretroviral efficacy.

Abbreviations: LDCs: lipid–drug conjugates; ARVs: antiretrovirals; HAART: highly active drugs for antiretroviral therapy; CNS: central nervous system; SLNs: solid lipid nanoparticles; NLCs: nanostructured lipid carriers; PLGA: poly(lactic-co-glycolic acid); ATP: adenosine triphosphate; TGs: triglycerides; UDCA: ursodeoxycholic acid; PLA_2: phospholipase A_2; EL: ether lipids; PKC: protein kinase C; BBB: blood brain barrier.

ARTICLE HISTORY
Received 6 August 2019
Revised 12 November 2019
Accepted 13 November 2019

KEYWORDS
HIV-1; antiretrovirals; lipid–drug conjugates; drug delivery; nanoparticles

1. Introduction

HIV is the causative agent for Acquired Immune Deficiency Syndrome (AIDS) (Sarma and Das 2019). About 40 million people are living with HIV-infection whilst more than 25 million people have died due to AIDS (Sharma et al. 2015; Collier et al. 2016). Out of 2.5 million people infected annually worldwide, 60% are women (Carias et al. 2013). The high vulnerability of women to HIV infection consequently places them at risk of transmitting the virus. In most cases, this can either be through direct (mother to child) or horizontal transmission (heterosexual contact) (Anderson et al. 1991; Morison et al. 2001). To date, the spread of HIV/AIDS is still estimated to increase across different countries, yet eradication of this infection remains a clinical challenge (Corsi et al. 2016). Various biological barriers have been shown to hinder the delivery of ARV drugs through membranes by limiting their absorption and bioavailability (Amly and Karaman 2016; Corsi et al. 2016). Owing to this, the prodrug approach has been developed (Amly and Karaman 2016) to overcome barriers such as blood–brain barrier (BBB) and intestinal mucosa by altering pharmacokinetic and physicochemical properties of the drug to enhance absorption. The approach can also block efflux pumps to improve transcellular delivery of the drug (Amly and Karaman 2016). Amongst prodrug approaches that have been developed to date, lipid–drug conjugation has been revealed to be one of the best (Hussain et al. 2015). Lipid–drug conjugates (LDCs) are some of the common lipid nanoparticles designed to prevent leakage of highly polar drugs from the lipid matrix (Adhikari et al. 2017). They were developed in the late 1990s because solid lipid nanoparticles (SLNs) and nanostructured lipid carriers (NLCs) possess the drawback of low drug loading capacity for hydrophilic drugs (Neupane et al. 2013). Recently, LDCs have gained great attention of researchers since metabolic pathways of lipids are designed in a way that benefits their action of targeting suitable organs with less side effects (Hussain et al. 2015; Banerjee and Kundu 2018). Thus, the similarities of LDCs with physiological lipids increase the solubility of therapeutic agents and thereby improving the bioavailability (Adhikari et al. 2017). Lipid-based drug carriers like LDCs have distinctive size-dependent properties. Hence, they provide higher degree of biocompatibility, versatility, safety, and efficacy. Therefore, LDCs are suitable for administration through different routes. Compared to other polymeric systems, LDCs protect the drug from enzymatic degradation and results in increased oral absorption (Hussain et al. 2015). However, it is worth noting that even with several reports that have been published on this delivery system, there is no comprehensive treatment for HIV infections that has been presented centred on the aspects of this technology (Adhikari et al. 2017). Therefore, this review presents in-depth report on LDCs and their associated carrier strategies for enhanced antiretroviral efficacy. This could be useful in the development of new therapeutics for HIV to overcome challenges associated with various biological barriers that reduce ARV bioavailability.

2. Advantages and drawbacks of LDCs

When a drug gets covalently attached to the corresponding functional group of a lipid through an ester, amide, or any other

CONTACT Viness Pillay viness.pillay@wits.ac.za Wits Advanced Drug Delivery Platform Research Unit, Department of Pharmacy and Pharmacology, School of Therapeutic Sciences, Faculty of Health Sciences, University of the Witwatersrand, Johannesburg, 7 York Road, Parktown, 2193, South Africa.
© 2019 Informa UK Limited, trading as Taylor & Francis Group

2.1 Introduction

Various biological barriers have been shown to hinder the delivery of ARV drugs through membranes by limiting their absorption and bioavailability (Amly and Karaman 2016; Corsi et al. 2016). Owing to this, the prodrug approach has been developed (Amly and Karaman 2016) to overcome barriers such as blood–brain barrier (BBB) and intestinal mucosa by altering pharmacokinetic and physicochemical properties of the drug to enhance absorption. The approach can also block efflux pumps to improve transcellular delivery of the drug (Amly and Karaman 2016). Among prodrug approaches that have been developed to date, lipid–drug conjugation has been revealed to be one of the best (Hussain et al. 2015).

Lipid–drug conjugates (LDCs) are some common lipid nanoparticles designed to prevent leakage of highly polar drugs from the lipid matrix (Adhikari et al. 2017). They were developed in the late 1990s because solid lipid nanoparticles (SLNs) and nanostructured lipid carriers (NLCs) possess the drawback of low drug loading capacity for hydrophilic drugs (Neupane et al. 2013). Recently, LDCs have gained great attention of researchers since metabolic pathways of lipids are designed in a way that benefits their action of targeting suitable organs with less side effects (Hussain et al. 2015; Banerjee and Kundu 2018). Thus, the similarities of LDCs with physiological lipids increase the solubility of therapeutic agents and thereby improving the bioavailability (Adhikari et al. 2017). Lipid-based drug carriers like LDCs have distinctive size-dependent properties. Hence, they provide higher degree of biocompatibility, versatility, safety, and efficacy.

Therefore, LDCs are suitable for administration through different routes. Compared to other polymeric systems, LDCs protect the drug from enzymatic degradation and results in increased oral absorption (Hussain et al. 2015). However, it is worth noting that even with several reports that have been published on this delivery system, there is no comprehensive treatment for HIV infections that has been presented based on the aspects of this technology (Adhikari et al. 2017). Therefore, this review presents an in-depth report on LDCs and their associated carrier strategies for enhanced antiretroviral efficacy. This could be useful in the development of new therapeutics for HIV to overcome challenges associated with various biological barriers that reduce ARV bioavailability.

2.2 Advantages and drawbacks of LDCs

When a drug gets covalently attached to the corresponding functional group of a lipid through an ester, amide, or any other bond, the product formed is an LDC, also known as lipidic or lipophilic prodrug (Sharma et al. 2012; Hussain et al. 2015). Since prodrugs are inactive, they need to be converted to their active form to show pharmacological action (Date et al. 2019). *In vivo* biological stimulation such as enzymatic transformation or pH can be used to trigger this conversion. However, to be metabolized, LDCs require enzymes having broad substrate specificity such as hydrolases, esterase, and amidases. Therefore, chemical bonds which get cleaved by highly substrate-specific enzymes should be avoided as they could lead to enzyme saturation and patient response variability (Date et al. 2019).

Advantages of LDCs include their ability to increase bioavailability, drug targeting, and intestinal permeability, thereby providing controlled drug release. Lipid–drug conjugation seems to be a good strategy to improve diffusivity of the drug, its permeability through the gastrointestinal (GI) walls, and stability in the GI environment. Furthermore, drugs with sufficient hydrophobic functional groups have been shown to have good GI permeability. Hence, chemical modification of drug structure using hydrophobizing moieties like lipids has been proven to be practically effective (Date et al. 2019).

Challenges associated with LDC formulations include chemical instability, aqueous solubility, and polymorphism. This is caused by differences in physicochemical properties of the prodrug and the parent drug; since by nature, the parent drug is more chemically stable than the prodrug (Jana et al. 2010). Taken together, LDCs are at the forefront of the fast-emerging field of nanotechnology, presenting numerous outstanding applications in drug delivery studies (Adhikari et al. 2017).

2.3 Methods for processing LDCs into lipidic delivery systems

Lipid-based drug delivery systems are a wide range approach used in the production of formulations containing a suspended or dissolved drug in lipidic excipients. This approach involves several techniques such as hot homogenization and ultrasonication methods. Many studies have employed these techniques in the formulation of LDCs, SLNs, NLCs, among others for drug delivery systems. Although, in preparation of LDC nanoparticles, the hot homogenization technique is the most suitable method. Other methods which can be used preparing this type of nanosystem include microemulsion, solvent emulsification–diffusion, and solvent injection (Adhikari et al. 2017; Nemati et al. 2019).

In 2019, Nemati et al. described the formulation of a dry powder inhaler for pulmonary administration using ethambutol-loaded solid lipid nanoparticles (EMB-loaded SLNs) for the treatment of tuberculosis. In their study, solid lipid (compritol) and oil phase surfactant (tween 80) were boiled at 80 °C under continuous stirring and melted to form an oil phase. Subsequently, poloxamer (aqueous phase) was dissolved in distilled water and the temperature was increased to that of the lipid phase. Thereafter, adequate amounts of EMB were dissolved in the aqueous phase and then added to the lipid phase. The solution was homogenized to generate a primary water-in-oil emulsion, and the remaining aqueous phase was added into the oil phase in a dropwise manner under continuous homogenization to obtain a final dispersion. Then the product acquired from homogenization was sonicated and EMB-loaded SLN dispersion was obtained by reducing the nanoemulsion to room temperature.

The findings of aerodynamic traits and flowability study showed suitability of EMB-loaded SLN DPI when spray dried with and without mannitol in the analysis conducted using next-generation impactor (NGI) (Nemati et al. 2019). In another related study carried out by Dolatabadi et al. (2018), the improvement of cellular toxicity and systemic bioavailability of Ketotifen (KT) was assessed using NLCs. The results of MTT and DAPI staining assays showed that the formulated KT-loaded NLCs possessed low toxicity, and it was proven safe on A549 cells. Furthermore, the findings suggested that this type of nano-delivery system can be used to surrogate the traditional use of KT in the treatment of allergic symptoms via topical or pulmonary routes of administration. There are several other studies (Dolatabadi et al. 2014; Bakhtiary et al. 2017) which have used hot homogenization and ultrasonication methods in preparing SLNs, NLCs, and other lipidic drug delivery systems.

2.4 Characterization techniques for LDCs

To assure therapeutic efficacy, dosage uniformity, and biological safety of LDCs in improving bioavailability of ARVs, the following characterization techniques and parameters are employed (Adhikari et al. 2017; Date et al. 2019):

(i) Fourier Transformed Infrared Spectra (FTIR): This is used to characterize functional groups formed in conjugates.
(ii) Differential Scanning Calorimetry (DSC): Used to establish melting point and crystallinity of the LDC formulations.
(iii) Partition Coefficient (logP) and Caco-2 permeability assay: Evaluate potential absorption or permeability of conjugates.
(iv) Stability assay: Verify chemical and aqueous stabilities of prodrugs targeted/ designed for enzymatic and chemical hydrolysis, respectively.

(v) Solubility assay: Compares prodrug solubility with that of the parent drug over the range of gastrointestinal pH.

(vi) Nuclear Magnetic Resonance (NMR): Confirms successful conjugate formation.

(vii) Mass spectroscopy: Determines molecular mass of the formed conjugate.

(viii) X-ray diffraction (XRD): Identifies the nature and distribution pattern of LDCs in the formulated nanoparticles.

(ix) Entrapment Efficiency (EE) and Drug loading capacity: Provide an estimate of the amount of drug loaded per unit amount of carrier.

(x) *In vitro* drug release: Establishes duration of dosing.

(xi) *In vivo* studies: Proves therapeutic efficacy of the conjugates.

(xii) Toxicity analysis: Proves safety of conjugates.

2.5 ARV drugs and lipid synthesized conjugates

Provided below is a report of ARV lipidic prodrugs (FDA approved and those in clinical trials) that have been designed with the purpose of improving HIV therapy. This is summarized in Table 2.1 and their chemical structures are presented in Figures 2.1 and 2.4. Generally, lipid selection in the production of LDCs is based on the function that they are intended to perform and the structure of the drug (Adhikari et al. 2017). Herein, lipids were selected based on their abilities to increase therapeutic efficacy of ARV drugs with poor bioavailability, to reduce their toxicity, and to increase permeation, potency, lipophilicity, and cellular uptake. Thus, lipids interact with ARV drugs via the covalent ester bond, which becomes cleaved during the replication cycle to produce compounds that target reverse transcriptase activity.

2.5.1 ARV lipidic prodrugs approved by the U.S. and EU FDA

2.5.1.1 Tenofovir disoproxil fumarate (TDF)

TDF is a prodrug form of tenofovir (TFV) phosphonate which has been developed to improve the oral bioavailability of TFV (Spinks et al. 2017). This prodrug is activated intracellularly through the phosphorylation process to achieve its therapeutic efficacy. During this process, TDF gets converted to its active form (TDF-DP) by cellular enzymes. As compared to TFV which has the solubility of ~5 mg/mL in aqueous medium, the solubility of TDF is ~2.5-fold higher at 13.4 mg/mL (Spinks et al. 2017). When tested *in vitro*, TDF showed increased antiretroviral activity by more than 100-fold and increased TFV-DP concentrations by more than 1000-fold compared to TFV (Hoang et al. 2018). Therefore, due to its increased potency in comparison with TFV, TDF was first approved by the U.S. FDA in 2001 for the treatment of HIV infections and sold under the brand name Viread® (Clercq 2018). It then became available as pills, which combine several antiviral drugs into a single dose. These include: (1) Truvada®

(combination of TDF and emtricitabine) which was approved in 2004 for treatment of HIV infections and in 2012 for prophylaxis of HIV infections. In 2016, Truvada® was also approved by the EU for prophylaxis infections (2) Atripla® (combination of TDF, emtricitabine, and efavirenz) approved in 2006 (3) Complera® in the USA and Eviplera® in the EU (combination of TDF, emtricitabine, and rilpivirine) approved in 2011 and, (4) Stribild® (combination of TDF, emtricitabine, elvitegravir, and cobicistat) approved in 2012; all for HIV infections (Clercq 2018).

2.5.1.2 Tenofovir alafenamide (TAF)

TAF, formerly known as GS-7340, is a prodrug with improved properties comparative to TDF (Ray et al. 2016; Spinks et al. 2017). Although TDF is potent and well tolerated overall, it has been associated with reductions in bone mineral density, changes in markers of renal function, and a rare incidence of serious renal adverse events, including Fanconi syndrome (Spinks et al. 2017). Hence, TAF was intended to be a more effective prodrug able to overcome such limitations. This is a lipophilic aryloxy phosphoramidate prodrug of TFV wherein phenol and an esterified amino acid moiety, alanine, are used as masking groups of the phosphonate functional group (Rautio et al. 2017). For its activation pathway, TAF involves several lysosomal serine protease enzymes, such as cathepsin A, capable of initial intracellular hydrolysis of the carboxyester bond. This is followed by a putative nucleophilic attack on the phosphorus by the negatively charged carboxyl group, causing phenol to be eliminated from a highly unstable five-membered ring. When this ring is opened by nucleophilic attack from the water molecule, a phosphoramidate intermediate with alanine conjugated to TFV is generated.

Subsequently, alanine is released either by enzymatic or by chemical degradation to release TFV that is later phosphorylated to the pharmacologically active metabolite TFV-DP (Ray et al. 2016; Rautio et al. 2017). As compared to TDF, TAF produces higher levels of intracellular TFV-DP because of its increased stability in the plasma, which allows for prolonged systemic exposure to the intact prodrug. Therefore, TAF has been shown to be 1000-fold more active against HIV than TFV and 10-fold more active than TDF *in vitro* (Ray et al. 2016). Additionally, regimens containing TAF showed a 90% reduction in plasma tenofovir concentrations and improved renal and bone safety (Spinks et al. 2017). TAF was first approved by the U.S. FDA in 2015 and marketed as Genvoya® (combination of emtricitabine, elvitegravir, and cobicistat). In 2016, it was approved alone with the trade name Vemlidy® and again as Odefsey® (combination of emtricitabine and rilpivirine). Thereafter, it was approved as Biktarvy® (combination of emtricitabine and bictegravir) in 2018. It has lately been approved as

Descovy® (combination of TAF and emtricitabine) on 3 October 2019 for HIV pre-exposure prophylaxis (PrEP) (Clercq 2018).

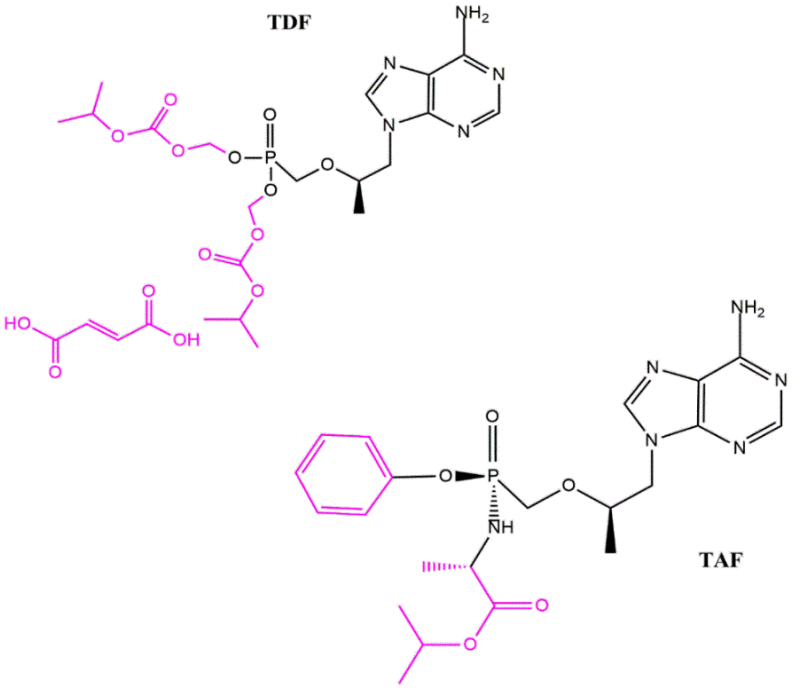


Figure 2.1. Chemical structures of ARV lipidic prodrugs approved by the FDA (TDF and TAF)

2.5.2 ARV lipidic prodrugs in clinical trials and those still under assessment

2.5.2.1 Tenofovir (TFV) and hexadecyl-oxypropyl (HDP) [HDP-TFV]

As a result of poor oral bioavailability and renal toxicity associated with TDF, an alternative TFV lipid conjugate (HDP-TFV, well known as CMX157) has been formulated (Spinks et al. 2017). This is an alkoxy alkyl-based prodrug comprised of TFV hydroxyl groups and hexadecyloxypropyl lipid moiety. Herein, CMX157 is intended to remain intact in the blood while it makes use of natural lipid uptake pathways by mimicking lysophosphatidylcholine (LPC) (Lanier et al. 2010). In doing so, TFV is converted to the active antiviral (TFV-DP) with higher intracellular concentrations and improved effectiveness against HIV. When administered orally to rats at 10, 30, and 100 mg/kg per day for 7 days, CMX157 was shown to be non-toxic, and it resulted in enhanced bioavailability. Furthermore, this prodrug showed great potential to effectively suppress replication of multi NRTI-resistant (MNR) HIV that cannot be treated with any currently available NRTIs, including TDF (Lanier et al. 2010). CMX157 has been tested in phase I clinical trials, and it was found to be 300-fold more active than TFV against multiple viruses in several cell systems and at least 267-fold more active against HIV-1. It was also found to have wide activity against both HIV subtypes (HIV-1 and HIV-2) in fresh human peripheral blood mononuclear cells (Sinikrot et al. 2017).

2.5.2.2 Cidofovir (CDV) and 1-0-hexadecyl-oxypropyl (HDP)

CDV, marketed as Vistide®, is used to treat cytomegalovirus (CMV) retinitis in HIV patients (Painter et al. 2012). This drug has shown clinical activity against various families of double-stranded DNA (dsDNA) viruses that cause diseases in humans. However, CDV can cause nephrotoxicity by uptake into renal tubules through human organic anion transporters (hOAT). Additionally, CDV has poor permeability in the BBB. Owing to this, brincidofovir, formerly known as CMX001, has been established (Florescu and Keck 2014). This is a lipid antiviral conjugate (LAC) comprised of the HDP lipid moiety and CDV. Just like CMX157, this conjugate similarly mimics LPC in the small intestine to allow the drug to use natural LPC uptake pathways (Painter et al. 2012; Florescu and Keck 2014). Once in the cell, CDV gets converted to the active antiviral agent, cidofovir diphosphate (CDV-PP).

In comparison with typical prodrugs which deliver drugs to the plasma, brincidofovir remains intact in the plasma and delivers drugs directly to the targeted cell. This produces higher intracellular levels of the active antiviral agent, while maintaining lower drug plasma concentrations of CDV (Painter et al. 2012; Florescu and Keck 2014). Consequently, brincidofovir significantly improves antiviral potency against dsDNA viruses compared to CDV alone. Moreover, since brincidofovir is not a substrate of hOAT like cidofovir, it does not accumulate in renal tubules and thereby reducing nephrotoxicity. Taken together, brincidofovir has been tested in a series of clinical trials for CMV retinitis, making it seem to be a promising prodrug under development.

2.5.2.3 Emtricitabine (FTC) and elvitegravir (ELG) with docosahexaenoic acid (DHA)

Owing to their high potencies, FTC and ELG form part of combination therapies (mentioned in Section 2.5.1) currently used by HIV-infected patients worldwide. However, their long-term efficiency is restricted by poor bioavailability, daily administration, and metabolism by cytochrome P450 3A4 (CYP3A4). Attributable to this, they have been modified using polyunsaturated fatty acid (PUFA) to synthesize prodrugs that are long-acting (Krovi et al. 2018). Success of this method is reliant on the degree of cleavage of the chemical bond within the parent drug and the derivatizing moiety. In models of tissue culture and *in vitro* drug release profiles, conjugation of FTC and ELG with DHA showed improved antiretroviral activities in contrast to drugs alone (shown in Figure 2.2). The release was sustained and controlled for 3–4 weeks, which was further confirmed by evaluating pharmacokinetic properties *in vivo* using CD1 mice, depicted in Figure 2.3 (Krovi et al. 2018).

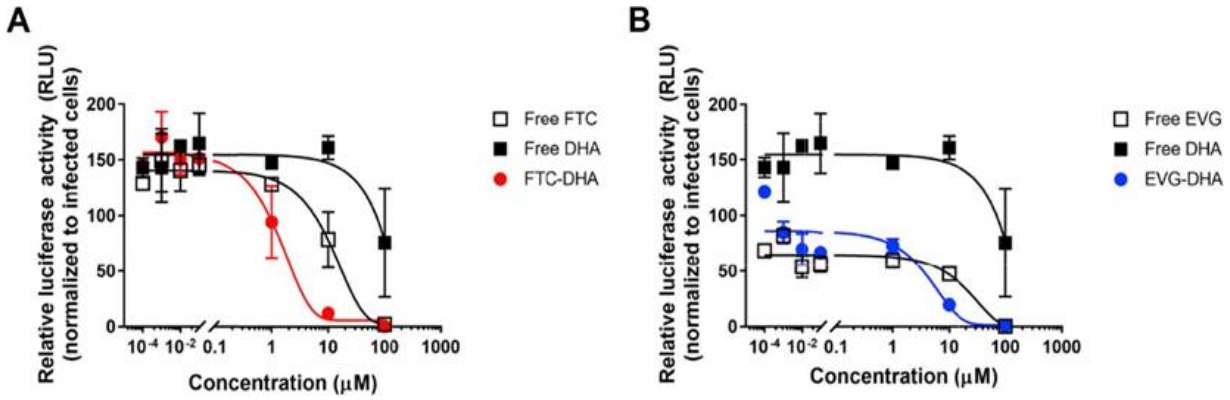


Figure 2.2. Results showing improved antiretroviral activities of FTC and ELG conjugated with DHA in CD1 mice (Figure adapted with permission from Krovi et al. 2018)

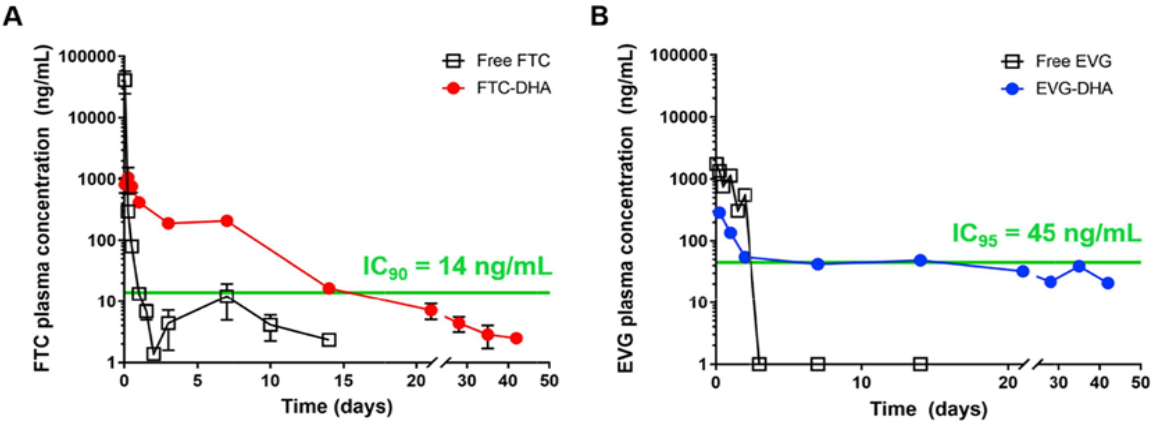


Figure 2.3. Results showing improved antiretroviral activities of FTC and ELG conjugated with DHA *in vitro* (Figure adapted with permission from Krovi et al. 2018)

2.5.2.4 Ganciclovir (GCV) and acyl ester

Same as CDV, GCV is also used to treat CMV retinitis in HIV patients. However, administration of GCV, both orally and intravenously, results in poor ocular bioavailability as well as insufficient therapeutic concentrations in the retina (Cholkar et al. 2014). In addition to this, high doses or frequent administrations of this drug lead to systemic toxicity. Therefore, to improve bioavailability and lipophilicity of GCV, its acyl ester derivatives have been synthesized through a one-step esterification reaction process. Herein, the reversed-phase high-performance liquid chromatography was used to determine purity of novel prodrugs whereas NMR and mass spectroscopy were used to confirm acyl ester-GCV conjugation (Cholkar et al. 2014). Thereafter, the toxicity of this prodrug was tested *in vitro* on human retinal pigment epithelial cells (ARPE-19 cell line) using the MTT assay. Results indicated that the GCV prodrug was safe, non-toxic, and well tolerated by these cells. Additionally, the hydrolyzed ester bond resulted in a sustained release of GCV. This denotes that long acyl ester-GCV conjugates may be further assessed for treatment of CMV retinitis and ocular delivery (Cholkar et al. 2014).

2.5.2.5 Emtricitabine (FTC) and lamivudine (3TC) with fatty acyl ester derivatives

Fatty acyl conjugates of both FTC and 3TC were designed and intended for topical anti-HIV microbicide development (Agarwal et al. 2012, 2013). Once in the cell, these ester conjugates are hydrolyzed by esterases to produce two anti-HIV active agents: (1) the nucleoside analogue targeting reverse transcriptase and (2) fatty acid targeting N-myristoyltransferase (NMT) enzymes. Results showed enhanced antiviral potency, lipophilicity, and cellular uptake in HIV target cells compared to drugs alone (Agarwal et al. 2012, 2013). Although, over time, mutations in HIV reverse transcriptase were reported to have produced several strains of FTC and 3TC-resistant viruses.

2.5.2.6 Zidovudine (AZT) and ether lipids

Given that AZT is the first successful clinical drug for AIDS treatment, serious adverse reactions such as suppression of bone marrow have been shown to limit its therapeutic potential (Tsotinis et al. 1996). Therefore, it has been conjugated with ether phospholipids such as alkoxyethyl and oxyalkyl wherein lipid molecules bear alkoxypropanols and long alkyl chains are replaced with aromatic groups. These lipids are covalently attached to AZT through the phosphodiester bond, resulting in compounds with improved anti-HIV activity and that are more potent compared to AZT alone (Tsotinis et al. 1996).

2.5.2.7 AZT and thioether lipid

AZT-thioether lipid conjugate [Fozivudine tidoxil (FZD)] was established to improve organ and cell selectivity (Girard et al. 2000). When administered intracellularly, FZD splits into the lipid moiety and AZT monophosphate (AZT-MP) which gets phosphorylated to its active metabolite (AZT triphosphate). As compared to free AZT, FZD was shown to be more effective and well tolerated by patients. Additionally, the viral load in patients receiving FZD was shown to have reduced whereas the plasma half-life was significantly increased (Girard et al. 2000). This explains the possibility of FZD to be taken once daily during short-term administration.

2.5.2.8 AZT and synthetic phosphocholine lipid

Using HAART treatment for long-term has been associated with toxic side effects, drug resistance in HIV variants, and poor pharmacokinetic properties (Kucera et al. 2004). As a result, a synthetic phosphocholine lipid–AZT conjugate (INK 20) has been synthesized. INK 20 is formed from the association of a phosphocholine lipid with a nucleoside analogue through a malonate diester bond. Upon cleavage of this bond in the viral replication cycle, INK-20 releases the nucleoside AZT, which becomes phosphorylated to AZT-triphosphate and inhibits HIV-induced reverse transcriptase. This prodrug showed little or no toxicity when assayed in PBMC and CEM-SS cells compared to AZT alone (Kucera et al. 2004).

Furthermore, the prodrug retained significant activity against viruses resistant to nevirapine, 3TC, and saquinavir whereas it showed excellent activity against multidrug-resistant clinical isolate. This suggests that INK 20 has the potential to reduce toxicity and for treatment of HIV drug resistant variants.

2.5.2.9 AZT and ursodeoxycholic acid (UDCA)

This conjugation was developed owing to several limitations that the AZT drug possesses. AZT has poor ability to permeate the CNS since it is a substrate of the AET (active efflux transporter) system, which is highly expressed in the brain. This leads to reduced effective treatment of CNS conditions such as AIDS dementia complex and HIV encephalopathy (Takasawa et al. 1997). Hence, UDCA–AZT conjugate was synthesized to escape the AET system by reducing transport mediation resistance and rate of hydrolysis in the plasma (Dalpiaz et al. 2014). Taken together, this prodrug shows significant safety and increased efficacy compared to previously mentioned AZT prodrugs, as it represents a potential carrier for AZT in the CNS. Furthermore, it has been incorporated into solid lipid microparticles (SLMs) for nasal administration, whereby its uptake was shown to have increased six times in the cerebrospinal fluid (CSF) (Dalpiaz et al. 2014).

2.5.2.10 Indinavir (IDV) with phosphatidylcholine and cholesterol lipid

This conjugation was designed to improve delivery of IDV to the lymphatic system in HIV-infected patients (Kinman et al. 2003). Since lipophilicity of IDV is pH-dependent and decreases by 1000- fold from 3 to 7 in an aqueous soluble state, its association with lipids has been optimized to form stable LDCs. An example for this is that of phosphatidylcholine and cholesterol (3:1 mol/mol) conjugated with IDV and adjusted to pH 7.4 using a lipid–drug (m/m) ratio of 5:1. In these conditions, conjugation of IDV with lipids is expected to be stable with a diameter of 69 ± 7 nm (Kinman et al. 2003). When administered in macaques infected with HIV-2287 for 30–33 weeks, this conjugate showed significant reduction in RNA viral load, increased half-life, and concentrations in the number of CD4 T cells compared to lipid-free IDV administered in humans.

Table 2.1. Lipid synthesized ARV-conjugate delivery systems

ARV drugs	Lipids	References
Zidovudine (AZT)	Thioether lipids, ether lipids, synthetic phosphocholine lipid & UDCA	(Tsotinis et al. 1996; Takasawa et al. 1997; Girard et al. 2000; Kucera et al. 2004)
Cidofovir (CDV)	1-0-hexadecyl-oxypropyl (HDP)	(Painter et al. 2012, Florescu and Keck 2014)
Ganciclovir (GCV)	Acyl ester	(Cholkar et al. 2014)
Tenofovir (TFV)	Hexadecyl-oxypropyl (HDP)	(Lanier et al. 2010)
Emtricitabine (FTC); Lamivudine (3TC)	Fatty acyl ester derivatives	(Agarwal et al. 2012, 2013)
Indinavir (IDV)	Phosphatidylcholine; cholesterol lipids	(Kinman et al. 2003)
Emtricitabine (FTC); Elvitegravir (ELG)	Docosahexaenoic acid (DHA)	(Krovi et al. 2018)

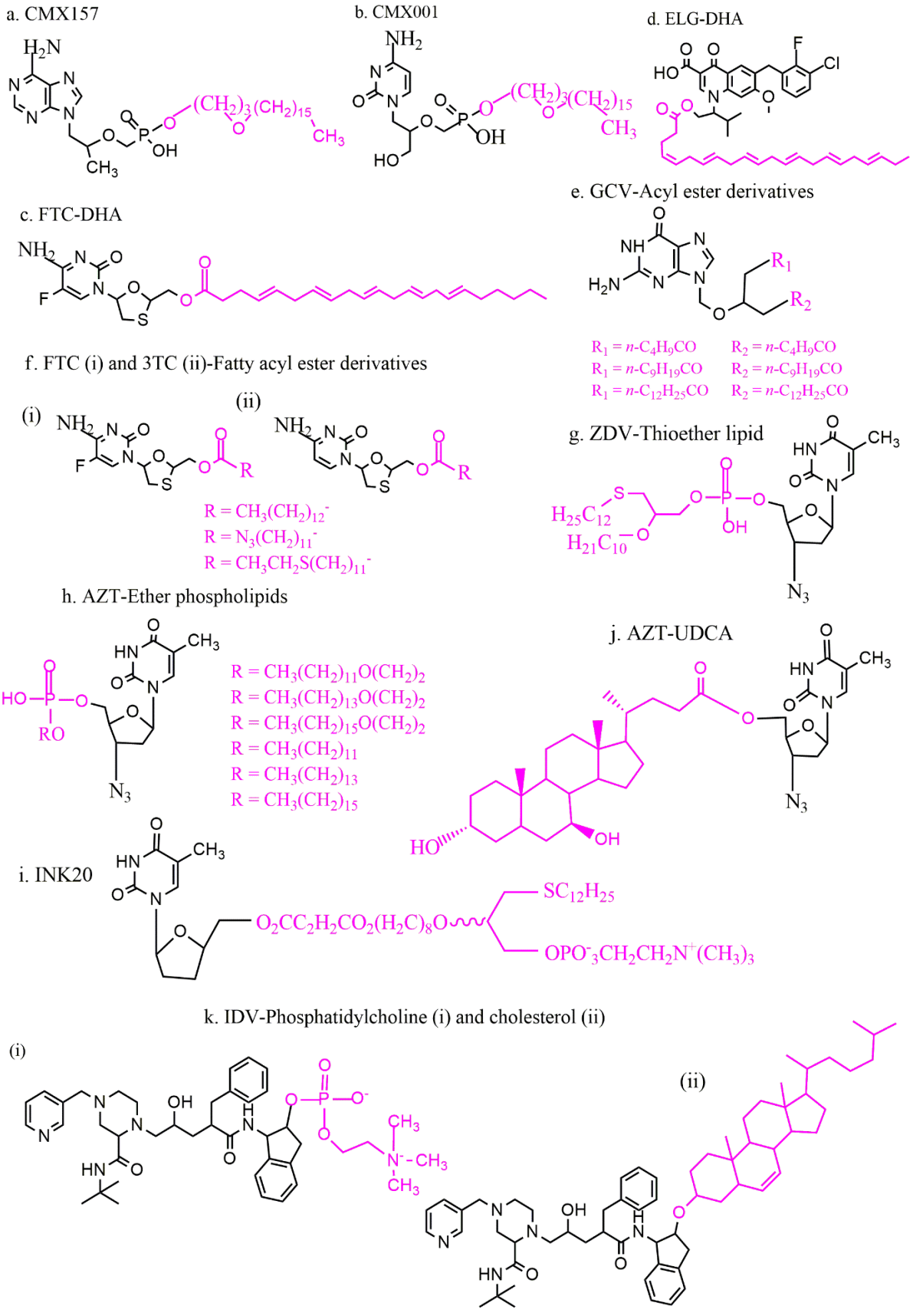


Figure 2.4. Chemical structures of lipid–drug conjugates

2.6 Strategies for the delivery of LDCs

The process of selecting lipid carriers to develop LDCs determines the functional role of a lipid. Lipid carriers can be classified into a group of fatty acids, glycerides, steroids, or phospholipids. These lipids are the most common in developing LDCs since their melting point properties are high (Date et al. 2019).

2.6.1 ARV drug-fatty acids conjugation

Fatty acids are made up of long aliphatic chains (4–28 carbon atoms) which may be saturated or unsaturated. Since they produce ATP (adenosine triphosphate) in large quantities during metabolism, they are regarded as important sources of fuel. Fatty acids are the most utilized lipid carriers because they grant high lipophilicity during the development of drug conjugation (Rajabi and Mousa 2016). They consist of a carboxylic acid and a hydrocarbon chain. Two ways through which fatty acids can be conjugated to drugs are: (i) through direct attachment of a drug to the carboxylic end of a lipid with hydroxyl or amino function to yield an ester or amide linkage (Zaro 2015). Herein, the most executed method is one whereby the -OH group is converted to a better leaving group by activating agents like carbodiimide. Then a drug containing an amine or alcohol group is added. (ii) Through keeping the carboxylic group free to allow fatty acids to bind serum albumin and gain recognition from transporters in the cell membrane while the drug attaches to the x-atom that has been altered (Markovic et al. 2019). It is worth mentioning that fatty acids with longer chains (>14) result in higher absorption and circulation stability in contrast to shorter chains. Therefore, fatty acid chain length has an impact on drug properties which may affect drug delivery (Zaro 2015).

2.6.2 ARV drug–glycerides conjugation

Triglycerides (TGs) are the major constituents of dietary fat. In this conjugation, three fatty acids within the glycerol molecule are linked through an ester bond, resulting in TGs. Thus, drugs can bind to sn-1, sn-2, or sn-3 carbon atoms during conjugation (Markovic et al. 2019). However, one fatty acyl group among these located at position two is replaced by a drug conjugate to benefit from the unique metabolic pathway of TGs; a process referred to as triglyceride deacylation–reacylation (Irby et al. 2017). This is a pathway whereby hydrolysis of TGs takes place in the gastrointestinal (GI) lumen, leading to the formation of 2-monoglyceride (2-MG) and free fatty acids. The monoglycerides are reacylated into enterocytes to yield triglycerides, which are then integrated into lipoproteins to accumulate in the lymphatic system (Han et al. 2014). The purpose of this conjugation is to target drugs in the lymphatic system while improving their absorption. As discussed under fatty acids, the chemistry of glyceride conjugation also involves activating agents that convert the hydroxyl group to a better leaving group, such as chlorine (Zaro 2015).

2.6.3 ARV drug–steroids conjugation

Steroids are considered an important class of hydrophobic (non-water-soluble) lipids. A steroid molecule consists of four rings [three referred to as cyclohexane rings (A, B, and C) and one known as cyclopentane ring (D)] (Rajabi and Mousa 2016). These rings are often attached with hydroxyl group(s), which are essential in the development of drug–steroid conjugation. Hence, the hydroxyl group (s) is used as the primary location in most studies (Irby et al. 2017). Examples of steroids that have been conjugated with drug molecules include cholesterol, cholic acid, and bile acid. Among these, cholesterol is the most prominent member. Interaction of cholesterol with proteins can influence functions of the cell and contribute to self-assembly of several nanostructures (Markovic et al. 2019). Furthermore, drugs that have been conjugated with cholesterol revealed less side effects, improved target delivery, and enhanced cellular uptake (Irby et al. 2017). Cholic acid, on the other hand, has been utilized as lithocholic acid (LCA) or ursodeoxycholic acid (UDCA). This is a bile acid that has the potential to penetrate the CNS. In contrast to cholesterol, UDCA consists of three hydroxyl groups which can be used for conjugation (Markovic et al. 2019).

2.6.4 ARV drug–phospholipids conjugation

Phospholipids are lipid structures comprising polar and nonpolar potions as well as a phosphorous element. Owing to the presence of alcohol groups, phospholipids can be divided into glycerophospholipids and sphingomyelins (Li et al. 2014). Glycerophospholipids are the main phospholipids containing α-structure, L-configuration, and glycerol as the backbone. The chemical structures of glycerophospholipids and sphingomyelins are closely related except that in sphingomyelins, the backbone is a sphingosine. During conjugation, drugs can attach to the glycerol backbone at position sn-2 using an enzyme called phospholipase A2 (PLA2) or they can directly attach to the phosphate group by replacing the fatty acid either in positions sn-1 or sn-2 (Markovic et al. 2019). Conjugates developed from these strategies can improve incorporation of drugs into lipid-based delivery systems to enhance absorption and stability of the drug (Arouri and Mouritsen 2011). Phospholipids compounds possess anti-HIV-1 activity which works by altering viral envelopes and membrane cell surface (Krugner-Higby et al. 1995).

2.7 Delivery systems for LDCs

AIDS can be diagnosed and treated using several nanotechnology approaches. These approaches are intended to improve physicochemical properties of drugs such as permeability state, stability, and solubility. Although LDCs can be administered without a delivery carrier, the most common delivery systems include lipid nanoparticles, polymeric nanoparticles,

micelles, liposomes, emulsions, and carbon nanotubes. Table 2.2 summarizes examples of ARV drugs conjugated with nanoparticles explained herein:

2.7.1 Lipid and polymeric nanoparticles

Nanoparticle-based drug delivery systems have the potential to deliver drugs that are poorly water-soluble through oral routes by encapsulating them within nanoparticles and protecting them from degradation, thereby allowing a sustained and controlled release (Beloqui et al. 2014). As a result of their small nanometer size (10–1000 nm), nanoparticles hold great promise for new therapeutics development to overcome numerous biological barriers (Bender et al. 1996; Chattopadhyay et al. 2008). Examples of lipid nanoparticles include SLNs, NLCs, and LDCs. Several drugs have been successfully incorporated into these colloidal drug delivery systems to protect them from physiological degradation (Neupane et al. 2013). The main advantages of SLNs over other lipid-based delivery systems are their ability to incorporate both hydrophilic and lipophilic compounds, their large surface area, high drug loading capacities, increased potential for controlled release, and enhanced cell uptake of various drugs. They also provide protection of the drug from the environment, thereby increasing its physicochemical stability and bioavailability (Nemati et al. 2019). Although, their inherent low drug incorporation caused by crystalline structure tends to cause undesired aggregation and unexpected dynamics of polymorphic transition (Dolatabadi and Omidi 2016). As compared to SLNs, NLCs have lower drug payload and drug expulsion during storage; they are more dispersed in water content and have increased long-term physical stability of suspension.

Hence, they do not possess significant problems associated with SLNs (Dolatabadi and Omidi 2016). Meanwhile, LDCs are used to transform water-soluble drugs into hydrophobic drugs, since the loading capacity of SLNs is inadequate for hydrophilic drugs encapsulation at times. In addition to this, LDCs have higher drug loading capacity, which allows them to deliver higher drug molecules to target cells with lower amount of lipid–drug conjugated with NPs. This results in minimal side effects and maximal drug delivery efficacy when compared to SLNs. Although drug-loading is more enhanced by liquid lipid as compared to solid lipid, both lipids have been used to deliver LDCs (Irby et al. 2017). Several studies revealed that lipid-based drug delivery systems can increase concentrations of drugs in the brain and circulatory system (Chattopadhyay et al. 2008; Reddy et al. 2018). For example, atazanavir has been reported to be a potential candidate for brain targeting when encapsulated in SLNs due to its lower toxicity, frequent use, and superior clinical profile. Additionally, ritonavir-loaded stealth SLNs showed better systemic circulation time of the drug, whereas polymeric nanoparticles such as PLGA [poly (lactic-co-glycolic acid)] and PLA-PEG [poly (lactic acid)-poly (ethylene) glycol]

have been reported to be the most used and the most studied delivery carriers for LDCs (Singh and Pai 2014; Irby et al. 2017; Reddy et al. 2018). ARV drugs such as emtricitabine have been conjugated with optimized PLGA nanoparticles, and the findings showed a controlled stable release formulation (Singh and Pai 2014).

2.7.2 Liposomes

Liposomes are spherical, with their sizes ranging from 25 nm to several microns (Ramana et al. 2010; Nayak et al. 2017). Herein, hydrophilic drugs are encapsulated in the aqueous core whereas hydrophobic drugs are incorporated in the phospholipid bilayer. The most common liposomes classified by lamellarity and size are multilamellar vesicles (MLVs) made up of multiple phospholipid bilayer with a size range greater or equal to 500 nm. Large unilamellar vesicles consisting of one phospholipid bilayer with a size of greater or equal to 100 nm, and small unilamellar vesicles comprised of one bilayer with a size range of 20–100 nm (Periyasamy et al. 2012). Liposomal drug delivery has been considered one of the most significant approaches for enhancing bioavailability and cellular uptake of ARV drugs such as saquinavir, tenofovir, and nevirapine (Ramana et al. 2015; Spinks et al. 2017). In the delivery of LDCs, liposomes comprising lipids such as cholesterol, egg phosphatidylcholine, and poly (ethylene glycol) 2000-distearoyl phosphatidylethanolamine (PEG-DSPE) have been used as carriers to reduce toxicity, provide longer circulation, and enhance stability of the drug (Jiao et al. 2013). This implies that liposomes are valuable drug carriers because of their good biocompatibility.

2.7.3 Polymeric nanomicelles

These are self-assembled nanocarriers made up of amphiphilic block copolymers. Their sizes range from 10 to 100 nm, and they consist of core-shell structures, with a shell structure comprising hydrophilic heads and the inner core comprising hydrophobic tails (Edagwa et al. 2014; Poudel et al. 2018). DSPE-PEG/tocopherol-PEG1000-succinate (TPGS) is an example of a well-known micelle that has been successfully used in the delivery of LDCs. It can increase drug concentrations in the systemic circulation and provide excellent drug loading stability (Wang et al. 2014; Li et al. 2016). In addition to this, micelle-forming block copolymers (PEO-PPO) have been formulated incorporating an ARV drug efavirenz. The results for this were tested in vivo and showed enhanced oral bioavailability with no mucosal irritation (Chiappetta et al. 2013). Furthermore, these copolymers have shown success in producing stable hydroxyapatite hollow nanoparticles (HA HNPs) using a method known as polymeric micelle templating wherein both the PEO and PPO copolymers are soluble in water below the CMT (critical micellar temperature) (Ye et al. 2010). However, at CMT, the PPO blocks begin to be insoluble to form spherical micelles whereas the PEO blocks remain soluble. Thus, the PPO

blocks occupy the inner hydrophobic core, while the PEO blocks fill in the hydrophilic shell. As the temperature increases, the PEO blocks start to lose water and become too insoluble at a certain temperature, referred to as cloud point. This technique allows HA HNPs to be adjusted during preparation, and, consequently, the HA HNPs result in higher drug load and improved efficiency compared to traditional nanoparticles (Ye et al. 2010).

2.7.4 Nanoemulsions

Nanoemulsions are kinetically stable isotropic mixtures containing either water-in-oil or oil-in-water dispersions and a combination of surfactants as stabilizers (Chrastina et al. 2018; Hobson et al. 2018). These are biocompatible carriers with their sizes ranging from 20 to 300 nm (Manyarara et al. 2018). The most used types of emulsions in the delivery of LDCs are the oil-in-water (o/w) emulsions wherein emulsifiers allow LDCs to be incorporated as oil droplets in a stable manner (Irby et al. 2017). Emulsions covered with PEG-PE (polyethylene glycol-modified phosphatidylethanolamine) have been developed to reduce uptake by the mononuclear phagocyte system. This formulation showed prolonged circulation time *in vivo* (Lundberg et al. 2023). Additionally, self-forming nanoemulsifying drug delivery systems (SNEDDS) and self-forming nanoemulsifying oily formulation (S-SNEOF) have recently been established using branched amphiphilic copolymers (Hobson et al. 2018). These systems showed improved bioavailability of poorly water-soluble ARV drugs such as efavirenz, lopinavir, and darunavir. It is worth mentioning that branched amphiphilic pH-responsive copolymers are excellent emulsifiers since they can form objects with high stability and hydrogen bonding that is reversible within emulsion droplets (Hobson et al. 2018).

2.7.5 Carbon nanotubes

Carbon nanotubes (CNTs) were developed in 1991 (Rafati and Afraz 2014). These are carbon-based nanocarriers which are cylindrical and contain hexagonal networks of carbon atoms. They have a unique geometry and a controllable size with a surface area that is large and reactive (Lee and Yeo 2015). As a drug carrier, CNTs have been shown to possess excellent properties suitable to incorporate LDCs (Shao et al. 2013). Herein, a long chain lipid molecule covalently attached to the drug binds to surfaces of CNTs via hydrophobic interactions. Zidovudine is an example of one of the ARV drugs that has been conjugated to silver nanofilm and multiwalled carbon nanotubes. This conjugate was immobilized on glassy carbon electrodes to fabricate a sensor. The findings showed that zidovudine responded well to this sensor and thereby showing potential to produce high electrocatalytic activity (Rafati and Afraz 2014). CNTs can be divided into two groups (functionalized and non-functionalized). In contrast to non-functionalized CNTs which have difficulties dissolving in solvents (both organic and inorganic) because of their structural features, functionalized CNTs (f-CNTs) can

overcome these difficulties. Thus, f-CNTs allow covalent or non-covalent chemical bonding within CNTs and the targeted material. Hence, they have resulted in improved toxicity profiles both *in vitro* and *in vivo* (Prajapati et al. 2011). On the other hand, single-walled carbon nanotubes (SWNTs) have shown potential as drug carriers which do not result in toxic effects owing to their ability to penetrate mammalian cells (Zhang et al. 2006).

Table 2.2. Lipid-ARV prodrugs and nanoparticle synthesized-conjugate delivery systems

Lipid-ARV prodrugs	Nanoparticles	Covalent bond	Mechanism of action of bond breakage	Significance	References
Myristoylated ABC	Poloxamer nanoparticles	Ester bond	Hydrolyzed by esterases to produce the nucleoside ABC targeting reverse transcriptase and myristic acid targeting *N-myristoyltransferase* (NMT) enzymes.	Extends the half-life and bioavailability of ABC.	(Singh et al. 2016)
AZT and ursodeoxycholic acid (UDCA)	Solid lipid microparticles (SLMs)	Ester bond	Hydrolyzed through esterification to produce an antiviral agent substrate (AZT) of active efflux transport systems (AET) and UDCA, a bile acid able to permeate into the central nervous system (CNS).	Improves uptake of AZT in the brain.	(Dalpiaz et al. 2014)
TDF with compritol 888 ATO & oleic acid	NLCs	Carbon-carbon bond (covalent bond)	compritol 888 ATO & oleic acid are degraded by oxidation *in vivo* to form acetyl-CoA (coenzyme A) which is an entry molecule of the citric acid cycle for energy production. TDF is also released during the oxidation process.	Results in stable, biocompatible and biodegradable formulation.	(Sarma and Das 2019)
1-O-hexadecylpropanediol-3-phospho-ganciclovir (HDP-P-GCV)	Liposomes	Ester bond	The valine ester of GCV is cleaved from the HDP-P-GCV conjugate by esterases to produce GCV in the blood stream.	Provides a prototype for intraocular drug delivery.	(Cheng et al. 2000)
AZT myristate (AZT-M)	Liposomes	Ester bond	The ester bond between AZT and myristic acid is hydrolysed by esterases to produce AZT which targets reverse transcriptase while the free myristic acid targets *N-myristoyltransferase* (NMT) enzyme.	Results in higher concentrations of AZT in the brain and reticuloendothelial system (RES) organs.	(Jin et al. 2005)

2.8 Nano-enabled particulate systems for LDCs

2.8.1 Myristoylated abacavir (ABC) in poloxamer nanoparticles

Conjugation of ABC with myristic acid in poloxamer nanoparticles was synthesized to improve the bioavailability and half-life of ABC (Singh et al. 2016) (summarized in Table 2.3). Herein, myristic acid was linked to the 5-hydroxy-cyclopentene group of ABC through esterification, and the prodrug formed was encapsulated into poloxamer nanoparticles. Thereafter, assessment of antiretroviral activity, chemical composition, cellular trafficking, cell uptake, and retention for both free myristoylated ABC and nanoformulated myristoylated ABC was carried out using proton NMR (Singh et al. 2016). This was tested in human monocyte-derived macrophages and further evaluated in mice. The results indicated that nano formulated myristoylated ABC extended the bioavailability of ABC by 2 weeks compared to ABC alone, which suggests that myristoylated ABC can be used as a long-acting antiretroviral treatment.

2.8.2 UDCA-AZT in solid lipid microparticles (SLMs)

This system was established to overcome the restraint of lower uptake of UDCA-AZT in the CSF (cerebrospinal fluid). In this formulation, stearic acid and tristearin were employed as lipidic carriers to produce SLMs through the hot emulsion technique. As shown in Figure 2.5, tristearin SLMs were effective in controlling the release of UDCA-AZT whereas stearic acid SLMs showed a significant increase in dissolution rate of this prodrug. From this information, it can be deduced that the effect of stabilization is lower for stearic acid SLMs and very high for tristearin SLMs (Dalpiaz et al. 2014). When UDCA-AZT was administered in the CSF of rats, there was no AZT or UDCA-AZT detected. However, when incorporated in stearic acid SLMs and in the presence of chitosan, its uptake was shown to be enhanced (depicted in Figure 2.6). This indicates that SLMs have the potential to improve the uptake of AZT in the brain (Dalpiaz et al. 2014).

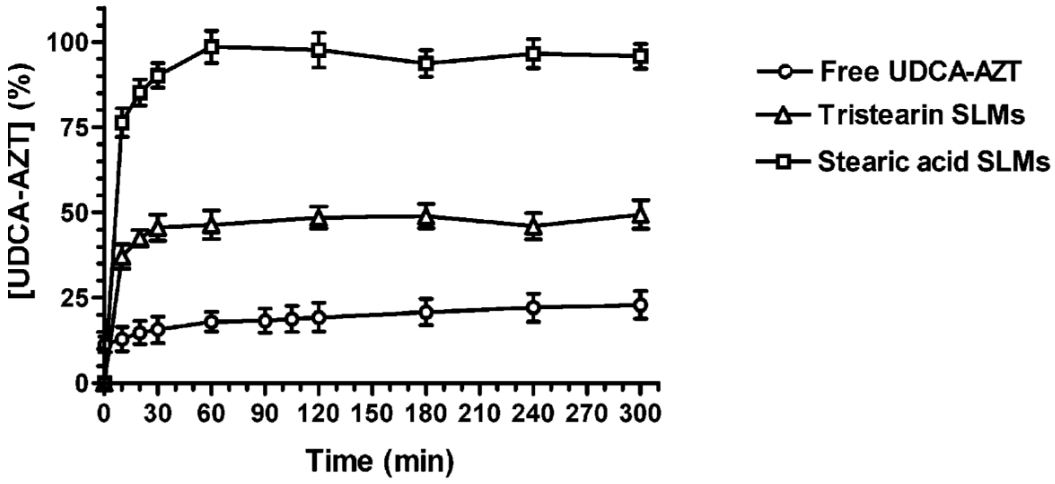


Figure 2.5. *In vitro* release of UDCA-AZT from SLMs based on tristearin or stearic acid (Figure adapted with permission from Dalpiaz et al. 2014)

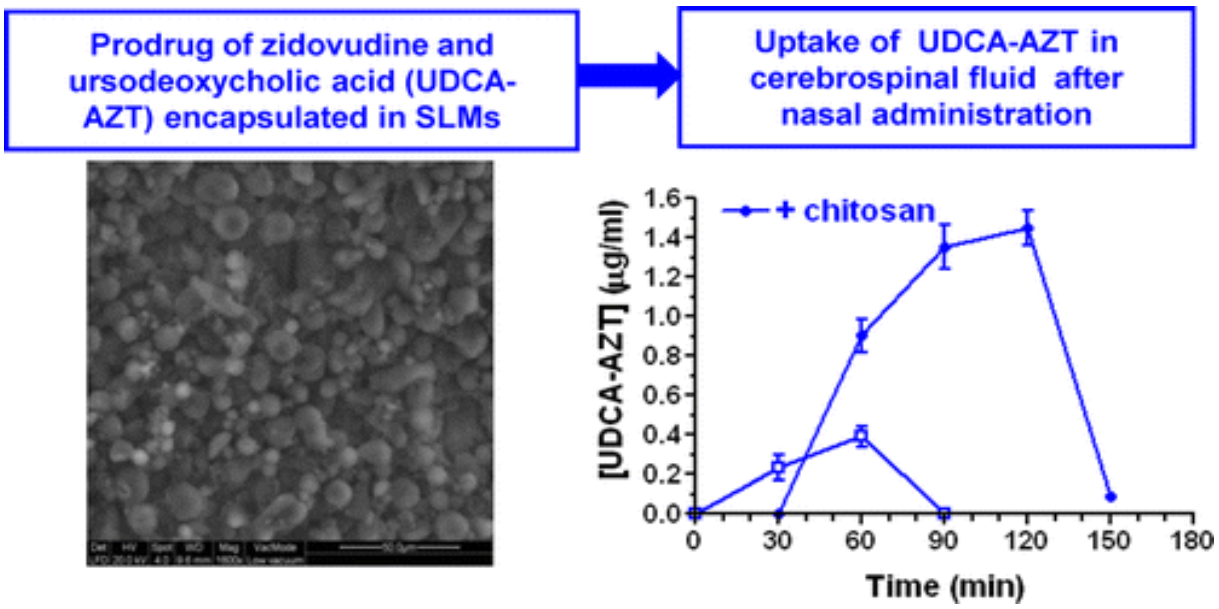


Figure 2.6. Uptake of UDCA-AZT-loaded stearic acid SLMs detected in the CSF after nasal administration in the presence of chitosan (Figure adapted with permission from Dalpiaz et al. 2014)

2.8.3 Tenofovir disoproxil fumarate (TDF) with Compritol 888 ATO & oleic acid in NLCs

Given that delivery of ARV drugs in the CNS is restricted by blood–brain and blood–CSF interfaces, a lipid prodrug formulation comprising TDF, Compritol 888 ATO, and oleic acid in NLCs has been synthesized. Both Compritol 888 ATO and oleic acid have been reported to be non-toxic and non-irritant materials which form acetyl-coA through degradation by oxidation *in vivo* (Sarma and Das 2019). Incorporating these materials into NLCs results in a stable, biocompatible, and biodegradable formulation. Hence, they have been widely used in NLCs drug delivery systems. TDF-loaded NLCs were designed using the modified emulsion solvent displacement method and optimized using response surface central composite design (CCD). Thereafter, it was evaluated for morphology, physicochemical, and *in-vitro* drug release characteristics. This formulation showed potential of brain delivery through non-invasive intranasal route (Sarma and Das 2019).

2.8.4 HDP-P-GCV (1-O-hexadecylpropanediol-3-phospho-ganciclovir) in liposomes

Although GCV has been shown to be effective against CMV retinitis in AIDS patients, it does not get rid of the virus completely. Therefore, its lipid prodrug (HDP-P-GCV) incorporated into liposomes has been produced (Cheng et al. 2000). This was tested both *in vitro* and *in vivo*. The findings showed that HDP-P-GCV resulted in a one-week complete protection of the retina at 0.2 mM intravitreal concentration compared to free GCV or liposomes. In addition to this, no ocular toxicity was observed except for cataracts in some eyes at higher doses *in vivo*. This suggests that self-assembling liposome systems may be appropriate for various compounds intended for intraocular diseases (Cheng et al. 2000).

2.8.5 AZT myristate (AZT-M) in liposomes

Due to low entrapment efficiency and fast leakage of AZT from the liposomal carrier, AZT-M has been synthesized and tested in rats (Jin et al. 2005). In comparison with free AZT, AZT-M liposomes resulted in higher concentrations of AZT in the brain and reticuloendothelial system (RES). This was expected in the RES, since liposomes are readily taken up by RES cells. From these results, it can be deduced that AZT-M liposomes hold great promise for HIV therapy owing to its high lipophilicity (Jin et al. 2005). This prodrug tactic can significantly reduce renal clearance rate and increase time of retention in the plasma compared with AZT solution. This is shown in Figure 2.7 wherein plasma levels of AZT-M liposomes were higher than those of AZT solution at each time point from 1 to 360 min. Therefore, an increase from 5.1 ± 0.7 μmol min ml^{-1} to 8.2 ± 1.7 μmol min ml^{-1} was observed in the $AUC_{0-\infty}$ of AZT-M liposome whereas total body clearance was decreased from 16.6 ± 2.3 ml/min to 10.8 ± 2.2 ml/min (Jin et al. 2005).

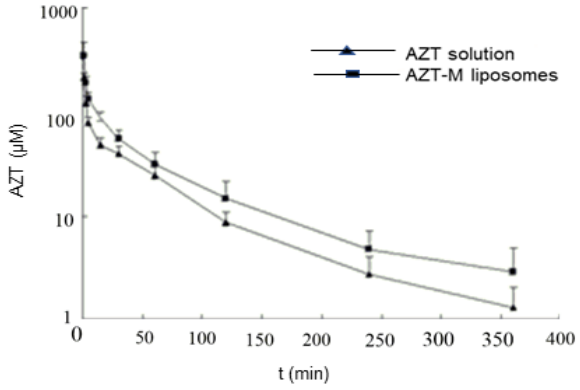


Figure 2.7. Plasma concentration profiles of AZT and AZT-M incorporated in liposomes (Figure adapted with permission from Jin et al. 2005).

Table 2.3. ARV drugs and nanoparticle synthesized-conjugate delivery systems

ARV drugs	Carrier systems	Advantages	Disadvantages	References
Saquinavir	Polyhexylcyanoacrylate nanoparticles	Improves efficacy and leads to dose-dependent reduction of HIV type 1 antigen production.	Inactive in chronically HIV-infected macrophages.	(Bender et al. 1996)
Efavirenz	Polymeric micelles	Increases oral bioavailability *in vivo.*	Release profiles not sustained.	(Chiappetta et al. 2013)
Saquinavir	Nanostructure lipid carriers	Increases saquinavir permeability in Caco-2 monolayers by up to 9-fold.	Mucus layer hinders NLCs access to the underlying epithelium.	(Beloqui et al. 2014)
Tenofovir	Liposomes	Minimal drug leakage & triggered release at the targeted site.	Significant differences in terms of drug release rate.	(Xu et al. 2012)
Enfuvirtide	Iron oxide nanoparticles	Increases translocation of enfuvirtide across blood brain barrier (BBB) *in vitro* and *in vivo.*	Dissociation of enfuvirtide from iron oxide nanoparticles in the endothelial cells.	(Fiandra et al. 2015)
Zidovudine	Silver nanofilm and multiwalled carbon nanotubes (MWCNTs)	Improves water solubility of MWCNTs and provide active surfaces for deposition of metals onto MWCNT surfaces.	Increases impurity of MWCNTs and cost of modification process.	(Rafati and Afraz 2014)
Saquinavir	Nano-emulsions	Increases drug permeation rate *ex-vivo* and *in vivo.*	Lower transport of drug across the BBB by passive diffusion.	(Mahajan et al. 2014)

2.9 Concluding remarks

LDCs show great potential for enhancing oral bioavailability, permeation, and absorption of poorly water-soluble ARV drugs since after enzymatic metabolism, the released drug can reach the site of action in maximum concentrations compared to free drug. In addition to this, the human body naturally digest lipid which suggests less toxicity data required to ensure safety issues. Given that lipidic prodrugs such as TDF and TAF have already been approved by the U.S. and EU FDA for current HIV therapy, the LDC approach seems to hold great promise for future enhanced antiretroviral efficacy. However, the remaining challenges of LDCs include their large-scale production, shelf-life stability, and sterilization of the parenteral product.

2.10 References

Adhikari P, Pal P, Das KA, Ray S, Bhattacharjee A, Mazumder B. 2017. Nano lipid-drug conjugate: an integrated review. Int J Pharm. 529(1–2):629–641.

Agarwal HK, Chhikara BS, Bhavaraju S, Mandal D, Doncel GF, Parang K. 2013. Emtricitabine prodrugs with improved anti-HIV activity and cellular uptake. Mol Pharm. 10(2):467–476.

Agarwal HK, Chhikara BS, Hanley MJ, Ye G, Doncel GF, Parang K. 2012. Synthesis and biological evaluation of fatty acyl ester derivatives of (-)-20 ,30 -dideoxy-30 -thiacytidine. J Med Chem. 55(10):4861–4871.

Amly W, Karaman R. 2016. Overview on the recent drugs delivery approaches. J Pharmacol Drug Design. 2(1):1–29.

Arouri A, Mouritsen OG. 2011. Anticancer double lipid prodrugs: liposomal preparation and characterization. J Liposome Res. 21(4):296–305.

Bakhtiary Z, Barar J, Aghanejad A, Saei AA, Nemati E, Ezzati Nazhad Dolatabadi J, Omidi Y. 2017. Microparticles containing erlotinib-loaded solid lipid nanoparticles for treatment of non-small cell lung cancer. Drug Dev Ind Pharm. 43(8):1244–1253.

Banerjee S, Kundu A. 2018. Lipid-drug conjugates: a potential nanocarrier system for oral drug delivery applications. Daru. (26):65–75.

Beloqui A, Solınıs MA, des Rieux A, Preat V, Rodrıguez-Gascon A. 2014. Dextran-protamine coated nanostructured lipid carriers as mucus-penetrating nanoparticles for lipophilic drugs. Int J Pharm. 468(1–2):105–111.

Bender AR, Von Briesen H, Kreuter J, Duncan IB, Rubsamen- Waigmann H. 1996. Efficiency of nanoparticles as a carrier system for antiviral agents in human immunodeficiency virus-infected human monocytes/macrophages in vitro. Antimicrob Agents Chemother. 40(6):1467–1471.

Chattopadhyay N, Zastre J, Wong H-L, Wu XY, Bendayan R. 2008. Solid lipid nanoparticles enhance the delivery of the HIV protease inhibitor, atazanavir, by a human brain endothelial cell line. Pharm Res. 25(10):2262–2271.

Cheng L, Hostetler KY, Chaidhawangul S, Gardner MF, Beadle JR, Keefe KS, Bergeron-Lynn G, Severson GM, Soules KA, Mueller AJ, et al. 2000. Intravitreal toxicology and duration of efficacy of a novel antiviral lipid prodrug of ganciclovir in liposome formulation. Invest Ophthalmol Vis Sci. 41(6):1523–1532.

Chiappetta DA, Hocht C, Opezzo JAW, Sosnik A. 2013. Intranasal administration of antiretroviral-loaded micelles for anatomical targeting to the brain in HIV. Nanomedicine. 8(2):223–237.

Cholkar K, Trinh HM, Vadlapudi AD, Mitra AK. 2014. Synthesis and characterization of ganciclovir long chain lipid prodrugs. Adv Ophthalmol Vis Syst. 1(2):1–7.

Chrastina A, Baron VT, Abedinpour P, Rondeau G, Welsh J, Borgstrom P. 2018. Plumbagin-loaded nanoemulsion drug delivery formulation and evaluation of antiproliferative effect on prostate cancer cells. Biomed Res Int. 2018:1–7.

Clercq ED. 2018. The acyclic nucleoside phosphonates (ANPs): Antonın Holy's legacy (2012–2018). J Infect. 1(2):11–13.

Corsi F, Sorrentino L, Mazzucchelli S, Truffi M. 2016. Antiretroviral therapy through barriers: a prominent role for nanotechnology in HIV-1 eradication from sanctuaries. J Pharm Pharmacol. 4: 328–339.

Dalpiaz A, Contado C, Mari L, Perrone D, Pavan B, Paganetto G, Hanuskova M, Vighi E, Leo E. 2014. Development and characterization of PLGA nanoparticles as delivery systems of a prodrug of zidovudine obtained by its conjugation with ursodeoxycholic acid. Drug Deliv. 21(3):221–232.

Date T, Paul K, Singh N, Jain S. 2019. Drug–lipid conjugates for enhanced oral drug delivery. AAPS J. 41(20):1–11.

Dolatabadi JEN, Azami A, Mohammadi A, Hamishehkar H, PanahiAzar V, Saadat YR, Saei AA. 2018. Formulation, characterization, and cytotoxicity evaluation of ketotifen-loaded nanostructured lipid carriers. J Drug Deliv Sci Technol. 46:268–273.

Dolatabadi JEN, Hamishehkar H, Valizadeh H. 2014. Development of dry powder inhaler formulation loaded with alendronate solid lipid nanoparticles: solid-state characterization and aerosol dispersion performance. Drug Dev Ind Pharm. 41(9):1431–1437.

Dolatabadi JEN, Omidi Y. 2016. Solid lipid-based nanocarriers as efficient targeted drug and gene delivery systems. Trend Anal Chem. 77:100–108.

Edagwa B, Zhou T, McMillan J, Liu X-M, Gendelman H. 2014. Development of HIV reservoir targeted long acting nanoformulated antiretroviral therapies. Curr Med Chem. 21(36): 4186–4198.

Fiandra L, Colombo M, Mazzuchelli S, Truffi M, Santini B, Allevi R, Nebuloni M, Capetti A, Rizzardini G, Prosperi D, et al. 2015. Nano formulation of antiretroviral drugs enhances their penetration across the blood brain barrier in mice. Nanomedicine. 11: 1387–1397.

Florescu DF, Keck MA. 2014. Development of CMX001 (Brincidofovir) for the treatment of serious diseases or conditions caused by dsDNA viruses. Expert Rev Anti-Infect Ther. 12(10):1171–1178.

Girard P-M, Pegram PS, Diquet B, Anderson R, Raffi F, Tubiana R, Sereni D, Boerner D. 2000. Phase II placebo-controlled trial of fozivudine tidoxil for HIV infection: pharmacokinetics, tolerability, and efficacy. J Acquir Immune Defic Syndr. 23(3):227–235.

Han S, Quach T, Hu L, Wahab A, Charman WN, Stella VJ, Trevaskis NL, Simpson JS, Porter CJH. 2014. Targeted delivery of a model immunomodulator to the lymphatic system: comparison of alkyl ester versus triglyceride mimetic lipid prodrug strategies. J Control Release. 177:1–10.

Hoang T, Date AA, Ortiza JO, Young TW, Bensouda S, Xiao P, Marzinke M, Rohan L, Fuchs EJ, Hendrix C, et al. 2018. Development of rectal enema as microbicide (DREAM): preclinical progressive selection of a tenofovir prodrug enema. Eur J Pharm Biopharm.138:23–29.

Hobson JJ, Edwards S, Slater RA, Martin P, Owen A, Rannard SP. 2018. Branched copolymer-stabilised nanoemulsions as new candidate oral drug delivery systems. RSC Adv. 8(23): 12984–12991.

Hussain A, Usman M, Siddique M, Singh SK, Samad A, Beg S, Wais M. 2015. Lipid-drug conjugates for oral bioavailability enhancement. Nanomedicine. 5(2):87–95.

Irby D, Du C, Li F. 2017. Lipid–drug conjugate for enhancing drug delivery. Mol Pharm. 14(5):1325–1338.

Jana S, Mandlekar S, Marathe P. 2010. Prodrug design to improve pharmacokinetic and drug delivery properties: challenges to the discovery scientists. Curr Med Chem. 17(32):3874–3908.

Jiao YY, Wang XQ, Lu WL, Yang ZJ, Zhang Q. 2013. A novel approach to improve the pharmacokinetic properties of 8- chloro-adenosine by the dual combination of lipophilic derivatisation and liposome formulation. Eur J Pharm Sci. 48(1–2): 249–258.

Jin SX, Bi DZ, Wang J, Wang YZ, Hu HG, Deng YH. 2005. Pharmacokinetics and tissue distribution of zidovudine in rats following intravenous administration of zidovudine myristate loaded liposomes. Pharmazie. 60(11):840–843.

Kinman L, Brodie SJ, Tsai CC, Bui T, Larsen K, Schmidt A, Anderson D, Morton WR, Hu S-L, Ho RJY, et al. 2003. Lipid-drug association enhanced hiv-1 protease inhibitor indinavir localization in lymphoid tissues and viral load reduction: a proof-of-concept study in HIV-2287-infected macaques. J Acquir Immune Defic Syndr. 34(4):387–397.

Krovi SA, Gallovic MD, Keller AM, Bhat M, Tiet P, Chen N, Collier MA, Gurysh EG, Pino EN, Johnson MM, et al. 2018. Injectable long-acting human immunodeficiency virus antiretroviral prodrugs with improved pharmacokinetic profiles. Int J Pharm. 552(1–2):371–377.

Krugner-Higby L, Goff D, Edwards T, Iyer N, Neufeld JAY, Kute T, Morris-Natschke S, Ishaq K, Piantadosi C, Kucera LS, et al. 1995. Membrane-interactive phospholipids inhibit HIV type 1-induced cell fusion and surface gpl60/gpl20 binding to monoclonal antibody. AIDS Res Hum Retrovir. 11(6):705–712.

Kucera LS, Morris-Natschke SL, Ishaq KS, Hes J, Iyer N, Furman PA, Fleming RA. 2004. Synthesis and evaluation of a novel synthetic phosphocholine lipid-AZT conjugate that double-targets wild type and drug-resistant variants of HIV. Nucleosides Nucleotides Nucleic Acids. 23(1–2):385–399.

Lanier ER, Ptak RG, Lampert BM, Keilholz L, Hartman T, Buckheit RW, Mankowski MK, Osterling MC, Almond MR, Painter GR, et al. 2010. Development of hexadecyloxypropyl tenofovir (CMX157) for treatment of infection caused by wild-type and nucleoside/nucleotide-resistant HIV. Antimicrob Agents Chemother. 54(7):2901–2909.

Lee J. H, Yeo Y. 2015. Controlled drug release from pharmaceutical nanocarriers. Chem Eng Sci. 125:75–84.

Li F, Snow-Davis C, Du C, Bondarev ML, Saulsbury MD, Heyliger SO. 2016. Preparation and characterization of lipophilic doxorubicin pro-drug micelles. J Vis Exp. 114:1–8.

Li J, Wang X, Zhang T, Wang C, Huang Z, Luo X, Deng Y. 2014. A review on phospholipids and their main applications in drug delivery systems. Asian J Pharm Sci. 10:81–98.

Lundberg BB, Risovic V, Ramaswamy M, Wasan KM. 2003. A lipophilic paclitaxel derivative incorporated in a lipid emulsion for parenteral administration. J Control Release. 86(1):93–100.

Mahajan HS, Mahajan MS, Nerkar PP, Agrawal A. 2014. Nanoemulsion-based intranasal drug delivery system of saquinavir mesylate for brain targeting. Drug Deliv. 21(2):148–154.

Manyarara TE, Khoza S, Dube A, Maponga CC. 2018. Formulation and characterization of a paediatric nanoemulsion dosage form with modified oral drug delivery system for improved dissolution rate of nevirapine. MRS Adv. 3:2203–2219.

Markovic M, Ben-Shabat S, Keinan S, Aponick A, Zimmermann EM, Dahan A. 2019. Lipidic prodrug approach for improved oral drug delivery and therapy. Med Res Rev. 39(2):579–607.

Nayak D, Boxi A, Ashe S, Thathapudi NC, Nayak B. 2017. Stavudine loaded gelatin liposomes for HIV therapy: preparation, characterization, and in vitro cytotoxic evaluation. Mater Sci Eng C. 73: 406–416.

Nemati E, Mokhtarzadeh A, Panahi-Azar V. 2019. Ethambutol-loaded solid lipid nanoparticles as dry powder inhalable formulation for tuberculosis therapy. AAPS J. 20(120):1–9.

Neupane YR, Sabir MD, Ahmad N, Ali M, Kohli K. 2013. Lipid drug conjugate nanoparticle as a novel lipid nanocarrier for the oral delivery of decitabine: ex vivo gut permeation studies. Nanotechnology. 24(41):415102–415113.

Painter W, Robertson A, Trost LC, Godkin S, Lampert B, Painter G. 2012. First pharmacokinetic and safety study in humans of the novel lipid antiviral conjugate CMX001, a broad-spectrum oral drug active against double-stranded DNA viruses. Antimicrob Agents Chemother. 56(5):2726–2734.

Periyasamy PC, Leijten JCH, Dijkstra PJ, Karperien M, Post JN. 2012. Nanomaterials for the local and targeted delivery of osteoarthritis drugs. J Nanomater. 2012:1–13.

Poudel AJ, He F, Huang L, Xiao L, Yang G. 2018. Supramolecular hydrogels based on poly (ethylene glycol)-poly (lactic acid) block copolymer micelles and a-cyclodextrin for potential injectable drug delivery system. Carbohydr Polym. 194:69–79.

Prajapati VK, Awasthi K, Gautam S, Yadav TP, Rai M, Srivastava ON, Sundar S. 2011. Targeted killing of Leishmania donovani in vivo and in vitro with amphotericin b attached to functionalized carbon nanotubes. J Antimicrob Chemother. 66(4):874–879.

Rafati AA, Afraz A. 2014. Amperometric sensing of anti-HIV drug zidovudine on Ag nanofilm-multiwalled carbon nanotubes modified glassy carbon electrode. Mater Sci Eng C. 39:105–112.

Rajabi M, Mousa AS. 2016. Lipid nanoparticles and their application in nanomedicine. Curr Pharm Biotechnol. 17(8):662–672. Ramana LN, Sethuraman S, Ranga U, Krishnan UM. 2010. Development of a liposomal nanodelivery system for nevirapine. J Biomed Sci. 17(1):57–59.

Ramana LN, Sharma S, Sethuraman S, Ranga U, Krishnan UM. 2015. Stealth anti-CD4 conjugated immunoliposomes with dual antiretroviral drugs- Modern trojan horses to combat HIV. Eur J Pharm Biopharm. 89:300–311.

Rautio J, Karkkainen J, Sloan KB. 2017. Prodrugs – recent approvals and a glimpse of the pipeline. Eur J Pharm Sci. 109: 146–161.

Ray AS, Fordyce MW, Hitchcock MJM. 2016. Tenofovir alafenamide: a novel prodrug of tenofovir for the treatment of human immunodeficiency virus. Antiviral Res. 125:63–70.

Reddy S, Rudhrabatla P, Sudhakar B. 2018. Ritonavir loaded surface modified stealth solid lipid nanoparticles: full factorial design and pharmacokinetic studies. Int J Pharm Sci Res. 10(1): 77–89.

Sarma A, Das MK. 2019. Formulation by design (FbD) approach to develop tenofovir disoproxil fumarate loaded nanostructured lipid carriers (NLCs) for the aptness of nose to brain delivery. J Drug Deliv Ther. 9(2):148–159.

Shao W, Paul A, Zhao B, Lee C, Rodes L, Prakash S. 2013. Carbon nanotube lipid drug approach for targeted delivery of a chemotherapy drug in a human breast cancer xenograft animal model. Biomaterials. 34(38):10109–10119.

Sharma P, Dube B, Sawant K. 2012. Synthesis of cytarabine lipid drug conjugate for treatment of meningeal leukemia: development, characterization and in vitro cell line studies. J Biomed Nanotechnol. 8(6):928–937.

Singh D, McMillan J, Hilaire J, Gautam N, Palandri D, Alnouti Y, Gendelman HE, Edagwa B. 2016. Development and characterization of a long acting nanoformulated abacavir prodrug. Nanomedicine. 11(15):1913–1927.

Singh G, Pai RS. 2014. Pharmacokinetics and in vivo biodistribution of optimized PLGA nanoparticulate drug delivery system for controlled release of emtricitabine. Drug Deliv. 21(8):627–635.

Sinikrot H, Smerat T, Najjar A, Karaman R. 2017. Advanced prodrug strategies in nucleoside and non-nucleoside antiviral agents: a review of the recent five years. Molecules. 22:1–18.

Spinks CB, Zidan AS, Khan AM, Habib MJ, Faustino PJ. 2017. Pharmaceutical characterization of novel tenofovir liposomal formulations for enhanced oral drug delivery: in vitro pharmaceutics and Caco-2 permeability investigations. Clin Pharmacol. 9:29–38.

Takasawa K, Terasaki T, Suzuki H, Sugiyama Y. 1997. In vivo evidence for carrier-mediated efflux transport of 39-azido-39-deoxythymidine and 29,39-dideoxyinosine across the blood-brain barrier via a probenecid-sensitive transport system. J Pharmacol Exp Ther. 281(1):369–375.

Tsotinis A, Calogeropoulou T, Koufaki M, Souli C, Balzarini J, De Clercq E, Makriyannis A. 1996. Synthesis and antiretroviral evaluation of new alkoxy and aryloxy phosphate derivatives of 3'-azido-3'-deoxythymidine. J Med Chem. 39(17):3418–3422.

Wang Y, Fan W, Dai X, Katragadda U, Mckinley D, Teng Q, Tan C. 2014. Enhanced tumor delivery of gemcitabine via PEG-DSPE/TPGS mixed micelles. Mol Pharm. 11(4):1140–1150.

Xu X, Khan MA, Burgess DJ. 2012. A two-stage reverse dialysis in vitro dissolution testing method for passive targeted liposomes. Int J Pharm. 426(1–2):211–218.

Ye F, Guo H, Zhang H, He X. 2010. Polymeric micelle-templated synthesis of hydroxyapatite hollow nanoparticles for a drug delivery system. Acta Biomater. 6(6):2212–2218.

Zaro JL. 2015. Lipid-based drug carriers for prodrugs to enhance drug delivery. AAPS J. 17(1):83–92.

Zhang Z, Yang X, Zhang Y, Zeng B, Wang S, Zhu T, Roden RB, Chen Y, Yang R. 2006. Delivery of telomerase reverse transcriptase small interfering RNA in complex with positively charged single-walled carbon nanotubes suppresses tumor growth. Clin Cancer Res. 12(16):4933–4939.

CHAPTER 3

Co-emulsified Alginate-Eudragit Nanoparticles: Potential Carriers for Localized and Time-defined Release of Tenofovir in the Female Genital Tract

AAPS PharmSciTech (2024) 25:15
https://doi.org/10.1208/s12249-023-02723-4

RESEARCH ARTICLE



Co-emulsified Alginate-Eudragit Nanoparticles: Potential Carriers for Localized and Time-defined Release of Tenofovir in the Female Genital Tract

Funanani Takalani[1] · Pradeep Kumar[1] · Pierre P. D. Kondiah[1] · Yahya E. Choonara[1]

Received: 23 September 2023 / Accepted: 5 December 2023
© The Author(s) 2024

Abstract
This research aimed to explore the possibilities of Eudragit S100 (ES100) and sodium alginate as carriers for tenofovir disoproxil fumarate (TDF) in the female genital tract. Alginate and alginate-ES100 nanoparticles were prepared using the ionic gelation and emulsion/gelation complexation method, respectively. The nanocarriers were tested using morphological, physicochemical, *in vitro* drug release, and cytotoxicity analyses. In SEM and TEM images, the presence of spherical and uniformly distributed nanoparticles was revealed. The FTIR spectrum showed that alginate and calcium chloride interacted due to ionic bonds linking divalent calcium ions and the -COO- of alginate groups. Alginate and ES100 interacted via the ester C=O amide stretching. The results obtained from XRD and DSC, on the other hand, revealed a favorable interaction between sodium alginate and ES100 polymers, as evidenced by the crystallization peaks observed. Under experimental design analysis and optimization, overall size distribution profiles ranged from 134.9 to 228.0 nm, while zeta potential results showed stable nanoparticles (−17.8 to −38.4 MV). The optimal formulation exhibited a maximum cumulative *in vitro* release of 72% (pH 4.2) up to 96 h. The cytotoxicity tests revealed the safety of TDF-loaded nanoparticles on vaginal epithelial cells at concentrations of 0.025 mg/mL, 0.5 mg/mL, and 1 mg/mL for 72 h. These results indicated that alginate-ES100 nanoparticles have the potential to preserve and sustain the release of the TDF drug in the FGT. The future goal is to develop a low-dose non-toxic microbicide that can be administered long term in the vagina to cater to both pregnant and non-pregnant HIV patients.

Keywords female genital tract · human immunodeficiency virus 1 · nanoparticles · sodium alginate · tenofovir disoproxil fumarate

Introduction

The female genital tract (FGT) possesses numerous characteristics in the mucosal immune system that render it suitable for the systemic dissemination of the human immunodeficiency virus (HIV-1) [1]. Nonetheless, nanotechnology for HIV-1 therapy has been cited as a technique capable of overcoming obstacles against HIV, thereby offering hope for HIV-1 care [2, 3]. Hence, nanomedicine-based therapies have been developed to facilitate the treatment of HIV-1 [4]. The primary objective is to formulate nanoparticles that can serve as carriers for delivering medications to precisely designated sites within the human body. Examples of these nanoparticles include polymeric nanoparticles, micelles, lipid nanoparticles, liposomes, and emulsions, which are further delineated in greater detail elsewhere [5].

Nanoparticles offer significant assurance in resolving issues related to various biological barriers, as they protect drugs from degradation through their controlled and sustained delivery [6]. Nanoparticles have also been used to improve the oral absorption of drugs that are accompanied by limited permeation, low solubility, and chemical instability [7]. One of these drugs is the Tenofovir Disoproxil Fumarate (TDF) HIV drug. The TDF is categorized within a group of antiretroviral medications known as nucleotide reverse transcriptase inhibitors (NRTIs). It is a preferred

✉ Yahya E. Choonara
yahya.choonara@wits.ac.za

[1] Wits Advanced Drug Delivery Platform Research Unit, Department of Pharmacy and Pharmacology, School of Therapeutic Sciences, Faculty of Health Sciences, University of the Witwatersrand, Johannesburg, 7 York Road, Parktown 2193, South Africa

Published online: 10 January 2024

3.1 Introduction

The female genital tract (FGT) possesses numerous characteristics in the mucosal immune system that render it suitable for the systemic dissemination of the human immunodeficiency virus (HIV-1) (Reis Machado et al., 2014). Nonetheless, nanotechnology for HIV-1 therapy has been cited as a technique capable of overcoming obstacles against HIV, thereby offering hope for HIV-1 care (Das & Chakraborty, 2015; Corsi et al., 2016). Hence, nanomedicine-based therapies have been developed to facilitate the treatment of HIV-1 (Irvin-Choy et al., 2020). The primary objective is to formulate nanoparticles that can serve as carriers for delivering medications to precisely designated sites within the human body.

Nanoparticles offer significant assurance in resolving issues related to various biological barriers, as they protect drugs from degradation through their controlled and sustained delivery (Beloqui et al., 2013). The use of nanoparticles has also been employed to enhance the oral absorption of drugs that exhibit limited penetration, low solubility, and chemical instability (Shailender et al., 2017). One of these drugs is the Tenofovir Disoproxil Fumarate (TDF) HIV drug. The TDF is categorized within a group of antiretroviral medications known as nucleotide reverse transcriptase inhibitors (NRTIs). It is a preferred first-line regimen for both men and women (Olojede et al., 2022). Several studies have incorporated TDF into nanoparticles for antiviral protection (Zhang et al., 2011; Shailender et al., 2017; Cautela et al., 2019; Sarma & Das, 2019).

However, although this drug effectively prevents mother-to-child transmission and manages pre-exposure prophylaxis (PrEP) and hepatitis B, there is a rising concern regarding its long-term effects (Olojede et al., 2022). On the contrary, it has been reported that Eudragit S100 (ES100) may prolong the release of drugs in various parts of the body. However, only a few studies have used this polymer in the FGT. Eudragits have been shown to regulate drug release due to their dissolution and osmotic release patterns (Sukhnir Singh, Neelam, Sandeep Arora, n.d.). Furthermore, the burst effect, which is associated with accelerated drug release and therapeutic effects, is diminished due to the insoluble nature of ES100 under acidic pH conditions (Anwer et al., 2017; Saraf et al., 2019).

Given this knowledge, we were intrigued by the investigation of TDF-loaded alginate-ES100 nanoparticles for use in the FGT. ES100 is a non-biodegradable polyanionic copolymer of methacrylic acid and methyl methacrylate (Thakral et al., 2013; Ansari et al., 2017; Cazorla-Luna et al., 2020). Eudragit polymers are generally recommended for developing novel drug delivery systems and fabricating sustained-release formulations (Sonje & Chandra, 2013; Ansari et al., 2017; Sukhnir Singh, Neelam, Sandeep Arora, n.d.). Furthermore, ES100 has

been demonstrated to possess a high degree of adhesion, moderate swelling, and superior mechanical properties (Cazorla-Luna et al., 2020). In contrast to ES100, sodium alginate is a biodegradable natural polymer that is readily accessible and renowned for its low-cost production (Joshy et al., 2017; Spadari et al., 2019; Choukaife et al., 2020). This hydrogel-based polymer is suited for the delivery of hydrophilic drugs, such as TDF, owing to its capacity to absorb substantial quantities of water while maintaining its structure (Choukaife et al., 2020). Lastly, its mucoadhesive and immunogenic properties make it an outstanding drug-delivery polysaccharide.

In this chapter, we aimed to develop co-emulsified alginate-ES100 nanoparticles and assess their potential as carriers for the TDF antiretroviral drug in the FGT. The utilization of alginate nanoparticles turned out to be the optimal choice, as it has been demonstrated to enhance the bioavailability of drugs (Choukaife et al., 2020). Together with ES100, they are both non-toxic and recommended for controlled drug delivery, as mentioned before. Various techniques including SEM, TEM, FTIR, XRD, and DSC were employed, followed by the execution of a cytotoxicity MTT assay for further analysis.

3.2 Materials and methods

3.2.1 Materials

The ES100, sodium alginate (low molecular weight), calcium chloride, methanol, dimethyl sulfoxide (DMSO), MTT assay, and the TDF drug were purchased from Leap Chem (Easey Com BLDG 253-261, Hong Kong). Life Bioscience (Oakleigh, VIC, Australia) provided vaginal cells (VK2), penicillin/streptomycin, and fetal bovine serum (FBS). All the supplementary reagents or chemicals utilized were of superior quality.

3.2.2 Preparation of Alginate and Alginate-ES100 TDF-loaded Nanoparticles

3.2.2.1 Alginate Nanoparticles

The ionic gelation technique (Zimet et al., 2018) was employed to prepare several trial formulations (Shown in Table 3.1) to evaluate the formation of alginate nanoparticles. To summarize and utilize the most successful trial formulation (Figure 3.1 (F3)), 90 mg of sodium alginate and 60 mg of TDF were dissolved in 15 mL of water, resulting in a 0.6% alginate solution. On the contrary, a concentration of 25 mg of $CaCl_2$ was dissolved in 45 mL of water to form a 0.06% $CaCl_2$ solution. Subsequently, the alginate solution was introduced in droplets into the $CaCl_2$ solution under the influence of the magnetic stirrer at 1.5 RPM. After an hour of stirring, the particles were collected by centrifugation for 10 min at 12100 RPM. In the end, the suspension was frozen at −80 °C and lyophilized at −37 °C for a duration of 12 h.

Table 3.1: Outline of the trial formulations that were used to test for the formation of alginate nanoparticles

Formulations	Alginate (mg)	TDF (mg)	$CaCl_2$ (mg)
F1	130	60	25
F2	90	60	15
F3	90	60	25
F4	130	60	15

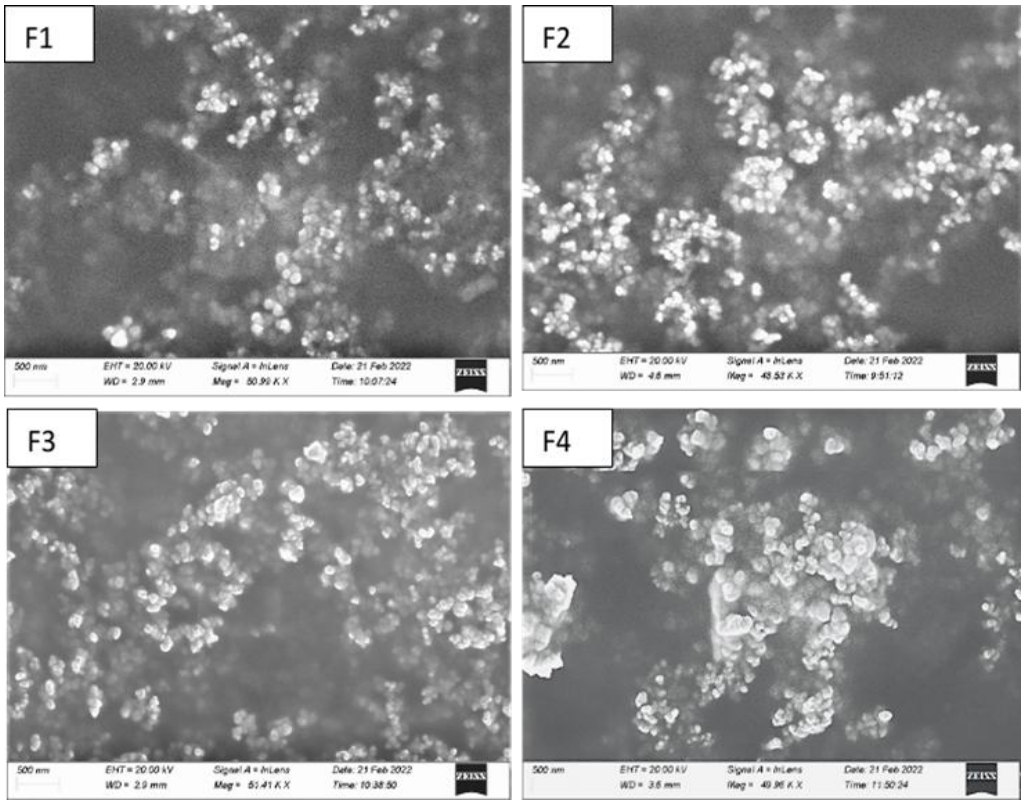


Figure 3.1. SEM images of the TDF drug loaded into alginate nanoparticles. Images taken at a scale of 500 nm

3.2.2.2 Alginate-ES100 Nanoparticles

As previously discussed, F3 (shown in Figure 3.1) was selected as the optimal alginate trial formulation, which resulted in the subsequent synthesis of alginate-ES100 nanoparticles. This was accomplished using the emulsion/gelation complexation method (Choukaife et al., 2020), which is the most widely used and recent manufacturing technique for alginate-based nanoparticle delivery systems (Choukaife et al., 2020). The preparation of the alginate-in-oil (w/o) emulsion is the first step in this technique, followed by the gelation of the alginate emulsion droplets with a covalent or ionic cross-linker. This method was most effective for mixing alginate and the ES100 polymer, which is partially soluble in water. Hence, we first dispersed it in methanol before combining it with alginate. Thus, different ratios (1:2, 1:1, 2:1, and 1:1.4) for Alginate: ES100 were employed, as presented in Table 3.2.

Using a 1:1 ratio as an example (F6), 90 mg of ES100 and 60 mg of TDF were mixed in 5-mL methanol under the magnetic stirrer to form a 2% ES100 solution. Afterward, 90 mg of alginate was thawed separately in 15 mL to create a 0.6% alginate solution. For 5 min, these two solutions were mixed under a magnetic stirrer, then further sonicated for another 5 min to create an emulsion. After this, the mixture was added dropwise to a 0.06% $CaCl_2$ solution, under the same magnetic stirrer at a stirring speed of 1.5 RPM. The composite was subjected to stirring for an hour under the fume hood to evaporate methanol, and nanoparticles were collected by centrifugation for 10 min at 12100 RPM. Finally, the suspension was frozen overnight and then lyophilized at −37 °C for 12 h. The same preparation steps were followed for TDF-free nanoparticles, except that the TDF drug was not added.

Table 3.2: Outline of the trial formulations for alginate-ES100 nanoparticles, prepared using F3 from table 3.1 as a standard for model formulation. All formulations were undertaken in triplicate

Formulations	Alginate:ES100 (mg)	TDF (mg)	$CaCl_2$ (mg)
F5	1:2	60	25
F6	1:1	60	25
F7	2:1	60	25
F8	1:1.4	60	25

3.3 Characterization of Nanoparticles

3.3.1 Morphological Analyses

The SEM (JEOL JSM, Tokyo) was used at an acceleration voltage of 15 keV to view the outward morphology of nanoparticles. Before visualization, the powder nanoparticles were placed on standard pin stubs and coated with gold palladium. Furthermore, TEM was employed to observe nanoparticles by utilizing high-energy electron beams. In this instance, a droplet of the suspension was fixed onto a carbon grid and subjected to analysis at a voltage of 120 keV using JEOL 1200 EX.

3.3.2 Nanoparticles Size, Zeta Potential, and Polydispersity Index (PDI)

The Malvern Zetasizer Nano ZS instrument, manufactured in Worcestershire, UK, was utilized. Here, 2 mL of the freshly prepared formulation was mixed with 3 mL of purified water for a total of 5 mL. The mixture was then sonicated for 2 min at a probe temperature of 20 °C with a 20% amplitude and pulsation (50 s of sonication with a 10-s pause). Afterward, the nanoparticles were analyzed for size, zeta potential, and PDI using the dynamic light scattering technique at an angle of 175°. Capillary cell cuvettes were employed, and intensity was recorded at 25 °C. Measurements were taken in three-fold increments.

3.3.3 Fourier Transform Infrared Spectroscopy (FTIR)

By observing vibrational frequency bands, we determined the structural variations of the nanoparticles formed. This was done to confirm the backbone structure and integrity of the main effective groups of the TDF drug, alginate, and ES100 polymers during nanoparticle formation. Samples were positioned on a diamond crystal and processed by a PerkinElmer Spectrum 2000 ATR-FTIR (PerkinElmer 100, Llantrisant, Wales, UK). The FTIR conditions were as indicated: 24 scans at a 4 cm^{-1} resolution and a wavelength number ranging from 4000 to 650 cm^{-1}.

3.3.4 X-ray Diffraction (XRD)

X-ray wave interference was observed to further analyze nanoparticles and characterize the stage categories involved. First, the spectra were recorded on a MiniFlex 600 benchtop diffractometer (Rigaku, Japan) using a copper anode (CuKα) at 40 kV radiation and 15 mA. Then, a scan of 2θ was conducted at a speed of ten degrees per minute, between 10 and 90 degrees. This was followed by diffraction analyses, which allowed for the observation of the nanoparticles' crystallinity degree.

3.3.5 Differential Scanning Calorimetry (DSC)

The thermodynamic compatibility between alginate, ES100, and the TDF drug was investigated using the DSC technique (Mettler Toledo, STARe System, Swchwerzenback, ZH, Switzerland). This was accomplished by evaluating their transition from glass to liquid and melting conditions. In this study, samples ranging from 3 to 10 mg were weighed, sealed in aluminum vessels, and subjected to warming at a temperature range of 10 to 350 °C. The melting rate was ten degrees per minute in a nitrogen gas atmosphere. Then, the DSC graphs were presented as the flow of heat *versus* temperature.

3.4 Determining the Entrapment Efficiency (EE%) and Drug Loading Capacity (DL%) of Nanoparticles

As shown below and reported by Schafroth and co-workers (2012), Eqs. (3.1) and (3.2) were used to calculate the EE% and DL% of TDF-loaded nanoparticles, respectively. Thus, the absorbance of the TDF was calculated using the ultraviolet-visible spectrophotometer (Specord 40 UV-vis Spectrophotometer, Analytic Jena AG, Jena, Germany) at 265 nm. The standard curve equation for the TDF drug was Y = 0.0192x (R^2 = 0.9999), as shown in Figure 3.2.

$$EE\% = \frac{drug\ within\ nanoparticle}{Initial\ amount\ of\ drug}\ X100 \qquad (3.1)$$

$$DL\% = \frac{amount\ of\ drug\ in\ nanoparticles}{amount\ of\ nanoparticle}\ X100 \qquad (3.2)$$

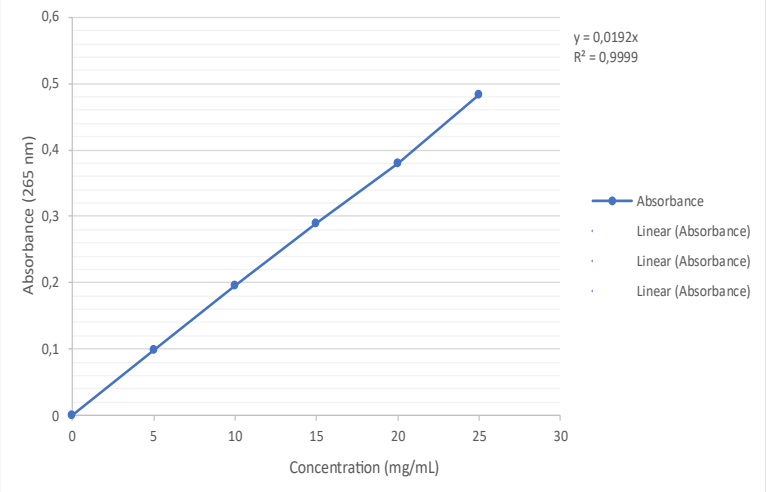


Figure 3.2. Standard calibration curve confirming quantification of the TDF drug at a wavelength of 265 nm

3.5 *In Vitro* Release of TDF-loaded Nanoparticles

The cumulative release profiles of TDF from TDF-loaded nanoparticles were determined by the dialysis bag diffusion method (Kianersi et al., 2021). In this instance, the simulated vaginal fluid (SVF, pH 4.2) was utilized as the release medium to preserve sink conditions for TDF. Briefly, 10 mg of TDF-loaded nanoparticles and 2 mL of SVF buffer were introduced into dialysis bags with a relative molecular mass cutoff of 12 kDa. These were submerged in 50-mL SVF buffer and placed in an orbital shaker, where they were stirred at 25 RPM, with the temperature set at 37 °C. Subsequently, at designated elapsed times (1 h, 3 h, 6 h, 9 h, 12 h, 24 h, 48 h, 72 h, and 96 h), 2 mL of the release buffer was withdrawn and promptly replaced with fresh release buffer. The amounts of TDF liberated from the samples were quantified at a wavelength of 265 using an ultraviolet-visible spectrophotometer, and the results were displayed as the cumulative release percentage of the drug over time. All procedures were undertaken in triplicate alongside a blank control formulation.

3.6 Development of the Experimental Design

To ensure the quality, safety, and efficacy of the formulations developed, the experiment design was generated. The response surface methodology (RSM) design was particularly applicable in this study as it requires few experimental runs (Aliemeke & Oladeinde, 2020; Karmoker et al., 2018). Hence, a fractional factorial design composing three factors, and three levels was generated using Minitab statistical software (MINITAB®, V15, Minitab, USA). The development of 15 formulations corresponding to 15 runs was conducted with a single centre point. Then, the upper and lower actual values for critical input factors were determined (shown in Table 3.3). In contrast, critical processing parameters such as temperature, volume, stirring speed, sizes of beakers, and sizes of stirrers were kept constant. The output critical responses, including drug release percentage (DR %), mean particle size (PS), zeta potential (ZP), and polydispersity index (PDI), were chosen for this design. Then, the results of these responses were incorporated into the quadratic polynomial equation as shown below:

$$\begin{aligned} Y = {} & [Alginate].[Eudragit].[CaCl2].[Alginate] * [Alginate].\ \ [Eudragit] \\ & * [Eudragit].[CaCl2] * [CaCl2].[Alginate] * [Eudragit].[Alginate] \\ & * [CaCl2].\ \ [Eudragit] \\ & * [CaCl2] \end{aligned} \tag{3.3}$$

Here, Y represents the measured responses, while Alginate, Eudragit, and $CaCl_2$ are input factors. The models were validated by applying an analysis of variance (ANOVA) test. A probability of 0.05 was considered to be the significant level with $P < 0.05$, and $P > 0.1$ was deemed non-significant due to a lack of fit. Furthermore, regression analysis and coefficient

of determination tests were conducted to evaluate the suitability of the models. Then, surface plots were employed to analyze the interactions among variables.

Table 3.3: Upper and lower actual values for input critical factors

Input variables	Lower values (mg)	Upper values (mg)
Alginate	90	130
ES100	90	180
$CaCl_2$	15	25

3.6.1 Optimization Using the Desirability Function

Based on the results obtained from the 15 formulations, the responses for PDI, mean particle size, and drug release % were further optimized following the desirability function approach (Reis et al., 2021). Therefore, three formulations were processed using the approximate values, as depicted in Table 3.4. These formulations were prepared following the same methods described in section 3.2.2. In addition to this, methods used to characterize or analyze responses for size/PDI, EE%/DL%, and DR% were also the same as those explained in section 3.3.2, 3.4 and 3.5, respectively. All experiments were undertaken in triplicate.

Table 3.4: Desirability and predicted values for the optimized formulations

Solution	Alginate (mg)	Eudragit (mg)	$CaCl_2$ (mg)	PDI fit	PS (nm) fit	DR% fit	Composite desirability
1	117.879	123.636	19.8485	0.143019	147.245	0.757158	0.932483
2	126.266	106.368	18.9104	0.142274	155.351	0.742039	0.884029
3	113.042	144.517	19.2536	0.157497	150.104	0.754622	0.879090

3.7 Cell Culture and Cytotoxicity Studies

The MTT assay was selected to analyze the toxic effects of TDF-loaded nanoparticles, drug-free nanoparticles, and TDF on vaginal epithelial cells (VK2). Therefore, cells were grown and maintained as described by Zhang and co-workers (Zhang et al., 2011). To summarize, VK2 cells were cultured in DMEM/F12 media, enriched with 1% penicillin-streptomycin and 10% FBS, in 25-cm^2 culture flasks until they reached 80–90% confluence. Then, the cells were slid into a 96-well plate with 1 × 104 cells per well. Afterward, the plates were left to equilibrate for 24 h at 37 °C to secure their attachment. Subsequently, the cells that were attached underwent treatment in pentaplicates (n = 5) with varying concentrations (0.025 mg/mL, 0.5 mg/mL, and

1 mg/mL) of TDF-loaded nanoparticles, drug-free nanoparticles, and TDF. An untreated medium was considered a positive control, whereas DMSO was considered a negative control. After the treatment, the well plates were left in the incubator for set time points, 24 h and 72 h. Then, 10 µL of MTT-media solution was poured into each well, and the plates were incubated for 4 h. Thereafter, 100 µL of media was taken out, and 100 µL of the solubilizing agent was introduced. This was followed by further overnight incubation of the plates at 37 °C to liquefy the formazan. Lastly, the multimodal microplate reader (Victor X3, manufactured by Perkin Elmer in Waltham, MA, USA) was employed to obtain the results at an absorbance of 570–690 nm.

3.8 Results and Discussion

3.8.1 Morphology of Alginate Nanoparticles as well as Alginate-ES100 Nanoparticles

SEM analysis demonstrated the existence of alginate nanoparticles, whereas both SEM and TEM results showed the existence of alginate-ES100 nanoparticles (Figure 3.3). The findings regarding alginate nanoparticles were in agreement with those reported by Thomas and co-workers in 2020 and 2021 (Thomas et al., 2020, 2021) and by Kumar and co-workers in 2014 and 2017 (Kumar et al., 2014, 2017), indicating the difficulties encountered in forming proper spherical nanoparticles by the alginate polymer. As a result, we introduced the ES100 polymer into the alginate system, and as we expected, the results of this confirmed the formation of nanoparticles that were more defined in shape and smooth on the surface, as shown in Figure 3.3. Similar outcomes have been reported for nanoparticle systems that have been incorporated with ES100, thereby confirming that ES100 is indeed capable of forming spherical nanoparticles. Some of these reports have been authored by Sharma et al. in 2011, Yoo et al. in 2011, Zhang et al. in 2011, , Anwer et al. in 2017, and Saraf et al. in 2019 (Sharma et al., 2011; Yoo et al., 2011; Zhang et al., 2011; Anwer et al., 2017; Saraf et al., 2019).

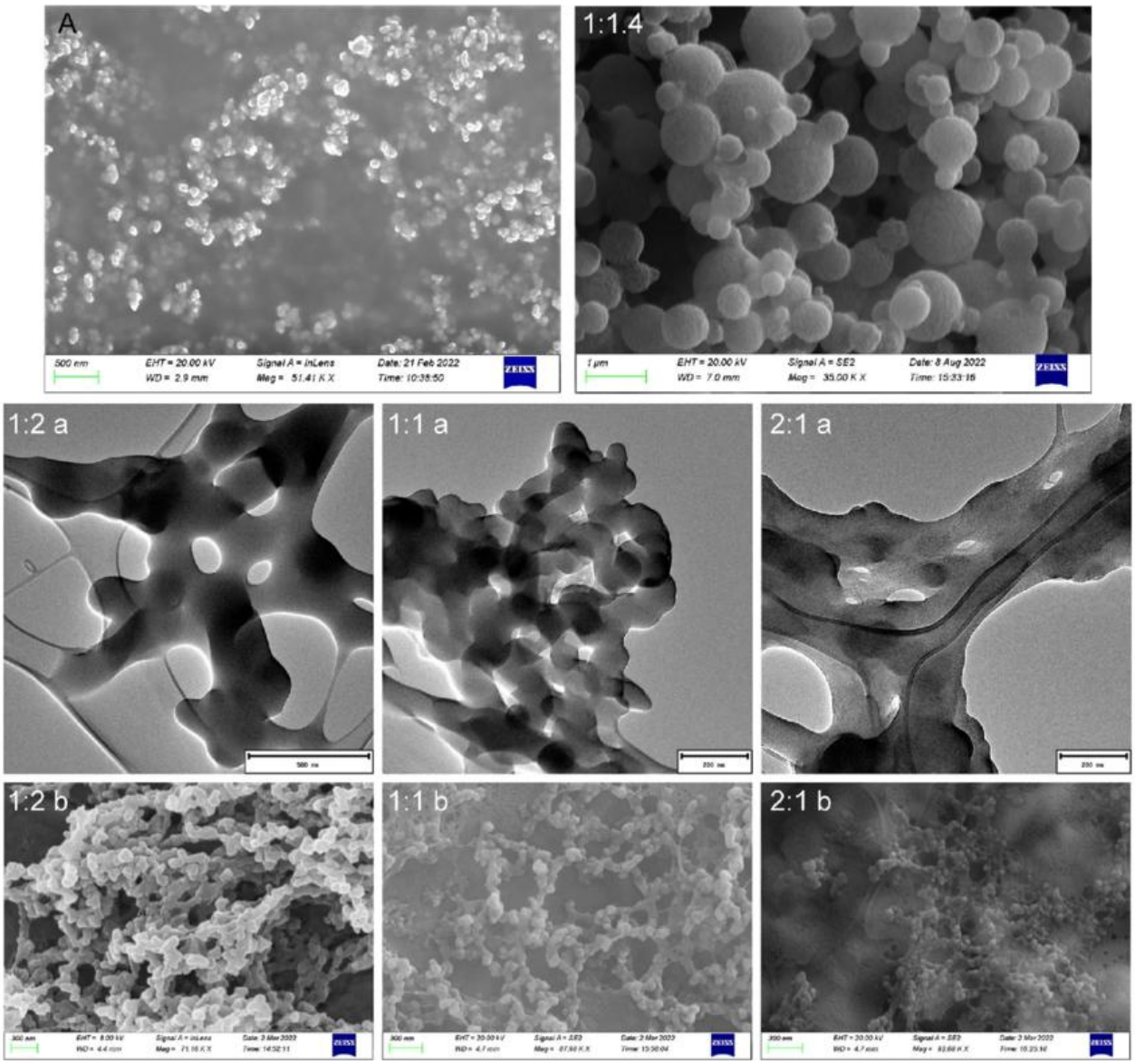


Figure 3.3. A SEM image of alginate nanoparticles taken at a scale of 500 nm. Ratios 1:1.4, 1:2b, 1:1b, and 2:1b: SEM images of the TDF drug loaded into alginate-ES100 nanoparticles. Images were taken at a scale of 1 µm and 500 nm. Ratios 1:2a, 1:1a, and 2:1a: TEM images of the TDF drug loaded into alginate-ES100 nanoparticles. Images were taken at a scale of 500 nm (1:2a) and 200 nm (1:1a and 2:1a)

3.8.2 Nanoparticle size, Polydispersity Index (PDI), and Zeta Potential

The mean particle size, the PDI, and the zeta potential are critical parameters for drug delivery systems (Spadari et al., 2019). Alginate-ES100 formulations had average sizes between 134.9 and 228.0 nm (Table 3.5), which could be explained by the encapsulation with a hydrophilic compound (Yoo et al., 2011). Moreover, the lower PDI values in the range of 0.129–0.363 indicate the physical stability of the systems and the uniform dispersion of particles (Saraf et al., 2019; Vlaia et al., 2021). The zeta potential results indicated that nanoparticles with high

negative charges were stable. System stability is indicated by zeta potentials around +/−30 MV (Saraf et al., 2019; Vlaia et al., 2021; Anicescu et al., 2022). As per the finding of Subudhi et al. (2015), elevated negative potentials result in an electric repulsion that prevents the degradation of particles. This contrasts with nanoparticles that possess a positive charge and bind to the cell membranes through electrostatic interaction with the negatively charged membrane. The mucosa's cellular uptake of negatively charged particles primarily pertains to the formation of loose assimilation of the particles, which encircle the surface of the plasma membrane. Secondly, it pertains to the production of nanoparticle clusters (Spadari et al., 2019).

In this study, negative zeta potentials were expected since both alginate and ES100 are anionic. Irvin-choy and colleagues reported that size and surface charge have the potential to influence the circulation of nanoparticles in living organisms (Irvin-Choy et al., 2020). Hence, zeta potential is regarded as a significant component that reveals the formation of nanoparticles because it indicates the net charges obtained by particles in a particular medium (Mujtaba & Alotaibi, 2020). Furthermore, negatively charged nanoparticles are more suitable for vaginal application, whereas larger sizes (>100 nm) could be utilized to target the placenta, since maternal blood is directly linked to the syncytial membrane (Menezes et al., 2012; Irvin-Choy et al., 2020).

Table 3.5: Box-Behnken Experimental Design: Formulation Variables and Responses of Alginate-ES100 Nanoparticles (All Analyses were Undertaken in Triplicate)

Run order	Alginate (mg)	ES100 (mg)	$CaCl_2$ (mg)	Maximum cumulative release % at 96 hrs.	Mean particle size (nm)	Zeta potential (MV)	PDI
F1	110	135	20	75%	146.9 ± 0.69	−29.9 ± 0.79	0.153 ± 0.02
F2	110	135	20	75%	147.5 ± 0.70	−30.7 ± 0.81	0.145 ± 0.02
F3	110	180	25	60%	157.7 ± 4.15	−25.1 ± 1.29	0.206 ± 0.01
F4	90	90	20	50%	228.0 ± 5.34	−17.8 ± 0.31	0.254 ± 0.04
F5	110	90	25	53%	150.7 ± 3.61	−30.8 ± 5.70	0.184 ± 0.02
F6	110	180	15	64%	178.8 ± 2.75	−25.1 ± 6.86	0.261 ± 0.01
F7	90	135	25	74%	182.6 ± 3.12	−32.4 ± 2.69	0.245 ± 0.01
F8	130	135	25	77%	179.7 ± 6.38	−31.9 ± 0.93	0.252 ± 0.01
F9	130	135	15	73%	179.5 ± 4.36	−35.5 ± 1.91	0.239 ± 0.01
F10	110	90	15	53%	149.9 ± 1,34	−38.4 ± 5.39	0.154 ± 0.01
F11	110	135	20	75%	148.7 ± 0.73	−28.2 ± 0.77	0.154 ± 0.02
F12	130	90	20	73%	157.9 ± 1.03	−38.4 ± 1.85	0.129 ± 0.02
F13	130	180	20	68%	185.8 ± 1.21	−32.6 ± 0.57	0.216 ± 0.01
F14	90	135	15	72%	194.6 ± 4.04	−35.2 ± 4.81	0.211 ± 0.02
F15	90	180	20	62%	198.9 ± 4,72	−29.5 ± 0.66	0.248 ± 0.01

3.8.3 Fourier Transform Infrared Spectroscopy

The FTIR spectra of neat polymers (Figure 3.4) revealed results like those previously reported. Thus, the infrared spectrum of ES100 revealed vibrational frequency bands at 1450 cm^{-1}, which correspond to the presence of the -CH_3 bend, and at 1275–1000 cm^{-1}, which are attributed to C=O amide stretching from esterified carboxylic groups and C-F bonds (Sharma et al., 2011; Silva et al., 2013; De Leo et al., 2020). The alginate spectrum, on the other hand, revealed absorption peaks at 1616 cm^{-1} and 1418 cm^{-1}, which correspond to COO- asymmetric and symmetric stretching vibrations, respectively (Jana et al., 2015; Joshy et al., 2017; Derkach et al., 2020). Furthermore, the bands at 1092 and 1032 correspond to the C-O and CO-C groups in the mannuronic and guluronic units, respectively. The vibration bands of alginates and ES100 carboxylic groups suggest that O-H exists in their structures at 3500–

3000 cm^{-1} (Kianersi et al., 2021). When the two polymers are cross-linked (Alg-ES100), slight variations were observed at 1616–1603 cm^{-1} and 1418–1410 cm^{-1} in comparison to the alginate spectra alone. The reduction in wave numbers confirmed a firm indication of intermolecular interactions, potentially related to the development of ionic bonds in divalent calcium ions and the -COO- groups of alginates (Daemi & Barikani, 2012; Thomas et al., 2020). In this context, the substitution of sodium ions with calcium ions in alginate blocks results in modifications in the atomic weight, charge density, and radius of cations. Upon the formation of nanoparticles, this creates a different setting around the carbonyl group (Daemi & Barikani, 2012; Thomas et al., 2020). Altogether, calcium chloride and alginate polymer interacted via the asymmetric and symmetric alginate stretching of COO- (Thomas et al., 2021).

Then, calcium alginate interacted with ES100 via the C=O ester bond to form a new strong anhydride bond at 1050–1040 cm^{-1}. A proposed mechanism for this interaction is depicted in chapter 1 (Fig.1.2). A shift in the carboxylate peak position from 1728 to 1560 cm^{-1} has been observed during the ionization process of ES100. This phenomenon is attributed to the anti-symmetrical COO- vibration (Raffin et al., 2006; Silva et al., 2013). Nonetheless, there was no discernible shift in the spectrum of Alg-TDF-ES100 pertaining to this band, indicating that no recent chemical bond was established either after the formulations production or during lyophilization. These results confirm the dispersion of TDF in the polymers and demonstrate an effective interaction between alginate and ES100 polymers. This interaction possesses characteristics that may have resulted in the entrapment of TDF within alginate-ES100 nanoparticles. Furthermore, the fusion of the polymers with the drug (Alg-TDF-ES100) showed peaks similar to those of Alg-ES100, which confirms that no interaction occurred between the polymers and the drug (Mehta et al., 2013).

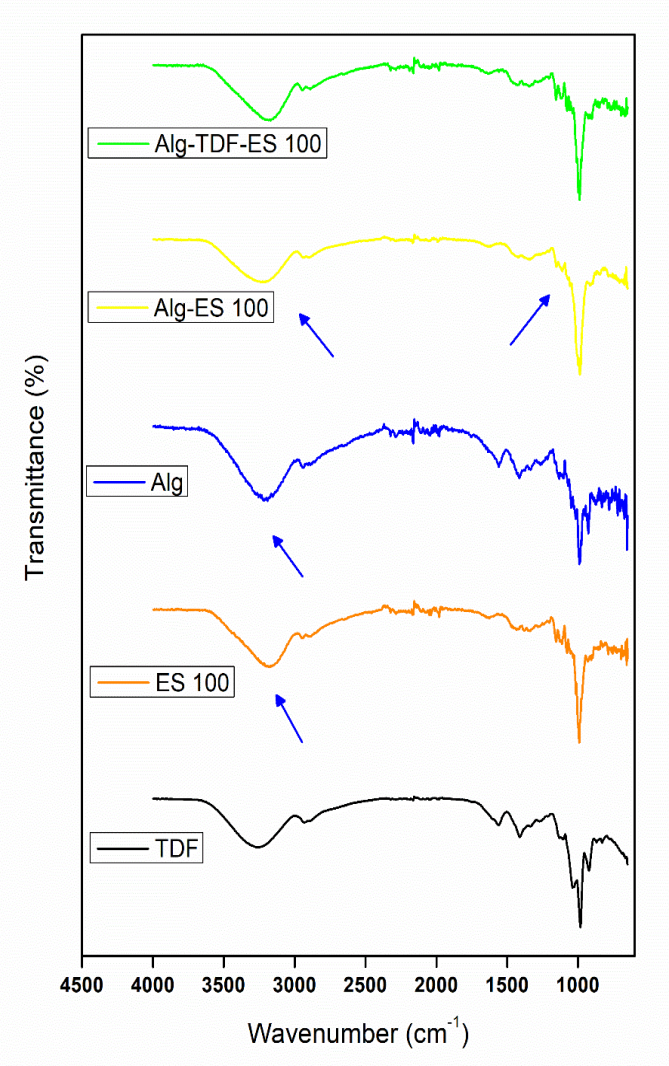


Figure 3.4. FTIR spectra of the TDF drug, ES100, alginate (Alg), unloaded (Alg-ES100), and TDF-loaded nanoparticles (Alg-TDF-ES100)

3.8.4 X-ray Diffraction

XRD was used to evaluate the crystalline structures of raw polymers and nanoparticles. Figure 3.5 shows the X-ray diffraction graphs of ES100, sodium alginate, and the TDF drug, as well as drug-free nanoparticles (Alginate-ES100) and TDF-loaded nanoparticles. This data indicated that alginate formed a semi-crystalline pattern, consistent with previous reports (Bhagyaraj & Krupa, 2020; Eltaweil et al., 2021; Nair et al., n.d.; Wang et al., 2022). Furthermore, the alginate diffraction peaks at 2θ = 14.5° and 22.0° correspond to the humidified atomic arrangement formed by hydrogen covalent bonding (Wang et al., 2022). On the contrary, ES100 is a nebulous powder devoid of crystalline structure, as exemplified by the diffraction pattern. These results agree with those reported by Sharma et al., 2011, Hu et al. 2012, Ding et al., 2020, and Yusuf et al., 2021 (Sharma et al., 2011; Hu et al., 2012; Ding et al., 2020; Yusuf et al., 2021).

The TDF drug powder is crystalline and shows clear, sharp peaks, unlike sodium alginate and ES100. According to El-Sheikh and co-workers (2018), sharp, clear peaks are associated with the high purity of the systems (El-Sheikh et al., 2019). Interestingly, sodium alginate and the ES100 polymer interacted well, as shown by the green graph of drug-free nanoparticles. This confirms nanoparticle formation. The interaction between these polymers could be attributed to the functional groups of the ES100 polymer, as similarities between the ES100, drug-free nanoparticles, and TDF-loaded nanoparticles graphs depict. Moreover, the sharp, clear peaks of the TDF drug that disappeared in TDF-loaded nanoparticles indicated that encapsulation had occurred (Anwer et al., 2017). In this invention, the TDF molecule was converted into a nebulous state to coincide with alginate and ES100 polymers.

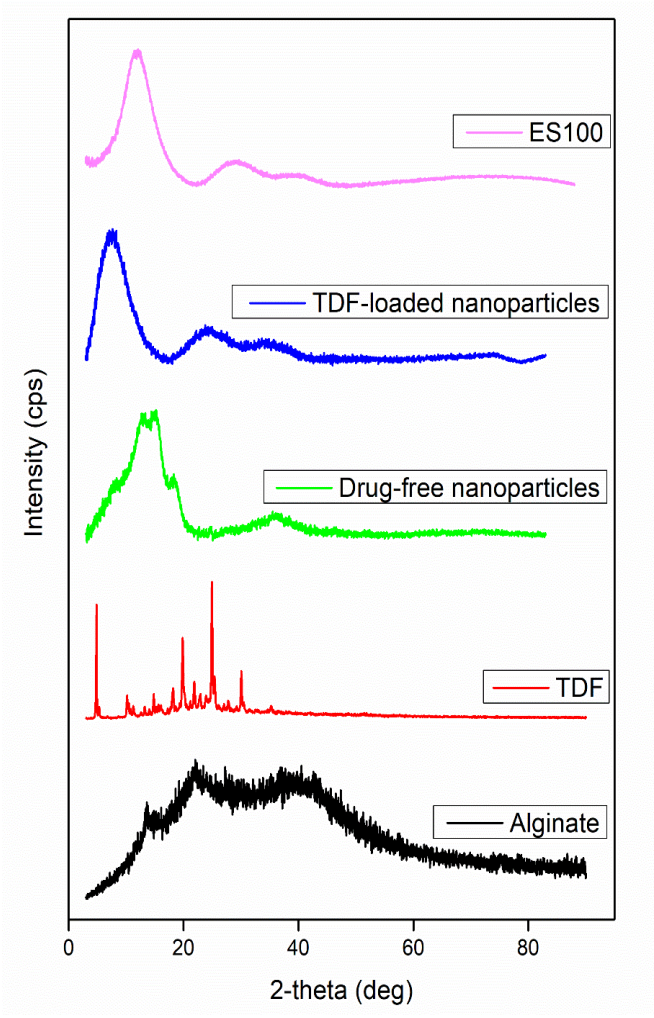


Figure 3.5. X-ray diffraction patterns of alginate, TDF drug, ES100, drug free (Alg-ES100), and TDF-loaded nanoparticles (Alg-TDF-ES100)

3.8.5 Differential Scanning Calorimetry

The DSC instrument is used to ascertain the melting behavior of polymers and the glass transition temperature (Jana et al., 2015). It is dependent on the sample's thermal capacity as a function of temperature (Sarmento et al., 2006). For the sodium alginate polymer, endothermic and exothermic peaks were observed at 123.57°C and 235.02 °C, respectively, as shown in Figure 3.6. As per the findings of Chawla et al. (2012) and Siddaramaiah et al. (2008), the endothermic peak is attributed to the evaporation of water and the carboxylate segment of the polymer (Chawla et al., 2012; Siddaramaiah et al., 2008), whereas the exothermic peak may be attributed to the diaxial and diequatorial links of the polymer segments (Siddaramaiah et al., 2008). The sodium alginate contains three polymer sections, one with varying units of sugar, the other with poly (β-D-mannopyranosyluronate), and the third with poly (α-L-guluo-pyranosyluronate). Based on the diaxial and diequatorial links between these segments, sodium alginate displays a weakened and narrow melting pinnacle at 220 °C (Siddaramaiah et al., 2008). Additionally, alginate is an amorphous polymer that does not crystallize due to its irregular or geometrical structure.

This conclusion is in accordance with the previous publications (Soares et al., 2004; El-Houssiny et al., 2016), wherein the authors reported that the thermal degradation of sodium alginate involves three distinct stages. The first step is an endothermic peak indicating the dehydration process and glass transition temperature at around 80 °C. Then, an endothermic peak nearing 200 °C, which is associated with the melting point, followed by an exothermic peak at around 240 °C (Soares et al., 2004; Siddaramaiah et al., 2008; El-Houssiny et al., 2016; Nair et al., n.d). In addition to the thermogram peaks for sodium alginate, endothermic peaks were observed for the unbound TDF, ES100, and nanoparticles loaded with TDF at 116.53 °C, 229.69 °C, and 164.93 °C, respectively, indicating their melting points and crystallization. The TDF and ES100 peaks are in agreement with previous findings (Jat et al., n.d.; Nunes et al., n.d.; Shailender et al., 2017). The overall results indicated that the endothermic peak of TDF was lowered in TDF-loaded nanoparticles. These findings suggest thermodynamic compatibility between alginate, ES100, and the TDF drug, as the shifts of the endothermic and exothermic peaks correspond to links connecting drugs and polymers (Sarmento et al., 2006; El-Houssiny et al., 2016).

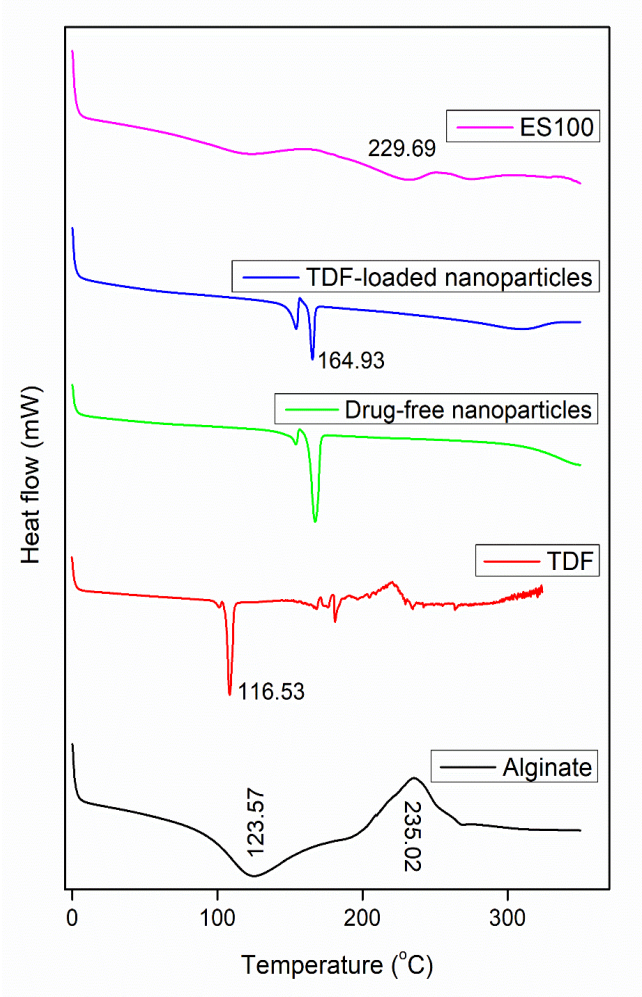


Figure 3.6. DSC thermograms of alginate, TDF drug, ES100, drug free (Alg-ES100), and TDF-loaded nanoparticles (Alg-TDF-ES100)

3.9 Determination of EE% and DL% of Nanoparticles

The results regarding entrapment efficiencies and drug loading capacities of the 15 formulations are presented in Figure 3.7. Entrapment efficiency refers to the percentage of TDF entrapped in the nanoparticles relative to the overall sum of TDF introduced during the production of the system (Politi et al., 2023). This is the primary factor affecting drug release and the overall efficacy of the formulation process. Our results confirmed that most of the drug was entrapped, ranging from 74% (F5) to 88% (F9). High entrapment efficiency was achieved by keeping the drug concentration and stirring speed constant while varying the alginate, calcium chloride, and ES100 concentrations. Pokharkar et al. (2015) and Cautela et al. (2018) have previously published comparable findings indicating a high EE% for the TDF drug encapsulated into nanoparticles (Pokharkar et al., 2015; Cautela et al., 2019). Drug loading, on the other hand, is described as the mass of TDF available in nanoparticles (100 mg) (Kumar et al., 2017). It is therefore dependent on the initial drug/polymer ratio (Schafroth et al., 2012). As depicted in Figure 3.7, the results obtained for drug loading capacities ranged from 13% (F13) to 20% (F4). Based on the drug release results in the "*In vitro* release of TDF-loaded

nanoparticles" section, these results confirmed successful loading, as the drug loading must ensure adequate release from the nano system (Ngema et al., 2022). Furthermore, Shen and colleagues (2017) reported that drug loading is considered high when it exceeds 10% (Shen Shihoong, Wu Youshen, 2017), as evidenced by our findings for all formulations. Overall, the formulations of alginate-ES100 nanoparticles demonstrated the ability to preserve the TDF drug, leading to a prolonged release.

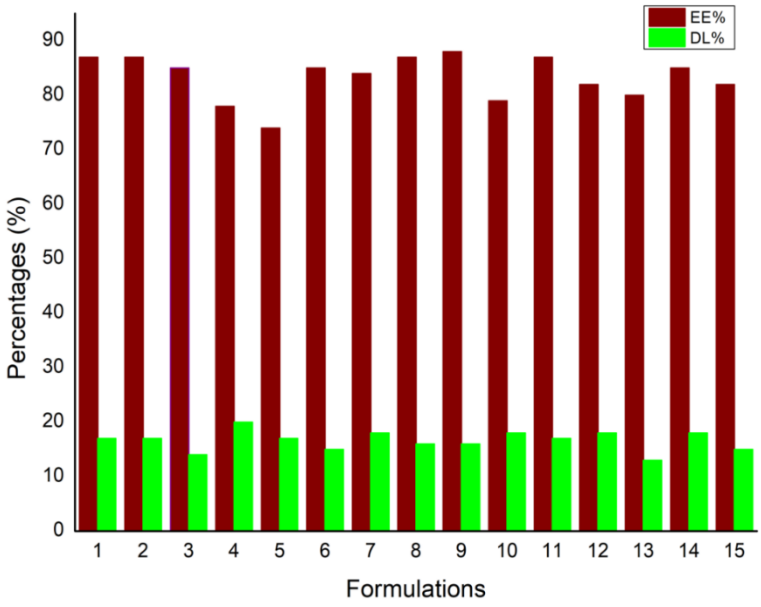


Figure 3.7. Entrapment efficiencies and drug loading capacities of the 15 formulations

3.10 *In Vitro* Release of TDF-loaded Nanoparticles

Graphs A–E (Figure 3.8) show that half of the TDF was released from alginate-ES100 nanoparticles within the initial 12 h, whereas the remaining concentration was sustained for 96 h. Table 3.5 shows that the maximum cumulative release of F1–F15 was achieved at 96 h. Increasing concentrations of alginate and eudragit resulted in an increased release of the drug. These outcomes are consistent with those reported by Zhang and co-workers (T. Zhang et al., 2011), who found that drug release increased with increasing concentrations of the ES100 polymer. The outcome was expected, as eudragits are known to regulate drug release due to their dissolution and osmotic release patterns (Singh, 2015). Furthermore, ES100 exhibits insoluble properties in acidic pH conditions, thereby reducing the burst effect, which is associated with accelerated drug release and therapeutic effects (Anwer et al., 2017; Saraf et al., 2019). On the contrary, calcium alginate undergoes a solvable transformation in the presence of sodium salts, thereby facilitating the extension of the encapsulated TDF release (Kumar et al., 2017). Our results demonstrated an improved cumulative release compared to previous reports on the release of the TDF drug (T. Zhang et al., 2011; Shailender et al., 2017; Cautela et al., 2019).

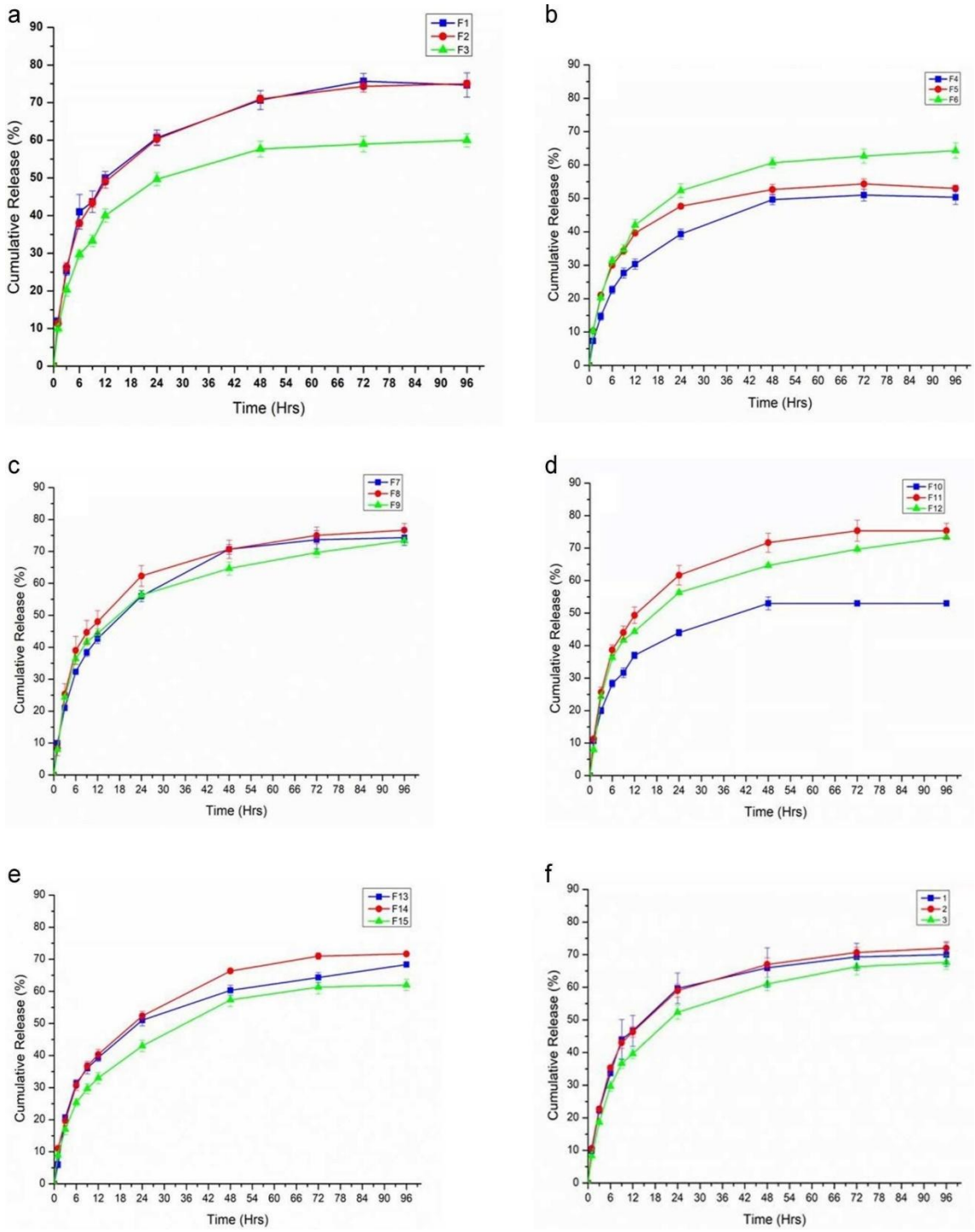


Figure 3.8. Cumulative *in vitro* release of the experimental design formulations [a–e (F1–F15)] and the optimized formulations [f (1–3)] in simulated vaginal fluid (SVF) at pH 4.2. The release was sustained for up to 96 h

3.11 Experimental Design Analysis

As depicted in Table 3.5, the model responses were determined based on the results of the 15 experimental runs. The adequacy of these models was then verified by applying several tests, such as ANOVA, regression analysis, and coefficient of determination. The results of the ANOVA test (shown in Tables 3.6-3.9) revealed that the probability values for the F-statistics of drug release % and mean particle size responses were both 0.004, which implies that these models were significant ($P < 0.05$) and that they fitted perfectly in the quadratic model. PDI (0.088) and zeta potential (0.403) responses were insignificant, which could be attributed to the fact that no statistical variation was detected for these models. However, the lack of fit *p* values was all significant ($P < 0.1$), except for the DR% model, which did not show any lack of ft. Therefore, the values of the lack of fit for PDI, mean particle size, and zeta potential models were 0.016, 0.006, and 0.042, respectively.

These models lacked prediction efficiency, as a lack of fit with high non-significant values ($P > 0.1$) is desired for a quadratic model (Karmoker et al., 2018; Huda et al., 2021). Under the coefficient of determination, the R^2 values were high and close to 1 (see Tables 3.6-3.9). This indicates that the mathematical model was adequate, and the optimization was appropriately validated (Aliemeke & Oladeinde, 2020; Bazdaric et al., 2021). Furthermore, the difference between R^2 and R^2-adjusted values is expected to be lower than 0.2, which was the case for drug release percentage and mean particle size models. This is an indication that the models adopted were significant (Benouis et al., 2022). However, the difference between the R^2 and the R^2-adjusted values for PDI and zeta potential was higher than 0.2. It is important to note that these results are consistent with those of the ANOVA test above.

Table 3.6: Model summary, analysis of variance and regression equation for drug release

Model Summary

S	R-sq	R-sq(adj)	PRESS	R-sq(pred)	AICc	BIC
0,0397762	90,79%	81,59%	0,10025	16,66%	-11,60	-41,23

Analysis of Variance

Source	DF	Seq SS	Contribution	Adj SS	Adj MS	F-Value	P-Value
Model	7	0,109218	90,79%	0,109218	0,015603	9,86	0,004
Linear	3	0,021475	17,85%	0,021475	0,007158	4,52	0,046
[Alginate]	1	0,013613	11,32%	0,013613	0,013613	8,60	0,022
[Eudragit]	1	0,007813	6,49%	0,007813	0,007813	4,94	0,062
[CaCl2]	1	0,000050	0,04%	0,000050	0,000050	0,03	0,864
Square	3	0,080518	66,93%	0,080518	0,026839	16,96	0,001
[Alginate]*[Alginate]	1	0,004906	4,08%	0,002083	0,002083	1,32	0,289
[Eudragit]*[Eudragit]	1	0,071407	59,36%	0,073667	0,073667	46,56	0,000
[CaCl2]*[CaCl2]	1	0,004206	3,50%	0,004206	0,004206	2,66	0,147
2-Way Interaction	1	0,007225	6,01%	0,007225	0,007225	4,57	0,070
[Alginate]*[Eudragit]	1	0,007225	6,01%	0,007225	0,007225	4,57	0,070
Error	7	0,011075	9,21%	0,011075	0,001582		
Lack-of-Fit	5	0,011075	9,21%	0,011075	0,002215	*	*
Pure Error	2	0,000000	0,00%	0,000000	0,000000		
Total	14	0,120293	100,00%				

Regression Equation in Uncoded Units

Drug Release (%)	=	-1,375 - 0,0046 [Alginate] + 0,02472 [Eudragit] + 0,0545 [CaCl2] + 0,000059 [Alginate]*[Alginate] - 0,000070 [Eudragit]*[Eudragit] - 0,001350 [CaCl2]*[CaCl2] - 0,000047 [Alginate]*[Eudragit]

Table 3.7: Model summary, analysis of variance and regression equation for mean particle size

Model Summary

S	R-sq	R-sq(adj)	PRESS	R-sq(pred)	AICc	BIC
10,4184	90,44%	80,89%	5714,42	28,12%	155,44	125,82

Analysis of Variance

Source	DF	Seq SS	Contribution	Adj SS	Adj MS	F-Value	P-Value
Model	7	7190,24	90,44%	7190,24	1027,18	9,46	0,004
Linear	3	1559,49	19,62%	1559,49	519,83	4,79	0,040
[Alginate]	1	1280,18	16,10%	1280,18	1280,18	11,79	0,011
[Eudragit]	1	150,51	1,89%	150,51	150,51	1,39	0,277
[CaCl2]	1	128,80	1,62%	128,80	128,80	1,19	0,312
Square	2	4698,60	59,10%	4698,60	2349,30	21,64	0,001
[Alginate]*[Alginate]	1	4331,16	54,48%	4490,69	4490,69	41,37	0,000
[Eudragit]*[Eudragit]	1	367,44	4,62%	367,44	367,44	3,39	0,108
2-Way Interaction	2	932,15	11,73%	932,15	466,08	4,29	0,061
[Alginate]*[Eudragit]	1	812,25	10,22%	812,25	812,25	7,48	0,029
[Eudragit]*[CaCl2]	1	119,90	1,51%	119,90	119,90	1,10	0,328
Error	7	759,80	9,56%	759,80	108,54		
Lack-of-Fit	5	758,12	9,54%	758,12	151,62	180,50	0,006
Pure Error	2	1,68	0,02%	1,68	0,84		
Total	14	7950,04	100,00%				

Regression Equation in Uncoded Units

Mean Particle Size (nm)	=	1532 - 21,89 [Alginate] - 2,48 [Eudragit] + 2,48 [CaCl2] + 0,0869 [Alginate]*[Alginate] + 0,00491 [Eudragit]*[Eudragit] + 0,01583 [Alginate]*[Eudragit] - 0,0243 [Eudragit]*[CaCl2]

Table 3.8: Model summary, analysis of variance and regression equation for PDI

Model Summary

S	R-sq	R-sq(adj)	PRESS	R-sq(pred)	AICc	BIC
0,0314322	80,95%	55,55%	0,0595635	0,00%	0,03	-47,89

Analysis of Variance

Source	DF	Seq SS	Contribution	Adj SS	Adj MS	F-Value	P-Value
Model	8	0,025192	80,95%	0,025192	0,003149	3,19	0,088
Linear	3	0,007940	25,52%	0,007940	0,002647	2,68	0,141
[Alginate]	1	0,002048	6,58%	0,002048	0,002048	2,07	0,200
[Eudragit]	1	0,005832	18,74%	0,005832	0,005832	5,90	0,051
[CaCl2]	1	0,000060	0,19%	0,000060	0,000060	0,06	0,813
Square	3	0,012995	41,76%	0,012995	0,004332	4,38	0,059
[Alginate]*[Alginate]	1	0,007204	23,15%	0,008345	0,008345	8,45	0,027
[Eudragit]*[Eudragit]	1	0,000306	0,98%	0,000535	0,000535	0,54	0,489
[CaCl2]*[CaCl2]	1	0,005485	17,62%	0,005485	0,005485	5,55	0,057
2-Way Interaction	2	0,004257	13,68%	0,004257	0,002128	2,15	0,197
[Alginate]*[Eudragit]	1	0,002450	7,87%	0,002450	0,002450	2,48	0,166
[Eudragit]*[CaCl2]	1	0,001806	5,80%	0,001806	0,001806	1,83	0,225
Error	6	0,005928	19,05%	0,005928	0,000988		
Lack-of-Fit	4	0,005879	18,89%	0,005879	0,001470	60,40	0,016
Pure Error	2	0,000049	0,16%	0,000049	0,000024		
Total	14	0,031120	100,00%				

Regression Equation in Uncoded Units

PDI = 2,463 - 0,03066 [Alginate] - 0,00214 [Eudragit] - 0,0484 [CaCl2]
+ 0,000119 [Alginate]*[Alginate] + 0,000006 [Eudragit]*[Eudragit]
+ 0,001542 [CaCl2]*[CaCl2] + 0,000027 [Alginate]*[Eudragit]
- 0,000094 [Eudragit]*[CaCl2]

Table 3.9: Model summary, analysis of variance and regression equation for zeta

Model Summary

S	R-sq	R-sq(adj)	PRESS	R-sq(pred)	AICc	BIC
5,04154	62,55%	12,62%	1963,81	0,00%	152,36	104,44

Analysis of Variance

Source	DF	Seq SS	Contribution	Adj SS	Adj MS	F-Value	P-Value
Model	8	254,711	62,55%	254,711	31,839	1,25	0,403
Linear	3	114,982	28,24%	114,982	38,327	1,51	0,305
[Alginate]	1	69,031	16,95%	69,031	69,031	2,72	0,150
[Eudragit]	1	21,451	5,27%	21,451	21,451	0,84	0,394
[CaCl2]	1	24,500	6,02%	24,500	24,500	0,96	0,364
Square	3	48,726	11,97%	48,726	16,242	0,64	0,617
[Alginate]*[Alginate]	1	13,757	3,38%	13,861	13,861	0,55	0,488
[Eudragit]*[Eudragit]	1	16,894	4,15%	14,221	14,221	0,56	0,483
[CaCl2]*[CaCl2]	1	18,074	4,44%	18,074	18,074	0,71	0,431
2-Way Interaction	2	91,002	22,35%	91,002	45,501	1,79	0,246
[Alginate]*[Eudragit]	1	76,563	18,80%	76,563	76,563	3,01	0,133
[Eudragit]*[CaCl2]	1	14,440	3,55%	14,440	14,440	0,57	0,480
Error	6	152,502	37,45%	152,502	25,417		
Lack-of-Fit	4	149,243	36,65%	149,243	37,311	22,89	0,042
Pure Error	2	3,260	0,80%	3,260	1,630		
Total	14	407,213	100,00%				

Regression Equation in Uncoded Units

Zeta Potential = -52 + 0,26 [Alginate] - 0,591 [Eudragit] + 5,03 [CaCl2]
- 0,00484 [Alginate]*[Alginate] + 0,00097 [Eudragit]*[Eudragit]
- 0,089 [CaCl2]*[CaCl2] + 0,00486 [Alginate]*[Eudragit]
- 0,0084 [Eudragit]*[CaCl2]

Figure 3.9a, on the other hand, displays linear regression models (normal probability plots), non-linear regression models (versus fits), histogram graphs, and versus order for all responses. Linear regression models revealed normal distribution analysis as evidenced by the straight lines and minor deviations from linear distribution (Sivakumar, 2013; Aliemeke & Oladeinde, 2020; Pathak et al., 2022). In contrast, non-linear regression models displayed randomness, with the standard error of the regression (S) for drug release %, mean particle size, PDI, and zeta potential being 0.0397762, 10.4184, 0.0314322, and 5.04154, respectively (see Tables 3.6-3.9). The dispersion of these responses is unbiased and forms constant variance as the small S values present it. The presence of smaller S values indicates that points are situated closer to the fitted line.

Histogram plots confirmed the uniform distribution of the results, as shown by the bell shapes evenly distributed around zero. Moreover, the versus order patterns displayed the overall results of the 15 formulations for each response. The formulas for multiple linear regression or quadratic polynomial equations for all responses are shown below [Eqs. (3.4) – (3.7)]. For the DR% model, the coefficient values are as follows: Alginate is −0,0046, eudragit is 0.02472, and $CaCl_2$ is 0.0545. For the PS model, alginate is −21,89, eudragit is −2,48, and $CaCl_2$ is 2,48. Similarly, for the PDI model, alginate is −0,03066, eudragit is −0,00214, and $CaCl_2$ is −0.0484. Lastly, for the ZP model, alginate is 0,26, eudragit is -0,591, and $CaCl_2$ is 5,03. These responses had intercepts of −1,375; 1532; 2,463; and −52, respectively.

$$\begin{aligned} DR\ \% = {} & -1{,}375\ -\ 0{,}0046\ [Alginate] +\ 0{,}02472\ [Eudragit] +\ 0{,}0545\ [CaCl2] \\ & +\ 0{,}000059\ [Alginate] * [Alginate] -\ 0{,}000070\ [Eudragit] * [Eudragit] \\ & -\ 0{,}001350\ [CaCl2] * [CaCl2] -\ 0{,}000047\ [Alginate] \\ & * [Eudragit] \end{aligned} \tag{3.4}$$

$$\begin{aligned} PS\ (nm) = {} & 1532\ -\ 21{,}89\ [Alginate] -\ 2{,}48\ [Eudragit] +\ 2{,}48\ [CaCl2] +\ 0{,}0869\ [Alginate] \\ & * [Alginate] +\ 0{,}00491\ [Eudragit] * [Eudragit] +\ 0{,}01583\ [Alginate] \\ & * [Eudragit] -\ 0{,}0243\ [Eudragit] * [CaCl2] \end{aligned} \tag{3.5}$$

$$\begin{aligned} PDI = {} & 2{,}463\ -\ 0{,}03066\ [Alginate] -\ 0{,}00214\ [Eudragit] -\ 0{,}0484\ [CaCl2] \\ & +\ 0{,}000119\ [Alginate] * [Alginate] +\ 0{,}000006\ [Eudragit] * [Eudragit] \\ & +\ 0{,}001542\ [CaCl2] * [CaCl2] +\ 0{,}000027\ [Alginate] * [Eudragit] \\ & -\ 0{,}000094\ [Eudragit] \\ & * [CaCl2] \end{aligned} \tag{3.6}$$

$$ZP = -52 + 0{,}26\,[Alginate] - 0{,}591\,[Eudragit] + 5{,}03\,[CaCl2] - 0{,}00484\,[Alginate] * [Alginate] + 0{,}00097\,[Eudragit] * [Eudragit] - 0{,}089\,[CaCl2] * [CaCl2] + 0{,}00486\,[Alginate] * [Eudragit] - 0{,}0084\,[Eudragit] * [CaCl2] \quad (3.7)$$

In addition to the aforementioned analysis, optimization of variables and their interaction was carried out using response surface and contour plots, Pareto charts, main effects and interaction plots. Response surface plots and their corresponding contour plots were used to examine additional interactions among process variables and the effects of these variables on responses. The effects of polymers and the cross-linking agent on DR%, PS, PDI, and ZP measurements were evaluated, as depicted in Figure 3.9b. This was presented as a function of alginate and eudragit, alginate and $CaCl_2$, and eudragit and $CaCl_2$. The percentages of drug release exhibited an increase with the increase in concentrations of both alginate and eudragit at any $CaCl_2$ concentration. However, particle size, zeta potential, and PDI increased with decreasing alginate concentrations and increasing concentrations of eudragit. It is noteworthy that as the concentrations of eudragit increase, the concentrations of $CaCl_2$ for particle size and PDI decrease.

Overall, the results suggested that alginate and eudragit play an important role in sustaining the release, stabilizing, dispersing, and controlling the particle size of the systems. These outcomes are in accordance with the findings presented in Table 3.5 and the "*In vitro* release of TDF-loaded nanoparticles" section. The nonlinear contour plots in Figure 3.10 show that there was no direct linear relationship between the selected independent variables (Yetilmezsoy et al., 2009). Except for the drug release response, in which the concentration of alginate increased with the increase in eudragit concentration. This is in accordance with the findings of the surface plots.

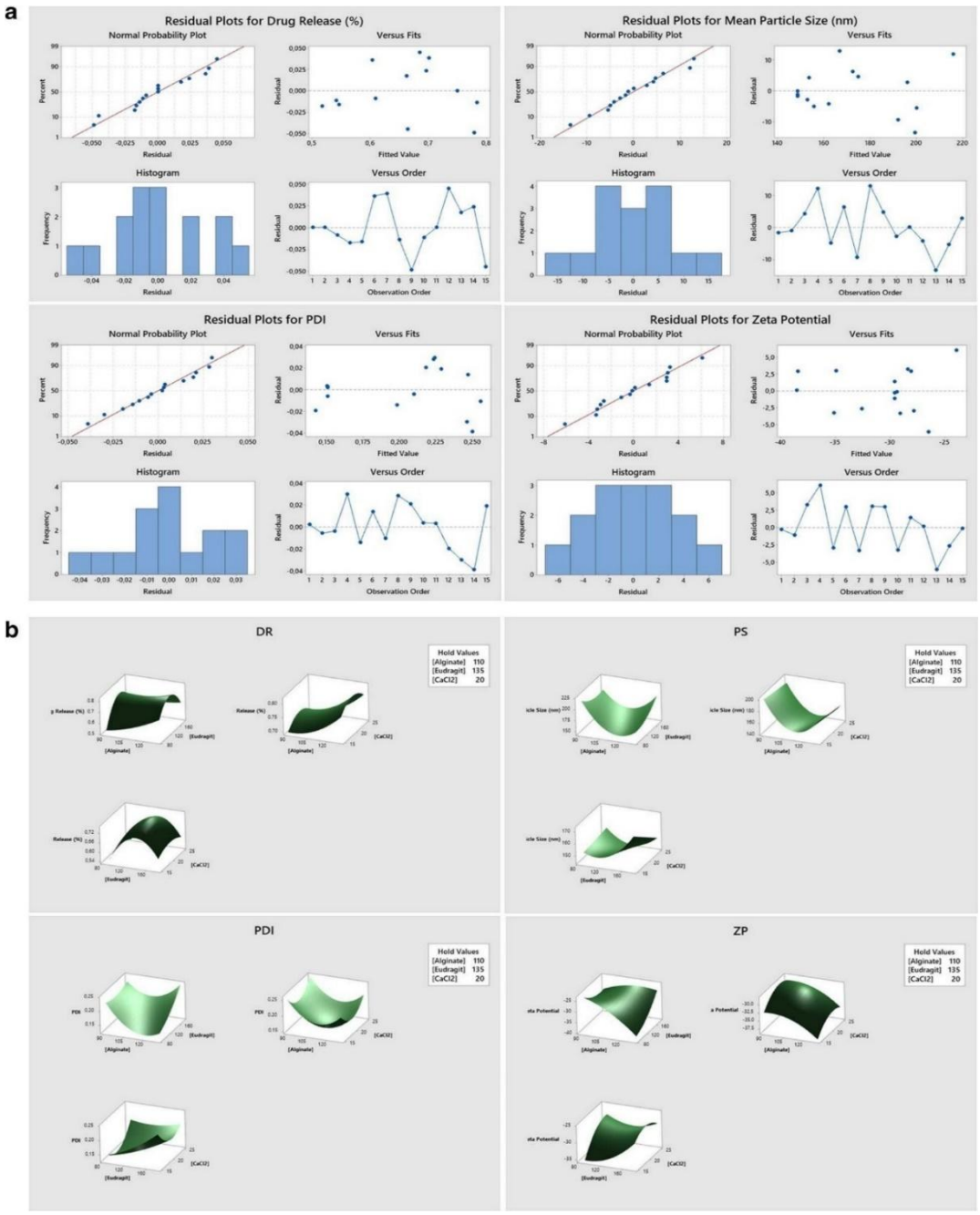


Figure 3.9. a Residual plots and **b** 3-D response surface plots for drug release, mean particle size, poly dispersity index, and zeta potential

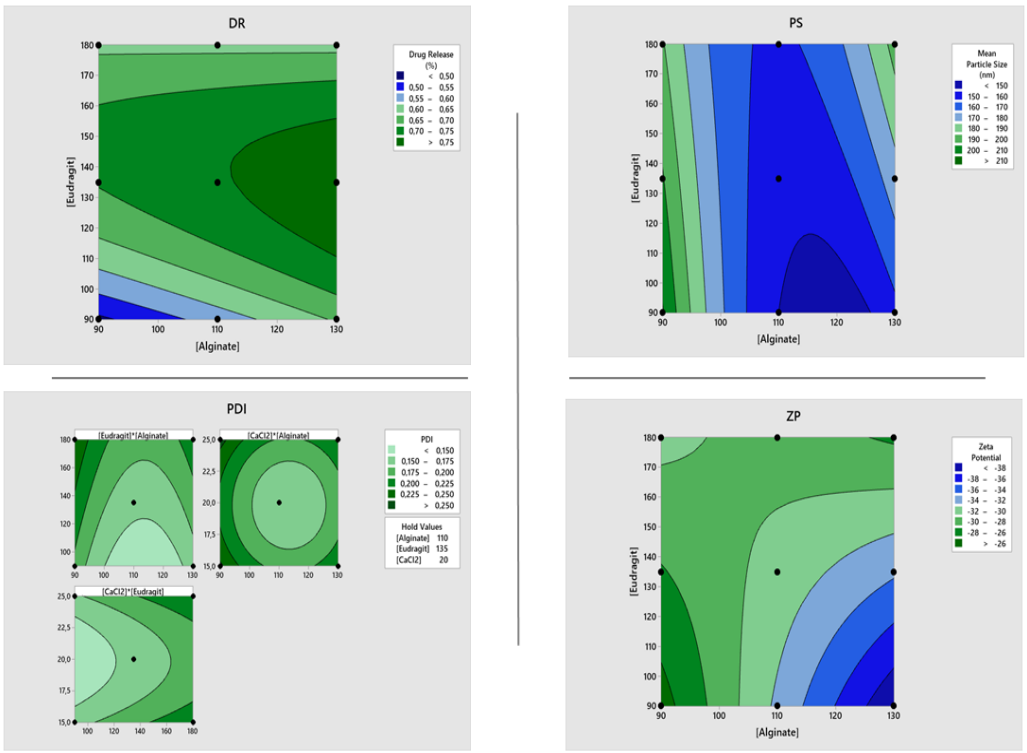


Figure 3.10 Contour plots for drug release, mean particle size, poly dispersity index, and zeta potential

Pareto charts were employed to calculate the effects of each factor, namely alginate, eudragit, and calcium chloride, on various responses. The objective was to ascertain the relative significance of the main and interaction effects. As depicted in Figure 3.11, the responses for mean particle size and zeta potential indicated that all factors and their interactions were significant, with confidence levels exceeding the reference lines above 0.711 and 0.718, respectively (Jegan et al., 2021). On the contrary, the calcium chloride factor did not exhibit significant effects on drug release and PDI responses, as their values were below the reference lines of 0.711 and 0.718, respectively. Nonetheless, their interactions (CC) demonstrated significant effects. The standardized effect of each factor on the response is indicated by the length of each bar in the chart (Yetilmezsoy et al., 2009). These results are in agreement with the main effects shown in Figure 3.12 and with the interaction plots in Figure 3.13. The means of the response variable for each level of a factor are plotted in a main effects plot, which helps identify which major effects are significant (Sibanda & Pretorius, 2013). As per the principle of sparsity-of-effect, a system is typically dominated by main effects and low-order interactions. Consequently, it is highly probable that main effects and two-factor interactions constitute the most significant responses in an experimental design (Sibanda & Pretorius, 2013).

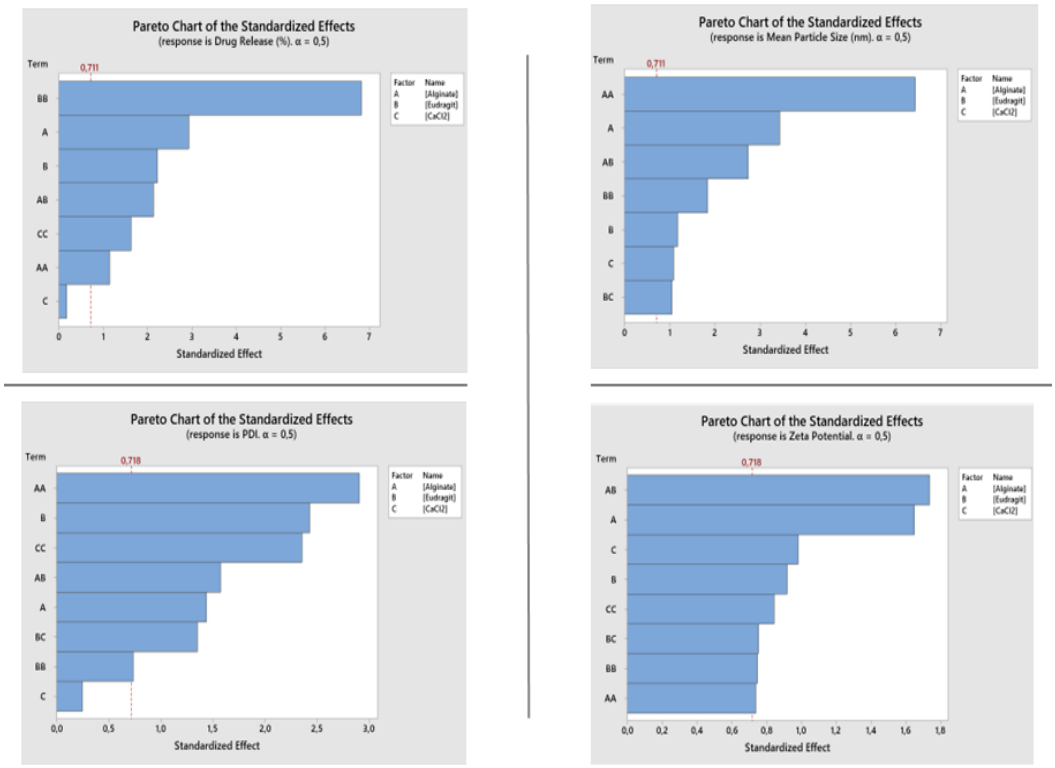


Figure 3.11 Pareto charts of the standardized effects for drug release, mean particle size, poly dispersity index, and zeta potential

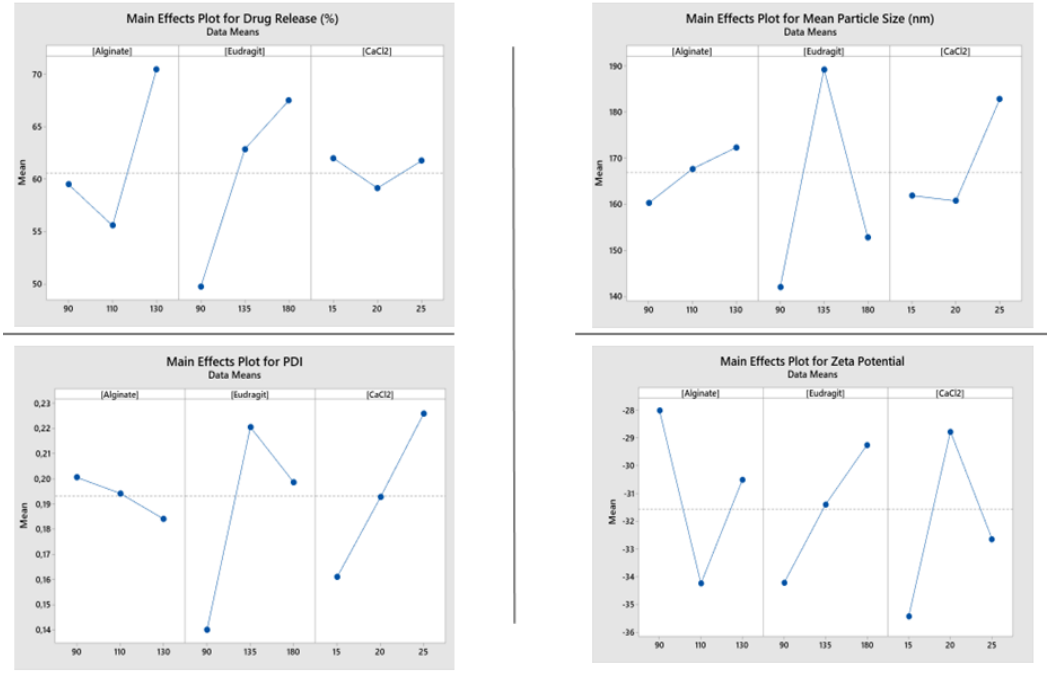


Figure 3.12 Main effects plots for drug release, mean particle size, poly dispersity index, and zeta potential

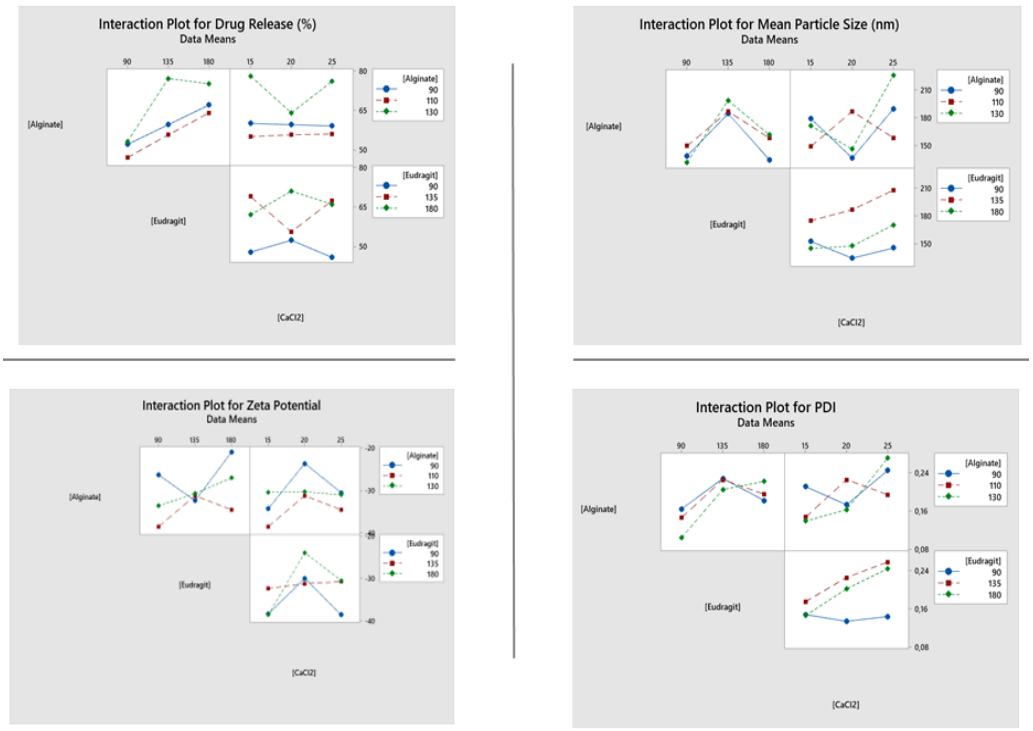


Figure 3.13 Interaction plots for drug release, mean particle size, poly dispersity index, and zeta potential

3.11.1 Optimization Using the Desirability Function

As shown in Table 3.4, the desirability indexes for the three optimized formulations (01, 02, and 03) were 0.932482, 0.884029, and 0.879090, respectively, considered within the acceptable range (Human et al., 2022). The experimentally derived PDI values for these formulations were 0.251 ± 0.03, 0.220 ± 0.04, and 0.197 ± 0.02, respectively, whereas mean particle size values were 134.9 ± 2.34, 155.9 ± 1.55, and 183.6 ± 2.17, respectively. It is necessary to conduct an analysis for both size and PDI, as they correlate. PDI shows how narrow the particle size distribution is. If the value is less than 0.1, it means that the distribution is minimal.

In drug delivery, a PDI of 0.3 or less is considered acceptable, which indicates a homogenous population of the nanocarrier (Zhang & Wang, 2023). Generally, for polymers and small particles (micron particles, nanoparticles, etc.), the more homogenous the particle size, the stronger their bonds are. The maximum cumulative release values for the optimized formulation were 70%, 72%, and 68%, respectively, as depicted in Figure 3.8f. These results are consistent with the predicted values (76%, 74% and 75%, respectively), see Table 3.4. However, the results for 02 closely match the approximated values, followed by 01 and 03. This confirms the reliability of the experimental design approach in predicting the most suitable formulation suitable for TDF release from alginate-ES100 nanoparticles. Furthermore, the

maximum cumulative release period for these formulations was 96 h. This formulation would require HIV patients to take it after every four days, compared to the current medication, which must be taken daily. On the contrary, the EE percentage of all formulations 01, 02, and 03 was 84%, whereas the DL percentage of 01 and 02 was 17% and the DL percentage of 03 was 16%. It is worth noting that the higher concentration of eudragit in formulation 03 resulted in a DL% that was lower than that of formulations 01 and 02. This supports the notion discussed in the "Determination of EE% and DL% of nanoparticles" section that higher concentrations of alginate/eudragit polymers result in lower DL%. Moreover, in contrast to the EE% range (74–88%) of the 15 formulations, the optimized formulations also exhibited EE% within this range, indicating that the majority of the drug was entrapped.

3.12 Cytotoxicity Assessment of Alginate-ES100 TDF-loaded Nanoparticles

The TDF drug has been reported to be tolerated for a short period by HIV patients, but if used for a long time, it can result in renal and bone cytotoxicity (Foster et al., 2009). In this research, the primary objective was to sustain the release of TDF by incorporating it into non-toxic polymers such as alginate and ES100. Hence, an MTT cytotoxicity assay was conducted utilizing TDF-loaded nanoparticles, drug-free nanoparticles, and TDF on VK2 cells. A vaginal microbicide is considered safe if it does not damage the vaginal epithelium, cause distress which would decrease patient compliance, and require low doses for therapy (Zhang et al., 2013; Meng et al., 2017). Moreover, it is imperative that the safety profiles for topical strategies to prevent HIV infection justify their implementation on the vaginal ecology and mucosal integrity (Zhang et al., 2011). Our data revealed that nanoparticles loaded with TDF did not exhibit any cytotoxic effects on VK2 cells for a duration of 24–72 h (as depicted in Figure 3.14) at concentrations of 0.025 mg/mL, 0.5 mg/mL, and 1 mg/ mL. The viability exhibited a significant increase with the increase in nanoparticle concentration, reaching its utmost level at 1 mg/mL.

Thus, cell viability remained above 90% at this concentration for up to 72 h, and no serious decrement was noticed compared to the positive control. These reactions are in agreement with those reported by Zhang et al. in 2013 (Zhang et al., 2013), who conducted cytotoxicity studies on tenofovir incorporated into eudragit S-100 sodium salt microspheres at a concentration of 1 mg/mL on VK2 cells. Furthermore, the findings presented by Yoo et al. in 2011 and Meng et al. in 2017 have demonstrated that alginate and eudragit S-100 polymers play a significant role in sustaining high cell viability on VK2 cells. Moreover, no significant reduction was observed for alginate and eudragit particles at various concentrations, up to 1 mg/mL (Yoo et al., 2011; Meng et al., 2017). In general, it appears that the cell viability of the pure TDF drug is lower than that of the TDF-loaded nanoparticles. This indicates that the

toxicity level of our designed formulation is superior to that of the TDF drug alone, rendering alginate and ES100 polymers suitable carriers for the TDF drug with the potential for sustained delivery in the FGT.

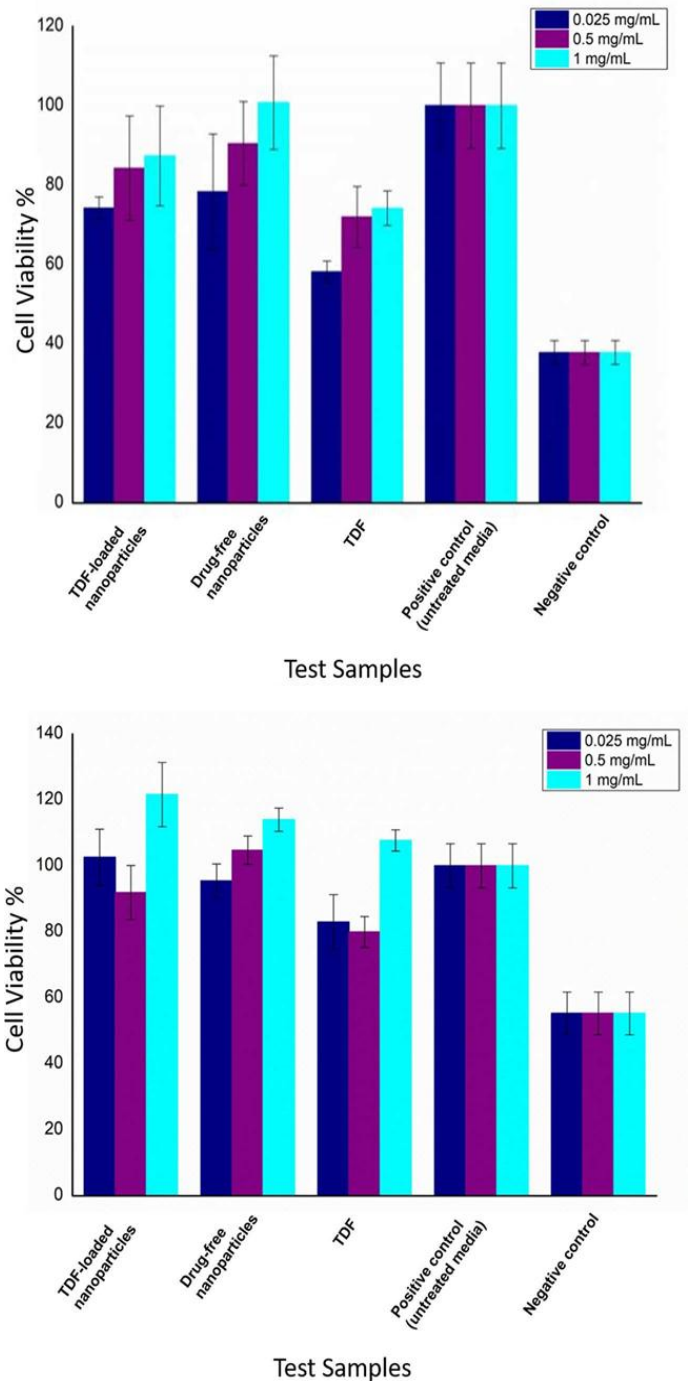


Figure 3.14. Cell viability for TDF-loaded nanoparticles, drug-free nanoparticles, and TDF at 24 h and 72 h

3.13 Clinical Significance of the Study

After the conception process, the fertilized egg divides into cells, resulting in the formation of a zygote. This embeds itself in the uterine wall, triggering the growth of the fetus and placenta (Irvin-choy et al., 2020). As gestation progresses, the chorionic villus begins to separate into various layers. Initially, extravillous trophoblasts penetrate and obstruct maternal spiral arteries, thereby preventing the flow of blood to the developing fetus. This provides a hypoxic condition for the fetus, which protects it from early damage caused by oxidative stress. Meanwhile, the uterine glands provide nutrients to the fetus (Irvin-choy et al., 2020). Secondly, villous trophoblasts produce syncytiotrophoblasts, a site where permeability glycoprotein (P-gp) is highly expressed in the placenta. The syncytiotrophoblasts directly interact with the maternal blood to form a strong barrier that unites the circulatory systems of the mother and child. Hence, at the commencement of the second trimester, the plug that encloses the maternal spiral arteries during differentiation is released, thereby allowing blood from the maternal region to flow into the placenta and fetus (Irvin-choy et al., 2020).

When taken together, the fetus has a greater capacity to be exposed to maternal drugs nearing birth term. It is noteworthy that the transport of drugs or other molecules from the maternal circulation to the placenta and fetus can be altered. Although, to attain this objective, nanomedicine must be constructed in a manner that enables them to overcome multiple biological obstacles to reach the fetus. The implementation of targeted treatments, with the aim of preventing transfer via the placenta or facilitating transport to treat the fetus, would yield significant advantages, resulting in optimal care for both the mother and the fetus. We are aiming to develop a topical delivery system that can be administered vaginally to pregnant women during the first trimester to increase the transfer of the TDF drug from maternal to fetal circulation.

3.14 Concluding remarks

This research describes the successful synthesis of the TDF antiretroviral drug loaded into alginate-ES100 nanoparticles. The particle size, encapsulation efficiency, and zeta potential were established to be suitable for the vaginal study. The drug release profiles showed a high release, sustained for 96 h at pH 4.2, corresponding to the vaginal pH. Following the statistical ANOVA test, the overall optimization results demonstrated that the mathematical model was adequate. This was exemplified by the R2 values, as well as the S and low F-statistics P values, which were found to be significant and within the desired ranges for nearly all models. The exception was the lack of fit P values for all models, which were not as high as anticipated to fit well in the quadratic model.

However, the system revealed significant interactions between dependent and independent variables, as shown in response surface plots and their corresponding contour plots, main effects, interaction plots and Pareto charts. The cytotoxicity evaluation demonstrated the safety of alginate-ES100 TDF-loaded nanoparticles in the vaginal cells. Hence, it can be inferred that alginate-ES100 nanoparticles possess the capability to effectively preserve and sustain TDF release in the FGT. However, it would be imperative to conduct a thorough investigation of the therapeutic implications of this system *in vivo* to ensure the viability of nanomedicine in the future. The long-term objective is to develop a low-dose non-toxic microbicide that can be administered long term in the vagina to cater to both pregnant and non-pregnant HIV patients.

3.15 References

Aliemeke, B. N. G., & Oladeinde, M. (2020). Box-behnken design optimization of sand-casting process parameters. IJET, 6(2), 25–36. https://doi.org/10.19072/ijet.714473

Anicescu, M. C., Dinu-Pîrvu, C. E., Talianu, M. T., Ghica, M. V., Anuța, V., Prisada, R. M., Nicoară, A. C., & Popa, L. (2022). Insights from a Box–behnken optimization study of microemulsions with salicylic acid for acne therapy. Pharmaceutics, 14(1). https://doi.org/10.3390/pharmaceutics14010174

Ansari, F., Pourjafar, H., Jodat, V., Sahebi, J., & Ataei, A. (2017). Effect of eudragit S100 nanoparticles and alginate chitosan encapsulation on the viability of *Lactobacillus acidophilus* and *Lactobacillus rhamnosus*. AMB Express, *7*(1). https://doi.org/10.1186/s13568-017-0442-x

Anwer, M. K., Al-Shdefat, R., Ezzeldin, E., Alshahrani, S. M., Alshetaili, A. S., & Iqbal, M. (2017). Preparation, evaluation, and bioavailability studies of Eudragit coated PLGA nanoparticles for sustained release of eluxadoline for the treatment of irritable bowel syndrome. Front. Pharmacol, 8(Nov). https://doi.org/10.3389/fphar.2017.00844

Bazdaric, K., Sverko, D., Salaric, I., Martinović, A., & Lucijanic, M. (2021). The abc of linear regression analysis: What every author and editor should know. Eur. Sci. Ed, 47. https://doi.org/10.3897/ese.2021.e63780

Beloqui, A., Solinís, M. Á., Gascón, A. R., Del Pozo-Rodríguez, A., Des Rieux, A., & Préat, V. (2013). Mechanism of transport of saquinavir-loaded nanostructured lipid carriers across the intestinal barrier. J. Contr. Release, 166(2), 115–123. https://doi.org/10.1016/j.jconrel.2012.12.021

Benouis, K., Alami, A., Khalfi, Y., Guella, S., & Khane, Y. (2022). Optimization of coagulation parameters for turbidity removal using box-behnken model. Proceedings of the 2nd international conference on industry 4.0 and Artificial Intelligence (ICIAI 2021), 175. https://doi.org/10.2991/aisr.k.220201.021

Bhagyaraj, S., & Krupa, I. (2020). Alginate-mediated synthesis of hetero-shaped silver nanoparticles and their hydrogen peroxide sensing ability. Molecules, 25(3). https://doi.org/10.3390/molecules25030435

Cautela, M. P., Moshe, H., Sosnik, A., Sarmento, B., & das Neves, J. (2019). Composite films for vaginal delivery of tenofovir disoproxil fumarate and emtricitabine. Eur. J. Pharm Biopharm, *138*, 3–10. https://doi.org/10.1016/j.ejpb.2018.02.001

Cazorla-Luna, R., Martín-Illana, A., Notario-Pérez, F., Miguel Bedoya, L., Tamayo, A., Ruiz-Caro, R., Rubio, J., & Veiga, M. D. (2020). Vaginal polyelectrolyte layer-by-layer films based on chitosan derivatives and eudragit® S100 for pH responsive release of tenofovir. Mar. Drugs, 18(1). https://doi.org/10.3390/md18010044

Chawla, A., Sharma, P., & Pawar, P. (2012). Eudragit S-100 coated sodium alginate microspheres of naproxen sodium: formulation, optimization, and *in vitro* evaluation. Acta Pharm, 62(4), 529–545. https://doi.org/10.2478/v10007-012-0034-x

Choukaife, H., Doolaanea, A. A., & Alfatama, M. (2020). Alginate nanoformulation: Influence of process and selected variables. In Pharm. 13(11), 1–35. MDPI AG. https://doi.org/10.3390/ph13110335

Corsi, F., Sorrentino, L., Mazzucchelli, S., Truffi, M., Capetti, A., Rizzardini, G., & Fiandra, L. (2016). Antiretroviral therapy through barriers: a prominent role for nanotechnology in HIV-1 eradication from sanctuaries. *4*, 328–339. https://doi.org/10.17265/2328-2150/2016.07.007

Daemi, H., & Barikani, M. (2012). Synthesis and characterization of calcium alginate nanoparticles, sodium homopolymannuronate salt and its calcium nanoparticles. Sci. Iran, 19(6), 2023–2028. https://doi.org/10.1016/j.scient.2012.10.005

Das, M. K., & Chakraborty, T. (2015). Progress in brain delivery of Anti-HIV drugs. J. Appl. Pharm. Sci, 5(7), 154–164. https://doi.org/10.7324/JAPS.2015.50724

De Clercq, E. (2016). Tenofovir alafenamide (TAF) as the successor of tenofovir disoproxil fumarate (TDF). Biochem Pharmacol, 119, 1–7. https://doi.org/10.1016/j.bcp.2016.04.015

De Leo, V., Di Gioia, S., Milano, F., Fini, P., Comparelli, R., Mancini, E., Agostiano, A., Conese, M., & Catucci, L. (2020). Eudragit s100 entrapped liposome for curcumin delivery: anti-oxidative effect in Caco-2 cells. Coat. J, 10(2). https://doi.org/10.3390/coatings10020114

Derkach, S. R., Voron'ko, N. G., Sokolan, N. I., Kolotova, D. S., & Kuchina, Y. A. (2020). Interactions between gelatin and sodium alginate: UV and FTIR studies. J Disper Sci Technol, 41(5), 690–698. https://doi.org/10.1080/01932691.2019.1611437

Ding, Y., Dou, C., Chang, S., Xie, Z., Yu, D. G., Liu, Y., & Shao, J. (2020). Core-shell eudragit S100 nanofibers preparedvia triaxial electrospinning to providea colon-targeted extended drug release. Polym. J, 12(9). https://doi.org/10.3390/POLYM12092034

El-Houssiny, A. S., Ward, A. A., Mostafa, D. M., Abd-El-Messieh, S. L., Abdel-Nour, K. N., Darwish, M. M., & Khalil, W. A. (2016). Drug-polymer interaction between glucosamine sulfate and alginate nanoparticles: FTIR, DSC and dielectric spectroscopy studies. Adv Nat Sci: Nanosci, *7*(2). https://doi.org/10.1088/2043-6262/7/2/025014

El-Sheikh, S. M., Barhoum, A., El-Sherbiny, S., Morsy, F., El-Midany, A. A. H., & Rahier, H. (2019). Preparation of superhydrophobic nanocalcite crystals using Box–Behnken design. Arab. J. Chem, 12(7), 1479–1486. https://doi.org/10.1016/j.arabjc.2014.11.003

Eltaweil, A. S., Mamdouh, I. M., Abd El-Monaem, E. M., & El-Subruiti, G. M. (2021). Highly Efficient Removal for Methylene Blue and Cu2+onto UiO-66 Metal-Organic Framework/Carboxylated Graphene Oxide-Incorporated Sodium Alginate Beads. ACS Omega. https://doi.org/10.1021/acsomega.1c03479

Foster, C., Lyall, H., Olmscheid, B., Pearce, G., Zhang, S., & Gibb, D. M. (2009). Tenofovir disoproxil fumarate in pregnancy and prevention of mother-to-child transmission of HIV-1: Is it time to move on from zidovudine? In HIV Med 10 (7), 397–406. https://doi.org/10.1111/j.1468-1293.2009.00709.x

Hu, D., Liu, L., Chen, W., Li, S., & Zhao, Y. (2012). A novel preparation method for 5-aminosalicylic acid loaded eudragit S100 nanoparticles. Int. J. Mol Sci, 13(5), 6454–6468. https://doi.org/10.3390/ijms13056454

Huda, A., Lim, K. W., Jayanthi, B., Palsan, S. A., Huda, M. A. S. N., Leony, T. Y. S., Ariff, A. L. Z., & Amizi, A. M. (2021). Optimization of rhodamine 6G removal from aqueous solution using box-behnken design. AIP Conference Proceedings, 2347. https://doi.org/10.1063/5.0052681

Human, C., De Beer, D., Bowles, S., & Joubert, E. (2022). Effect of electrospraying conditions on the properties of aspalathin-Eudragit S100 nanoparticles and assessment of orogastrointestinal stability and membrane permeability. Food Front., 3(2), 285–299. https://doi.org/10.1002/fft2.131

Irvin-Choy, N. S., Nelson, K. M., Gleghorn, J. P., & Day, E. S. (2020). Design of nanomaterials for applications in maternal/fetal medicine. In J. Mater. Chem B 8(31) 6548–6561. Royal Society of Chemistry. https://doi.org/10.1039/d0tb00612b

Jana, S., Kumar Trivedi, M., & Tallapragada, R. M. (2015). Characterization of physicochemical and thermal properties of chitosan and sodium alginate after biofield treatment. Pharm. Anal. Acta, 6(10). https://doi.org/10.4172/2153-2435.1000430

Jegan, J., Praveen, S., Kumar, B. M., Pushpa, T. B., & Gokulan, R. (2021). Box–behnken experimental design for the optimization of basic violet 03 dye removal by groundnut shell derived biochar. Desalin Water Treat., 209, 379–391. https://doi.org/10.5004/dwt.2021.26495

Jat, R., Jain, S., Singh, S. K., & Gupta, R. (n.d.). Formulation and In Vitro-In Vivo Evaluation of Quercetin Loaded Eudragit S100 Microspheres. In AJP, 12(1).

Joshy, K. S., George, A., Jose, J., Kalarikkal, N., Pothen, L. A., & Thomas, S. (2017). Novel dendritic structure of alginate hybrid nanoparticles for effective anti-viral drug delivery. Int. J. Biol. Macromol, 103, 1265–1275. https://doi.org/10.1016/j.ijbiomac.2017.05.094

Karmoker, J., Hasan, I., Ahmed, N., Saifuddin, M., & Selim Reza, M. (2018). Development and optimization of acyclovir loaded mucoadhesive microspheres by box-behnken design. J. Pharm. Sci. 18(1)

Kianersi, S., Solouk, A., Saber-Samandari, S., Keshel, S. H., & Pasbakhsh, P. (2021). Alginate nanoparticles as ocular drug delivery carriers. J. Drug Deliv. Technol, 66. https://doi.org/10.1016/j.jddst.2021.102889

Kumar, S., Bhanjana, G., Sharma, A., Sidhu, M. C., & Dilbaghi, N. (2014). Synthesis, characterization and on field evaluation of pesticide loaded sodium alginate nanoparticles. Carbohydr. Polym, 101(1), 1061–1067. https://doi.org/10.1016/j.carbpol.2013.10.025

Kumar, S., Bhanjana, G., Verma, R. K., Dhingra, D., Dilbaghi, N., & Kim, K. H. (2017). Metformin-loaded alginate nanoparticles as an effective antidiabetic agent for controlled drug release. J. Pharm. Pharmacol, 69(2), 143–150. https://doi.org/10.1111/jphp.12672

Menezes, V., Malek, A., & A. Keelan, J. (2012). Nanoparticulate drug delivery in pregnancy: placental passage and fetal exposure. Curr Pharm Biotechnol, 12(5), 731–742. https://doi.org/10.2174/138920111795471010

Mehta, R., Chawla, A., Sharma, P., & Pawar, P. (2013). Formulation and in vitro evaluation of Eudragit S-100 coated naproxen matrix tablets for colon-targeted drug delivery system. JAPTR, 4(1), 31–41. https://doi.org/10.4103/2231-4040.107498

Meng, J., Agrahari, V., Ezoulin, M. J., Purohit, S. S., Zhang, T., Molteni, A., Dim, D., Oyler, N. A., & Youan, B. B. C. (2017). Spray-dried thiolated chitosan-coated sodium alginate multilayer microparticles for vaginal HIV microbicide delivery. AAPS J, 19(3), 692–702. https://doi.org/10.1208/s12248-016-0007-y

Mujtaba, M. A., & Alotaibi, N. M. (2020). Chitosan-sodium alginate nanoparticle as a promising approach for oral delivery of rosuvastatin calcium: formulation, optimization and *in vitro* Characterization. J. Pharm. Res. Int, 50–56. https://doi.org/10.9734/jpri/2020/v32i130394

Nair, R. M., Bindhu, B., & L, R. V. (n.d.). A polymer blend from Gum Arabic and Sodium Alginate - preparation and characterization. J. Polym. Res. (2020) 27: 154. https://doi.org/10.1007/s10965-020-02128-y/Published

Ngema, L. M., Adeyemi, S. A., Marimuthu, T., Ubanako, P., Wamwangi, D., & Choonara, Y. E. (2022). Synthesis of novel conjugated linoleic acid (CLA)-coated superparamagnetic iron oxide nanoparticles (SPIONs) for the delivery of paclitaxel with enhanced *in vitro* anti-proliferative activity on A549 lung cancer cells. Pharm, 14(4). https://doi.org/10.3390/pharmaceutics14040829

Nunes, R., Bogas, S., Faria, M. J., Gonçalves, H., Lúcio, M., Viseu, T., Sarmento, B., & Das Neves, J. (n.d.). Electrospun fibers for vaginal administration of tenofovir disoproxil fumarate and 1 emtricitabine in the context of topical pre-exposure prophylaxis. https://doi.org/10.1101/2021.02.01.429162

Olojede, S. O., Lawal, S. K., Dare, A., Naidu, E. C. S., Rennie, C. O., & Azu, O. O. (2022). Evaluation of tenofovir disoproxil fumarate loaded silver nanoparticle on testicular morphology in experimental type-2 diabetic rats. Artif. Cells Nanomed. Biotechnol, 50(1), 71–80. https://doi.org/10.1080/21691401.2022.2042009

Pathak, A., Khandegar, V., & Kumar, A. (2022). Statistical investigation in conjunction with a box–behnken design for the removal of dyes using electrocoagulation. J. Hazard. Toxic Radioact. Waste, 26(2). https://doi.org/10.1061/(asce)hz.2153-5515.0000679

Pokharkar, V. B., Jolly, M. R., & Kumbhar, D. D. (2015). Engineering of a hybrid polymer-lipid nanocarrier for the nasal delivery of tenofovir disoproxil fumarate: Physicochemical, molecular, microstructural, and stability evaluation. Eur. J. Pharm. Sci, 71, 99–111. https://doi.org/10.1016/j.ejps.2015.02.009

Politi, F. A. S., Carvalho, S. G., Rodero, C. F., dos Santos, K. P., Meneguin, A. B., Sorrechia, R., Chiavacci, L. A., & Chorilli, M. (2023). Piperine-loaded nanoparticles incorporated into hyaluronic acid/sodium alginate-based membranes for the treatment of inflammatory skin diseases. Int. J. Biol. Macromol, 227, 736–748. https://doi.org/10.1016/j.ijbiomac.2022.12.147

Raffin, R. P., Colomé, L. M., Pohlmann, A. R., & Guterres, S. S. (2006). Preparation, characterization, and in vivo anti-ulcer evaluation of pantoprazole-loaded microparticles. Eur J Pharm Biopharm, 63(2), 198–204. https://doi.org/10.1016/j.ejpb.2006.01.013

Reis Machado, J., Da Silva, M. V., Cavellani, C. L., Antônia Dos Reis, M., Monteiro, M. L. G. D. R., Teixeira, V. D. P. A., & Rosa Miranda Corrêa, R. (2014). Mucosal immunity in the female genital tract, HIV/AIDS. In Biomed Res. Int. Hindawi Limited. https://doi.org/10.1155/2014/350195

Reis, S. D. S., Quintanilha Junior, V. D. S., Boto, G. D. S., Da Silva, T. M., Macedo, E. V., Peregrino, C. A. de F., Mourão, S. C., & De Araújo, E. M. (2021). Use of Box–behnken design for optimization of compounded medication: acyclovir capsules report. Drug Anal. Res, 5(1) 59-67.

Saraf, A., Dubey, N., Dubey, N., & Sharma, M. (2019). Box behnken design-based development of curcumin loaded eudragit s100 nanoparticles for site-specific delivery in colon cancer. RJPT, 12(8), 3672–3678. https://doi.org/10.5958/0974-360X.2019.00627.9

Sarma, A., & Das, M. K. (2019). Formulation by design (FbD) approach to develop tenofovir disoproxil fumarate loaded nanostructured lipid carriers (NLCs) for the aptness of nose to brain delivery. J. Drug Deliv. Ther, 9(2), 148–159. https://doi.org/10.22270/jddt.v9i2.2391

Sarmento, B., Ferreira, D., Veiga, F., & Ribeiro, A. (2006). Characterization of insulin-loaded alginate nanoparticles produced by ionotropic pre-gelation through DSC and FTIR studies. Carbohydr Polym, 66(1), 1–7. https://doi.org/10.1016/j.carbpol.2006.02.008

Schafroth, N., Arpagaus, C., Jadhav, U. Y., Makne, S., & Douroumis, D. (2012). Nano and microparticle engineering of water insoluble drugs using a novel spray-drying process. Colloids Surf. B Biointerfaces, 90(1), 8–15. https://doi.org/10.1016/j.colsurfb.2011.09.038

Shailender, J., Ravi, P. R., Saha, P., Dalvi, A., & Myneni, S. (2017). Tenofovir disoproxil fumarate loaded PLGA nanoparticles for enhanced oral absorption: effect of experimental variables and *in vitro*, *ex vivo* and *in vivo* evaluation. Colloids Surf. B Biointerfaces, 158, 610–619. https://doi.org/10.1016/j.colsurfb.2017.07.037

Sharma, M., Sharma, V., Panda, A. K., & Majumdar, D. K. (2011). Development of enteric submicron particle formulation of papain for oral delivery. Int J Nanomedicine, 6, 2097–2111. https://doi.org/10.2147/ijn.s23985

Shen Shihoong, Wu Youshen, L. Y. and W. D. (2017). High drug-loading nanomedicines: progress, current status, and prospects. Int J Nanomedicine, 12, 4085–4109.

Sibanda, W., & Pretorius, P. (2013). Comparative study of the application of central composite face-centred (CCF) and Box–Behnken designs (BBD) to study the effect of demographic characteristics on HIV risk in South Africa. Netw Model Anal Health Inform Bioinforma (2013) 2:137–146. https://doi.org/10.1007/s13721-013-0032-z

Siddaramaiah, Swamy, T. M. M., Ramaraj, B., & Lee, J. H. (2008). Sodium alginate and its blends with starch: thermal and morphological properties. J. Appl. Polym. Sci, 109(6), 4075–4081. https://doi.org/10.1002/app.28625

Silva, A. E., Oliveira, E. E., Gomes, M. C. S., Marcelino, H. R., Silva, K. C. H., Souza, B. S., Nagashima, T., Ayala, A. P., Oliveira, A. G., & Egito, E. S. T. Do. (2013). Producing xylan/Eudragit® S100-based microparticles by chemical and physico-mechanical approaches as carriers for 5-aminosalicylic acid. J. Microencapsul, 30(8), 787–795. https://doi.org/10.3109/02652048.2013.788087

Soares, J. P., Santos, J. E., Chierice, G. O., & G Cavalheiro, E. T. (2004). Thermal behavior of alginic acid and its sodium salt. Ecl. Quím., São Paulo, 29(2): 53-56. www.scielo.br/eq

Sonje, A., & Chandra, A. (2013). Comprehensive review on eudragit polymer. Int. Res. J. Pharm, 4(5), 71–74. https://doi.org/10.7897/2230-8407.04515

Spadari, C. de C., de Bastiani, F. W. M. da S., Lopes, L. B., & Ishida, K. (2019). Alginate nanoparticles as non-toxic delivery system for miltefosine in the treatment of candidiasis and cryptococcosis. Int J Nanomedicine, 14, 5187–5199. https://doi.org/10.2147/IJN.S205350

Singh, S., Neelam., Arora, S., Singla, Y. P. (2015). An overview of multifaceted significance of eudragit polymers in drug delivery systems. Asian J Pharm Clin Res, 8(5), 1-6

Sivakumar, D. (2013). Application of Box Behnken design to optimize the parameters for turning Inconel 718 using coated carbide tools. Int. J. Sci. Eng. Res, 4(4), 620-642. http://www.ijser.org

Takalani, F., Kumar, P., Kondiah, P. P. D., Choonara, Y. E., & Pillay, V. (2020). Lipid–drug conjugates and associated carrier strategies for enhanced antiretroviral drug delivery. In Pharm Dev Technol, 25(3), 267–280. Taylor and Francis Ltd. https://doi.org/10.1080/10837450.2019.1694037

Thakral, S., Thakral, N. K., & Majumdar, D. K. (2013). Eudragit®: A technology evaluation. In Expert Opin. Drug Deliv, 10 (1), 131–149. https://doi.org/10.1517/17425247.2013.736962

Thomas, D., Kurien Thomas, K., & Latha, M. S. (2020). Preparation and evaluation of alginate nanoparticles prepared by green method for drug delivery applications. Int. J. Biol. Macromol, 154, 888–895. https://doi.org/10.1016/j.ijbiomac.2020.03.167

Thomas, D., Mathew, N., & Nath, M. S. (2021). Starch modified alginate nanoparticles for drug delivery application. Int. J. Biol. Macromol, 173, 277–284. https://doi.org/10.1016/j.ijbiomac.2020.12.227

Vlaia, L., Coneac, G., Muţ, A. M., Olariu, I., Vlaia, V., Anghel, D. F., Maxim, M. E., Dobrescu, A., Hîrjău, M., & Lupuleasa, D. (2021). Topical biocompatible fluconazole-loaded microemulsions based on essential oils and sucrose esters: formulation design based on pseudo-ternary phase diagrams and physicochemical characterization. Processes, 9(1), 1–21. https://doi.org/10.3390/pr9010144

Wang, H., Chen, X., Wen, Y., Li, D., Sun, X., Liu, Z., Yan, H., & Lin, Q. (2022). A Study on the correlation between the oxidation degree of oxidized sodium alginate on its degradability and gelation. Polym J, 14(9). https://doi.org/10.3390/polym14091679

Yetilmezsoy, K., Demirel, S., & Vanderbei, R. J. (2009). Response surface modeling of Pb (II) removal from aqueous solution by Pistacia vera L.: Box-Behnken experimental design. J. Hazard. Mater, 171(1–3), 551–562. https://doi.org/10.1016/j.jhazmat.2009.06.035

Yoo, J. W., Giri, N., & Lee, C. H. (2011). PH-sensitive Eudragit nanoparticles for mucosal drug delivery. Int. J. Pharm, 403(1–2), 262–267. https://doi.org/10.1016/j.ijpharm.2010.10.032

Yusuf, H., Rahmawati, R. A., Rijal, M. A. S., & Isadiartuti, D. (2021). Curcumin micelles entrapped in eudragit S-100 matrix: A synergistic strategy for enhanced oral delivery. Future. Sci. OA, *7*(4). https://doi.org/10.2144/fsoa-2020-0131

Zhang, T., Sturgis, T. F., & Youan, B. B. C. (2011). PH-responsive nanoparticles releasing tenofovir intended for the prevention of HIV transmission. Eur J Pharm Biopharm, 79(3), 526–536. https://doi.org/10.1016/j.ejpb.2011.06.007

Zhang, T., Zhang, C., Agrahari, V., Murowchick, J. B., Oyler, N. A., & Youan, B. B. C. (2013). Spray drying tenofovir loaded mucoadhesive and pH-sensitive microspheres intended for HIV prevention. Antivir. Res, 97(3), 334–346. https://doi.org/10.1016/j.antiviral.2012.12.019

Zimet, P., Mombrú, Á. W., Faccio, R., Brugnini, G., Miraballes, I., Rufo, C., & Pardo, H. (2018). Optimization and characterization of nisin-loaded alginate-chitosan nanoparticles with antimicrobial activity in lean beef. LWT, 91, 107–116. https://doi.org/10.1016/j.lwt.2018.01.015

CHAPTER 4

Characterization, and *in vitro* drug release studies of alginate-ES100 nanoparticles loaded with tenofovir disoproxil fumarate within the film matrix

4.1 Introduction

Studies of the tenofovir disoproxil fumarate (TDF) drug loaded into nanoparticles and further incorporated into vaginal delivery systems have been reported for antiviral protection (Zhang et al., 2011; Cautela et al., 2019; Sarma & Das, 2019;). Polymeric nanoparticles, liposomes, dendrimers, and inorganic nanoparticles are some nanoparticles investigated for use in the female genital tract, while vaginal implants successfully developed include intravaginal films, intravaginal rings, and gels (Ghosal et al., 2016; Misra & Shahiwala, 2020; Takalani et al., 2020; Notario-Pérez et al., 2021; Pritchard et al., 2021). Among these implants, it has been demonstrated that vaginal films offer a broader timeframe of protection against HIV transmission. Moreover, the advantages of vaginal films encompass reduced or no leakage during usage and discreetness (Notario-Pérez et al., 2021).

Adhering to the LDCs approach, TDF is a phosphonate prodrug, which relies on a unique metabolic pathway to deliver its active form, tenofovir-DP. Therefore, the prodrug moieties of TDF undergo sequential removal through the action of esterases and subsequent spontaneous degradation of the hemiacetal intermediate, thereby delivering tenofovir. Thus, tenofovir only requires two phosphorylation steps (AMP-kinase) to produce active tenofovir-DP (Amblard et al., 2022). Nonetheless, despite the fact that LDCs, similar to TDF, can be administered without a delivery carrier, they are typically integrated into suitable delivery systems, specifically polymeric (alginate) and synthetic (ES100) nanoparticles in this study. It is noteworthy that among the ARV medications that have been developed to date, only TDF and TAF have been approved by the FDA as lipidic prodrugs (Amblard et al., 2022).

Despite the existence of numerous reports on LDCs, there has been no comprehensive treatment for HIV infections that has been presented centered on the aspects of this technology (Adhikari et al. 2017). In this chapter, TDF-loaded alginate-ES100 nanoparticles were further incorporated into the HPMC films for continued characterization and *in vitro* drug release analyses. Since the recommended dosage regimen of TDF is taken once daily (Spinks et al., 2017), this chapter was aimed at developing a novel long-lasting delivery system for vaginal use. The films were analyzed using SEM, FTIR, DSC, and *in vitro* drug release methods.

4.2 Materials and methods

4.2.1 Materials

Sodium alginate (low molecular weight), HPMC (2% viscosity in H_20), ES100, calcium chloride, and methanol were purchased from Sigma-Aldrich (St. Louis, Missouri, USA) whereas the TDF drug was purchased from Leap Chem (Easey Com BLDG 253-261, Hong Kong). Components of the simulated vaginal fluid (SVF) such as glucose, sodium chloride, lactic acid, potassium hydroxide, glacial acetic acid, urea, calcium hydroxide and glycerin were also purchased from Sigma–Aldrich (St. Louis, Missouri, USA).

4.2.2 Preparation of Alg-ES100 nanoparticles and films

4.2.2.1 Alg-ES100 nanoparticles

The optimal nanoparticle formulation was prepared using the emulsion/gelation complexation method described previously (Takalani et al., 2024). Briefly, 106.368 mg of ES100 and 60 mg of the TDF drug were dispersed in 5 mL of methanol under the magnetic stirrer to form a 2% ES100 solution. Subsequently, a concentration of 126.266 mg of alginate was separately dissolved in 15 mL of distilled water, resulting in a solution containing 0.8% alginate. These two solutions were mixed under the magnetic stirrer for 5 min, then further sonicated for 5 min to create an emulsion. Thereafter, the resultant emulsion was added dropwise to a 0.04% $CaCl_2$ solution under the magnetic stirrer at a stirring speed of 1.5 RPM. The mixture was allowed to stir for 1 h under the fume hood to evaporate methanol. Nanoparticles were collected by centrifugation for 10 min at 12100 RPM. The ultimate step involved freezing the suspension overnight and lyophilizing it at -37 °C for 12 h. The experiment was conducted in triplicate.

4.2.2.2 Film preparation

The films were prepared using the casting method described by De Moura and co-workers (De Moura et al., 2008). For this purpose, different weights of HPMC powder (0.6 g, 1.5 g, and 2.1 g) were dissolved in 60 mL of distilled water and stirred for 12 h to form 1%, 2.5%, and 3.5% HPMC solutions, respectively. The prepared nanoparticle powders were then dispersed into each HPMC solution and stirred for 15 min to achieve a homogeneous mixture. Thereafter, the mixtures were left to settle for an hour to eliminate air bubbles. Subsequently, the mixtures were poured into glass petri dishes (90 mm × 60 mm) for casting purposes. Then, the petri dishes were left to dry in the fume hood at ambient temperature for a duration of 24 h. Finally, the dried films were placed in sealed plastic bags and placed into the desiccator for

further analysis. To prepare control films, the same preparation steps were followed, except that the TDF drug was not added.

4.2.3 Scanning electron microscope

SEM (JEOL JSM, Tokyo, Japan) was used to study the surface morphology of TDF-loaded nanoparticles in films at different concentrations (1%, 2.5% and 3.5%). This was performed at an acceleration beam voltage of 15 keV. Before visualization, samples were mounted on aluminum stubs using carbon tapes and coated with gold-palladium. Magnifications of 60 000X were used.

4.2.4 In vitro drug release for TDF-loaded nanoparticles in films

The release profiles of TDF from TDF-loaded films were carried out as described previously (Notario-Pérez et al., 2021). Herein, the simulated vaginal fluid (SVF, pH 4.2) was used as the release media to maintain sink conditions for TDF. Briefly, three 2 × 2 cm^2 shaped films for each formulation (1%, 2.5% and 3.5%) were immersed in 100 mL glass bottles containing 50 mL of the SVF buffer. These bottles were placed in an orbital shaker at 37 °C with a stirring rate of 25 rpm. Then, at predetermined time intervals (1, 3, 6, 9, 12, 24, 48, 72 & 96 h), 2 mL of the release medium was withdrawn and immediately replaced by a fresh release medium. Amounts of TDF released from the samples were quantified at wavelength 265 using a UV-visible spectrophotometer, and the results were presented as the cumulative percentage of released compound versus time. The standard curve equation for the TDF drug was Y= 0.0192x (R^2=0.9999).

4.2.5 Fourier transform infrared spectroscopy

To identify the potential chemical interfaces between TDF-loaded alginate-ES100 nanoparticles and the HPMC polymer, a spectral research review of FTIR was conducted using the ATR-FTIR spectrophotometer (PerkinElmer 100, Llantrisant, Wales, UK). A PerkinElmer Spectrum 2000 was used to process film samples after they were positioned on a diamond crystal. The FTIR conditions were as outlined: 24 scans with a resolution of 4 cm^{-1} and a wavelength range of 4000 to 650 cm^{-1}.

4.2.6 Differential Scanning Calorimetry

To investigate the thermodynamic compatibility between the TDF-loaded alginate-ES100 nanoparticles and the HPMC polymer, the DSC technique (Mettler Toledo, STARe System, Swchwerzenback, ZH, Switzerland) was employed. The instrument operated at 10 degrees per minute in an atmosphere of nitrogen gas. Samples ranging from 3 to 10 mg were weighed,

sealed in aluminum vessels, and subjected to screening at temperatures ranging from 10 to 350 °C. The DSC graphs were presented as the flow of heat versus temperature.

4.3 Results and Discussion

4.3.1 The scanning electron microscope images depicting the optimized alginate-ES100 nanoparticles incorporated into HPMC films

Alginate-ES100 nanoparticles in the HPMC matrix were uniformly distributed, as shown in Figure 4.1. Although, with increasing concentrations of the HPMC, the degree of porosity decreased. Thus, the 1% film exhibited a significant degree of porosity in comparison to the 2.5% and 3.5% compact films. These findings substantiate the efficacy of the technique employed for the preparation of cast films, resulting in properties that are appropriate for various uses (de Moura et al., 2012). According to Pitpisutkul & Prachayawarakorn (2022), the salting out of the sodium salts of alginate nanoparticles in HPMC solution could have influenced the porous structures (Pitpisutkul & Prachayawarakorn, 2022). The incorporation of sodium salts may facilitate the separation of solid-liquid phases in HPMC solutions during drying, resulting in HPMC-based microporous films following water evaporation(Pitpisutkul & Prachayawarakorn, 2022).

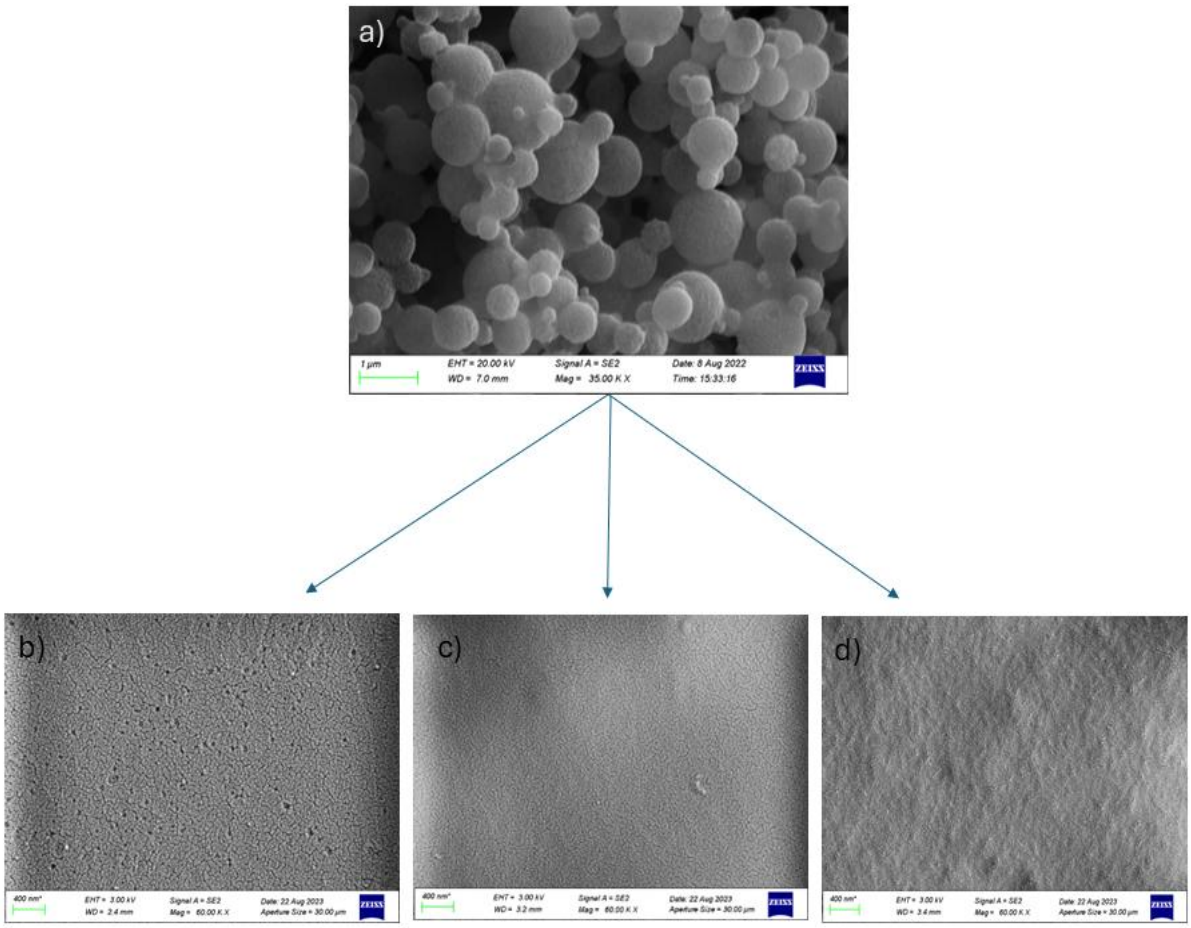


Figure 4.1. Scanning electron microscope of the optimized TDF-loaded nanoparticles (a) in HPMC films at different concentrations: (b) 1%, (c) 2.5 % and (d) 3.5 %. Film images were taken at a scale of 400 nm whereas nanoparticles were taken at a scale of 1 µm

4.3.2 *In vitro* drug release for alginate-ES100 nanoparticles in HPMC films

Figure 4.2 illustrates the release profiles of TDF-loaded nanoparticles in HPMC at various concentrations (1%, 2.5% and 3.5%). All films were sustained for up to 96 h, which supports the statement reported previously that films prepared with water dissolve slowly (de Moura et al., 2012). The Eudragit-based films are also associated with a slower drug release, compared to other films (Notario-Pérez et al., 2021). Out of the three films designed, the 2.5% film achieved the highest maximum release of 54%. The acidic environment of SVF could have been responsible for this, as films can only release a small amount of the drug (Notario-Pérez et al., 2021). The reason for this is that film-forming agents, particularly HPMC, are stable in the pH range of 3-11 (Milinković and Đekić, 2024). Additionally, HPMC contains moderate bioadhesive properties within a concentration range from 2% to 20%, making it suitable for controlled or delayed drug release applications (Milinković and Đekić, 2024). Lastly, incorporating alginate-ES100 nanoparticles into the HPMC film during synthesis resulted in a

higher sustained release, as polymer compositions can significantly impact properties of the film, such as mechanical strength and disintegration time (Garg et al., 2010). Consequently, this can affect the drug release rate. Thus, films based on 100% HPMC have previously been developed, and they had a high swelling index and disintegrated within 60 minutes. Therefore, they were considered unsuitable for the required long-time drug release purposes (Calvo et al., 2021).

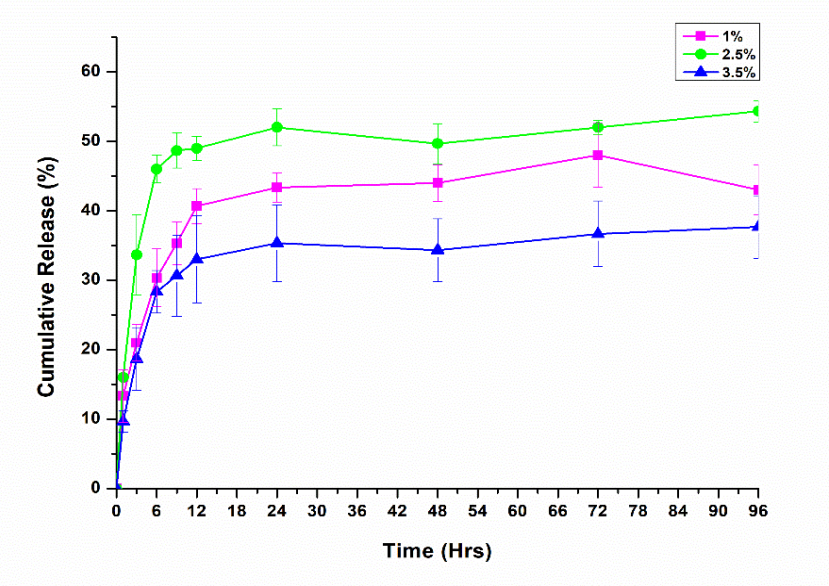


Figure 4.2. The cumulative *in vitro* release of TDF-loaded nanoparticles in HPMC film with concentrations of 1%, 2.5%, and 3.5% in simulated vaginal fluid (SVF) at pH 4.2. The release was sustained for up to 96 h

4.3.3 Fourier transform infrared spectroscopy of TDF-loaded alginate-ES100 nanoparticles in film

As shown in Figure 4.3, the HPMC spectrum shows a characteristic broad peak at 3434 cm^{-1} due to the stretching vibration of (–OH) and the intermolecular hydrogen bonding. It also shows a peak at 1062 cm^{-1}, which represents stretching vibration of (C–O) (Darwesh et al., 2024). However, the absorption band experienced a slight decrease from 3434 cm^{-1} for the HPMC polymer to 3422.93 cm^{-1} for the HPMC with nanoparticles. This implies that TDF-loaded nanoparticles interacted with the HPMC polymer via the medium stretching of the N-H bond. Another slight shift from 1050.75 cm^{-1} to 1050.98 cm^{-1} confirms that TDF-loaded nanoparticles interact with the HPMC polymer through a strong anhydride bond (Takalani et al., 2024). These results support the successful incorporation of TDF-loaded nanoparticles into the HPMC polymer.

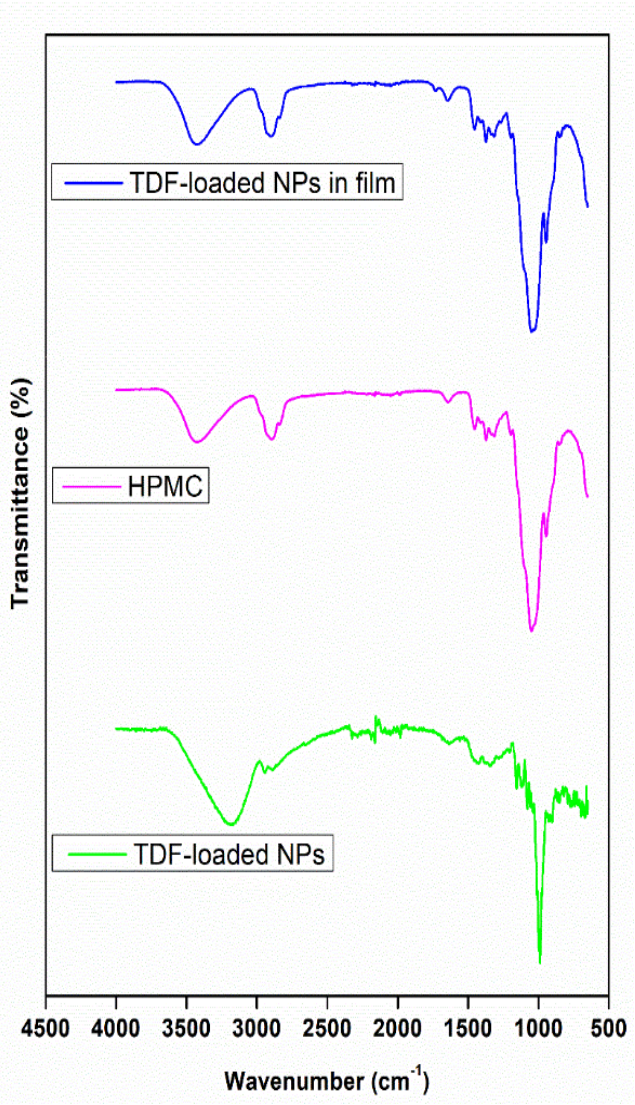


Figure 4.3. Fourier transform infrared spectra of TDF-loaded nanoparticles, HPMC, and TDF-loaded nanoparticles in film

4.3.4 Differential scanning calorimetry of TDF-loaded alginate-ES100 nanoparticles in film

The inert HPMC film was observed to have a thermal stability up to 300 °C, as previously reported (Porfirio et al., 2015). Then, from this temperature, thermal decomposition events began, which could be attributed to the characteristic of the polymer. The disappearance of endothermic peaks at 164.93 °C and 304 °C in TDF-loaded NPS in film supports the conclusion that TDF-loaded nanoparticles were successfully incorporated within the HPMC polymer during the synthesis (Porfirio et al., 2015; Jayaramudu et al., 2021), depicted in Figure 4.4. Thus, the heat transfer/melting temperature in HPMC was enhanced by nanoparticles and HPMC polymer chains were broken more readily in the presence of TDF-loaded nanoparticles. This confirms that HPMC has good biocompatibility with both natural and synthetic polymers, as reported previously (Pitpisutkul & Prachayawarakorn, 2022).

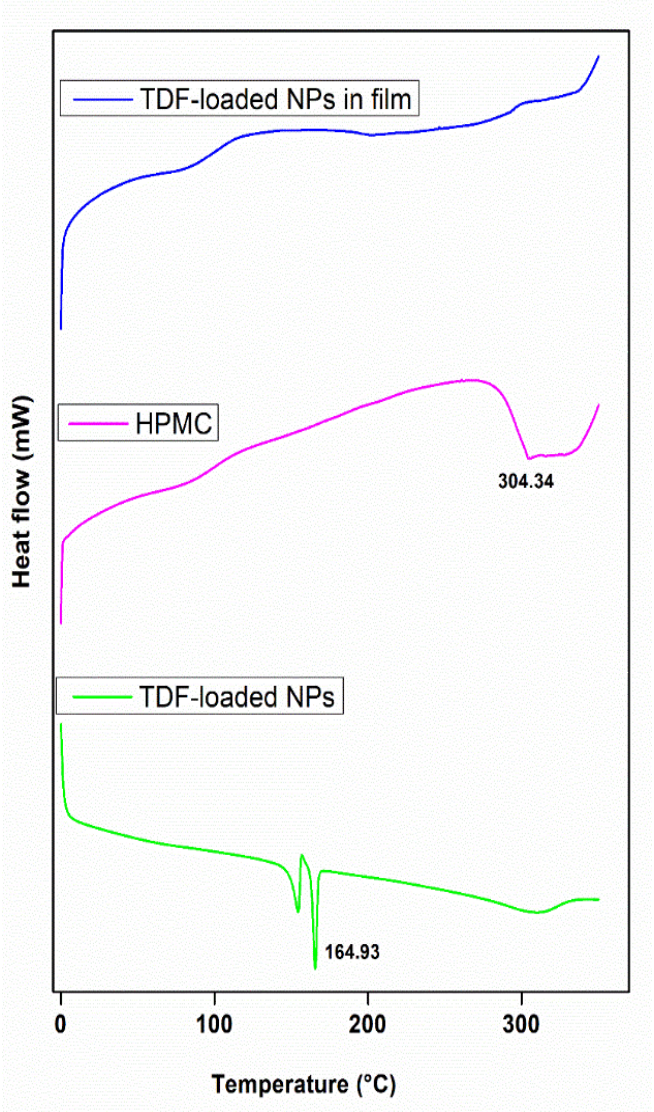


Figure 4.4: Differential scanning calorimetry thermograms of TDF-loaded nanoparticles, HPMC, and TDF-loaded nanoparticles in film

4.4 Concluding remarks

This chapter describes the successful loading of the lipidic prodrug (TDF) into alginate-eudragit S100 nanoparticles, which were then incorporated into the HPMC films for vaginal use. The film delivery system demonstrated that the release lasted for 96 hours at a pH of 4.2, which corresponds to the vaginal pH. As per the SEM images, the films exhibited significant levels of porosity and compactness. A novel and potent anhydride bond was formed when alginate and ES100 interacted via the ester C=O amide stretching, according to FTIR results. HPMC was additionally adhered to this anhydride bond, and the DSC results confirmed the successful incorporation of TDF-loaded nanoparticles into the HPMC matrix.

4.5 References

Adhikari, P., Pal P, Das KA, Ray S, Bhattacharjee A, Mazumder B. (2017). Nano lipid-drug conjugate: an integrated review. Int J Pharm, 529(1–2):629–641

Amblard, F., Patel D, Michailidis E, Coats S.J, Kasthuri M, Biteau N, Tber Z, Ehteshami M, Schinazi R.F. (2022). HIV nucleoside reverse transcriptase inhibitors. Eur. J. Med. Chem, 240 (2022) 114554

Calvo, N.L., Tejada, G., Svetaz, L.A., Quiroga, A.D., Alvarez, V.A., Lamas, M.C., Leonardi, D. (2021). Development and optimization of a new tioconazole vaginal mucoadhesive film using an experimental design strategy. Physicochemical and biological characterization. J. Pharm. Biomed. Anal. https://doi.org/10.1016/j.jpba.2021.114303

Cautela, M. P., Moshe, H., Sosnik, A., Sarmento, B., & das Neves, J. (2019). Composite films for vaginal delivery of tenofovir disoproxil fumarate and emtricitabine. Eur J Pharm Biopharm, 138, 3–10. https://doi.org/10.1016/j.ejpb.2018.02.001

Darwesh, A.Y., Helmy, A.P., Abdelhakk, H.M., Giri, B., & Maniruzzaman, M. (2024). 3D-printed short nanofibers/hydrogel-based vaginal films as a novel system for the delivery of anti-HIV microbicide drugs. J. Drug Deliv. Sci. Tech, 97 (2024) 105775. https://doi.org/10.1016/j.jddst.2024.105775

De Moura, M. R., Avena-Bustillos, R. J., McHugh, T. H., Krochta, J. M., & Mattoso, L. H. C. (2008). Properties of novel hydroxypropyl methylcellulose films containing chitosan nanoparticles. J. Food Sci, 73(7). https://doi.org/10.1111/j.1750-3841.2008.00872.x

De Moura, M. R., Monteiro Cordeiro de Azeredo, F. A. A. H., & Capparelli Mattoso, L. H. (2012). Microfluidizer technique for improving microfiber properties incorporated into edible and biodegradable films. Advances in Microfluidics, May 2014. https://doi.org/10.5772/38922

Garg, S., Goldman, D., Krumme, M., Rohan, L.C., Smoot, S., & Friend, D.R. (2010). Advances in development, scale-up and manufacturing of microbicide gels, films, and tablets. Antiviral Res, 88S (2010) S19–S29

Ghosal, K., Taran Hazra, B., Brata Bhowmik, B., & Thomas, S. (2016). Formulation development, physicochemical characterization and *in vitro-in vivo* drug release of vaginal films. Curr. HIV Res, 14(4), 295–306. https://doi.org/10.2174/1570162x14666151113123040

Jayaramudu, T., Varaprasad, K., Pyarasani, R. D., Reddy, K. K., Akbari-Fakhrabadi, A., Carrasco-Sánchez, V., & Amalraj, J. (2021). Hydroxypropyl methylcellulose-copper nanoparticle and its nanocomposite hydrogel films for antibacterial application. Carbohydr. Polym, 254 (October 2020). https://doi.org/10.1016/j.carbpol.2020.117302

Milinković, S., & Đekić, A. (2024). Hypromellose-based films and film-forming systems for topical application: current status and perspective in drug delivery. Arh. Farm, 74, 709 – 734

Misra, A., & Shahiwala, A. (2020). Applications of polymers in drug delivery., January 2014, 1–570. https://doi.org/10.1016/B978-0-12-819659-5.00017-3

Notario-Pérez, F., Galante, J., Martín-Illana, A., Cazorla-Luna, R., Sarmento, B., Ruiz-Caro, R., das Neves, J., & Veiga, M. D. (2021). Development of pH-sensitive vaginal films based on methacrylate copolymers for topical HIV-1 pre-exposure prophylaxis. Acta Biomater, 121, 316–327. https://doi.org/10.1016/j.actbio.2020.12.019

Pitpisutkul, V., & Prachayawarakorn, J. (2022). Hydroxypropyl methylcellulose/carboxymethyl starch/zinc oxide porous nanocomposite films for wound dressing application. Carbohydr. Polym, 298(May), 120082. https://doi.org/10.1016/j.carbpol.2022.120082

Porfirio, L., Costa, A.A., Conceic¸a˜o, R.R., Matos, T., Almeida, E., Sarmento, V.H.V., Arau´jo, A.A.S., Nunes, R.S., and Lira, A.A.M. (2015). Compatibility study of hydroxypropyl methylcellulose films containing zidovudine and lamivudine using thermal analysis and infrared spectroscopy. J Therm Anal Calorim (2015) 120:817–828

Pritchard, N., Kaitu'U-Lino, T., Harris, L., Tong, S., & Hannan, N. (2021). Nanoparticles in pregnancy: the next frontier in reproductive therapeutics. Hum. Reprod. Update, 27(2), 280–304. https://doi.org/10.1093/humupd/dmaa049

Sarma, A., & Das, M. K. (2019). Formulation by design (FbD) approach to develop tenofovir disoproxil fumarate loaded nanostructured lipid carriers (NLCs) for the aptness of nose to brain delivery. J. Drug Deliv. Ther, 9(2), 148–159. https://doi.org/10.22270/jddt.v9i2.2391

Spinks CB, Zidan AS, Khan AM, Habib MJ, Faustino PJ. (2017). Pharmaceutical characterization of novel tenofovir liposomal formulations for enhanced oral drug delivery: in vitro pharmaceutics and Caco-2 permeability investigations. Clin Pharmacol. 9:29–38

Takalani, F., Kumar, P., Kondiah, P. P. D., & Choonara, Y. E. (2024). Co-emulsified alginate-eudragit nanoparticles: potential carriers for localized and time-defined release of tenofovir in the female genital tract. AAPS PharmSciTech, 25(1). https://doi.org/10.1208/s12249-023-02723-4

Takalani, F., Kumar, P., Kondiah, P. P. D., Choonara, Y. E., & Pillay, V. (2020). Lipid–drug conjugates and associated carrier strategies for enhanced antiretroviral drug delivery. Pharm. Dev. Technol, 25(3), 267–280. https://doi.org/10.1080/10837450.2019.1694037

Zhang, T., Sturgis, T. F., & Youan, B. B. C. (2011). PH-responsive nanoparticles releasing tenofovir intended for the prevention of HIV transmission. Eur J Pharm Biopharm, 79(3), 526–536. https://doi.org/10.1016/j.ejpb.2011.06.007

CHAPTER 5

In vivo assessment of TDF-loaded nanoparticles-in-films in large white female pigs

5.1 Introduction

In vitro studies are conducted to mimic *in vivo* conditions. However, drug carriers are not exposed to the full functionality of an *in vivo* environment, which is crucial for providing more reliable and quantifiable pharmacokinetic data (Mumtaz et al., 2018). In this chapter, TDF-loaded Alg-ES100 nanoparticles incorporated into the HPMC films were assessed vaginally in large white female pigs. The pigs were chosen for their multiple similarities to humans in terms of body and organs, as well as anatomical, pathophysiological, and physiological similarities. Furthermore, they enable the development and evaluation of novel diagnostic and therapeutic interventions (Kalla et al., 2020).

Oral PrEP has shown success as a prevention platform for individuals who are at high risk of being infected by HIV-1. However, challenges that come with oral PrEP include stricter user adherence, decreases in condom use, bone and renal toxicity and antiviral resistance development (Marrazzo et al., 2015; Tyo et al., 2017). Vaginal route, on the other hand, is good for drug administration because it has a large surface area, low enzymatic activity, avoidance of first-pass liver metabolism, rich blood supply, and high suitability for bioadhesive drug delivery systems (Alexander et al., 2004; Acarturk, 2009; Ghosal et al., 2016). However, vaginal secretions and variations may cause the removal of the formulation, although properly designed formulations such as those made of mucoadhesive polymers (e.g., sodium alginate and HPMC) may overcome this drawback (Acarturk, 2009).

Compared to other vaginal delivery systems (e.g. gels and intravaginal rings) that have been developed to date, intravaginal films have been shown to stand a better chance for improved drug delivery as they could be more acceptable to women due to their quick dissolving nature, small size for administration, and the lack of need of an applicator (Srinivasan et al., 2016). In this study, folded film containing 60 mg of the TDF drug within nanoparticles were inserted into the pig vagina. The aim of this chapter was to undertake histopathological analyses to identify potential changes when this films delivery system was inserted in the pig vagina for four days. The vaginal tissues were excised from the euthanized pigs after 4 days of insertion.

5.2 Materials and methods

5.2.1 Materials

The materials used to develop alginate-ES100 nanoparticles and HPMC films are listed in chapter 4 (section 4.2.1). White large female pigs were procured from Niemen Stud Stoet, the supplier of the Wits Research Animal Facility (WRAF). All other chemicals or reagents used were of analytical grade.

5.2.2 Ethical approval for the use of animals in this study

The animal research ethics committee (AREC) of the University of the Witwatersrand approved the testing of the delivery system (TDF loaded alginate-ES100 nanoparticles encapsulated in a film) in large white female pigs with the ethics clearance number 23-07-002C (Appendix C).

5.2.3 Preparation of Alg-ES100 nanoparticles and films

Alginate-ES100 nanoparticles and HPMC films were prepared as previously described in chapter 4. Thus, alginate nanoparticles were prepared using the ionic gelation method (Zimet et al., 2018), while alginate-ES100 nanoparticles were prepared using the emulsion/gelation complexation method (Choukaife et al., 2020). Films were developed using the casting method (De Moura et al., 2008).

5.2.4 Transportation and housing of the experimental animals

The pigs were purchased from Niemen Stud Stoet, the supplier of the Wits Research Animal Facility (WRAF), who is also responsible for the pigs' welfare during transportation. To reduce total transportation time, these pigs were transported by road using the shortest possible route. The transportation was conducted according to the country's animal transportation laws and carried out by trained and experienced personnel to minimize acute stress. Appropriate procedures for pre-transport handling, loading, journeying, and unloading at WRAF were implemented according to the WRAF standard operating procedures (SOPs). Upon their arrival at WRAF, the pigs were assessed for any indications of stress and placed in quarantine to recuperate before proceeding with experimentation. The pigs were cared for by a competent and skilled staff at WRAF. Initially, the pigs were housed together in a single pen of an appropriate size, which allowed them to move freely, turn around, and lie down comfortably. However, following surgery, each pig was placed in its pen to facilitate easy identification and surveillance. A straw bedding was utilized, and both food and water were provided. Food was

furnished twice daily, and the temperature was maintained at 21–24 degrees, with 12 h of darkness and 12 h of light.

5.2.5 Experimental design

The *in vivo* experimentation involved 5 large white female pigs weighing approximately 35-40 kg. These pigs were allowed to habituate for one week from their day of arrival. Then they were weighed before the surgical procedure for the insertion of the catheters. This was done to keep track of any weight changes that occurred and to avoid any potential controversies with the established procedures of the study. The AREC team at the University of the Witwatersrand was mandated to exclude any pig that had lost more than 10% of its body weight from the study. All animals were closely monitored for any changes in their behavior or any indications of discomfort or reluctance to move. The experiment involved the division of 5 pigs into three groups, one containing 3 pigs and the other two containing one pig each. The two groups which comprised one pig each were utilized as controls to observe any behavioral disparities between the drug-treated and non-drug-treated animals. This is shown below:

Group 1 (Control-pig 1): Contained one large white pig without any formulations administered. This group was utilized to obtain pharmacokinetic data for comparative purposes.

Group 2 (Control-pig 2): consisted of one large white pig, administered with a drug-free system. This group was utilized to obtain pharmacokinetic outcomes, which would enable comparison between the optimized drug-free formulation and drug-dosed formulation.

Group 3 (Tests-pig 3,4 & 5): comprised of three large white pigs, which were all administered with the optimized TDF-loaded nanoparticle-in-film formulation (containing TDF at a concentration of 60 mg). Thus, the experiment was performed in triplicate.

5.2.6 Insertion of a catheter into the jugular vein

The surgical implantation of catheters into the pig's jugular vein was undertaken after one week of habituation. All pigs were anesthetized using ketamine (11 mg/kg), dormicum (0.3 mg/kg), and finadyne (2.2 mg/kg). The anesthesia in pigs was maintained by medical oxygen (100%) and isoflurane gas (5%) for 30–40 min to allow enough time for the surgical implantation of the catheter into the right jugular vein. The surgical insertion of the 7-gauge double lumen 40 cm catheter (CS28702, Arrow Deutschland GmbH, and Erding, Germany) into the jugular vein was carried. Then, the 25 cm length of the catheter remaining after insertion was tunneled subcutaneously to an exit point towards the cranial position, at the dorsal aspect of the scapula, which was stitched to avoid detachment. The external injection

ports of the catheter were sutured to the skin to prevent excess bending. After surgery, all pigs were observed critically to ensure full recovery from anesthesia.

5.2.7 Vaginal administration of films to large white female pigs

Before the vaginal implant, all pigs were allowed to fully recover for a period of three days. The pigs underwent overnight fasting and the subsequent day before implant. Then, they were anesthetized by injection of Ketamine HCL (40 mg/kg) through the implanted catheter. The anesthesia was sustained through the utilization of topical procaine and oxygen. When the pig was stabilized under anesthesia, the folded film delivery system containing 60 mg of the TDF was administered, as depicted in Figure 5.1. After administration, the pig was taken back to its pen and observed until full recovery and consciousness were obtained.



Figure 5.1: HPMC film solutions of 60 ml containing nanoparticle powders loaded with 60 mg of the drug were dried on glass petri dishes measuring 90 mm × 60 mm. Subsequently, the dried films were folded and inserted into the vagina of the large white female pig.

5.2.8. Vaginal tissue sample collection for histopathology assessment

The pigs were euthanized after 4 days of film insertion using an intravenous injection of Phenobarbital (200 mg/kg) into one of the ear veins to enable vaginal tissue collection. The vaginal tract was excised from the pelvic canal after midline dissection through the symphysis pubis. Thereafter, the vaginal tract was dissected to expose the vaginal mucosa. These tissues were fixed in 10% neutral-buffered formalin and stored at 4 ºC until histopathological analysis.

5.3 Results and discussion

5.3.1 Histopathology analysis of porcine vaginal epithelia

Table 5.1 and Figure 5.2 contain the histopathology results for the excised vaginal tissues. Pig 1 was the control with no insertion, whereas pig 2 was the control containing the delivery system without the drug. Pigs 3, 4, and 5 had the same optimal film delivery system (2.5%) inserted with 60 mg of TDF drug. Histopathologic description for each pig is provided below:

Pig 1 exhibited three distinct sections of vaginal tissue. Most sections revealed a thin, uniform layer of nonkeratinized squamous epithelium with only mild hyperplasia. Several scattered intraepithelial neutrophils have been observed, as well as occasional mild multifocal submucosal lymphoplasmacytic infiltrates. There was a mild hemorrhage within the muscular layer. Perivascular inflammation or significant fibrosis were absent.

Pig 2 had three segments of the vaginal tissue visible. Most segments only showed mild mucosal hyperplasia, with no significant inflammation. There were two foci which showed the presence of moderate mucosal hyperplasia with formation of deep invagination. Mild neutrophilic influx into the epithelium accompanied by a moderate inflammatory infiltrate in the adjacent submucosa was observed, consisting of macrophages and neutrophils with occasional lymphocytes and plasma cells. Degenerate neutrophils and desquamated squamous cells were visible within the lumen of the invagination, but there was no sign of ulceration. A slight micro pustule development was observed in the second focus. There was no sign of stromal fibrosis or perivascular lymphoplasmacytic cuffing.

Pig 3 demonstrated the presence of three sections of vaginal tissue. The mucosa consisted of mildly hyperplastic nonkeratinized squamous epithelium with shallow rete peg formation and a few invaginations. There were occasional mild submucosal lymphoplasmacytic infiltrates, including a few scattered secondary lymphoid follicles. One segment showed the presence of focal ulceration with fibrinopurulent exudation in one of the invaginations. This was accompanied by underlying haemorrhage and fibrin deposition, as well as infiltration by macrophages, neutrophils with scattered lymphocytes and plasma cells. Mild lymphangiectasia were visible, along with mild stromal fibrosis. There was no sign of perivascular infiltration.

Pig number 4 also showed three sections of the genital tissue. The vaginal mucosa was composed of nonkeratinized squamous epithelium with moderate to deep rete peg formation and had moderate hyperplasia. There was moderate underlying infiltration in the submucosa

by lymphocytes and plasma cells, as well as small secondary lymphoid follicle development multifocally. The epithelium also showed moderate spongiosis, with occasional areas of moderate intraepithelial neutrophil infiltration. No ulceration or tissue necrosis was present. Nevertheless, a mild case of stromal fibrosis was detected.

Pig 5 exhibited three distinct sections of vaginal tissue. There was a mild hyperplasia of the vaginal mucosa (nonkeratinized squamous epithelium), and this was accompanied by a moderate submucosal infiltrate of lymphocytes and plasma cells. Additionally, the mucosa was infiltrated with moderate numbers of neutrophils, with occasional small pustule formation. We observed moderate mucosal spongiosis and mild lymphangiectasia. Furthermore, the tunica muscularis showed multifocal infiltration by macrophages and neutrophils, as well as occasional clusters of lymphocytes and plasma cells. A mild stromal fibrosis was present. However, there were no signs of perivascular inflammation.

As demonstrated by the results obtained from pig 2, it is evident that the nano carriers, specifically the alginate-ES100 nanoparticles present in the HPMC film, did not cause or resemble any toxic behavior. This was anticipated as alginate, ES100, and HPMC polymers are known for their non-toxic properties (Thakral et al., 2013; Ghosal et al., 2014; Joshy et al., 2017; Ghadermazi et al., 2019). Films prepared with bioadhesive polymers, particularly HPMC and sodium alginate, have been reported to be non-irritant to the mucous membrane (Ghosal et al., 2014). Hence, they are capable of controlling the long-term efficacy and stability of the formulation. On the other hand, the presence of the TDF drug resulted in minimal epithelial erosion/ulceration, mild epithelial exocytosis, and subepithelial leukocyte influx, as observed in pigs 3, 4, and 5.

Additionally, Stromal fibrosis was noticed in all pigs administered with the delivery system and loaded with the TDF drug. The reason for this could be that bioadhesive polymers form a strong bond with the mucin-epithelial cell surfaces and adhere quickly to soft tissue, allowing easy incorporation of the drug (Ghosal et al., 2014). However, we expected the toxicity of the TDF drug to be severe after four days of insertion, considering previous reports of the TDF drug being administered for a long time (Foster et al., 2009; De Clercq, 2016). Therefore, these results suggest that our designed formulation can help reduce the toxicity effects associated with administering the TDF drug over a prolonged period. Pig 5 had a muscle injury because of the needle stitching during surgery. An excessive amount of bleeding was noticed specifically on this pig during vaginal insertion. Overall toxicity results showed mild to slight changes.

Table 5.1: Histopathological observations of the vaginal sections excised from pigs 1-5

Pig identification	**1**	**2**	**3**	**4**	**5**
Epithelial erosion/ulceration	0	0	1	0	0
Epithelial proliferation	1	1	1	2	1
Epithelial exocytosis	1	1	1	2	2
Subepithelial leukocyte influx	1	1	1	2	2
Stromal fibrosis	0	0	1	1	1
Perivascular cell cuffing	0	0	0	0	0
Tissue necrosis	0	0	0	0	0

0- no abnormality

1- minimal abnormality

2- mild abnormality

3- moderate abnormality

4- severe abnormality

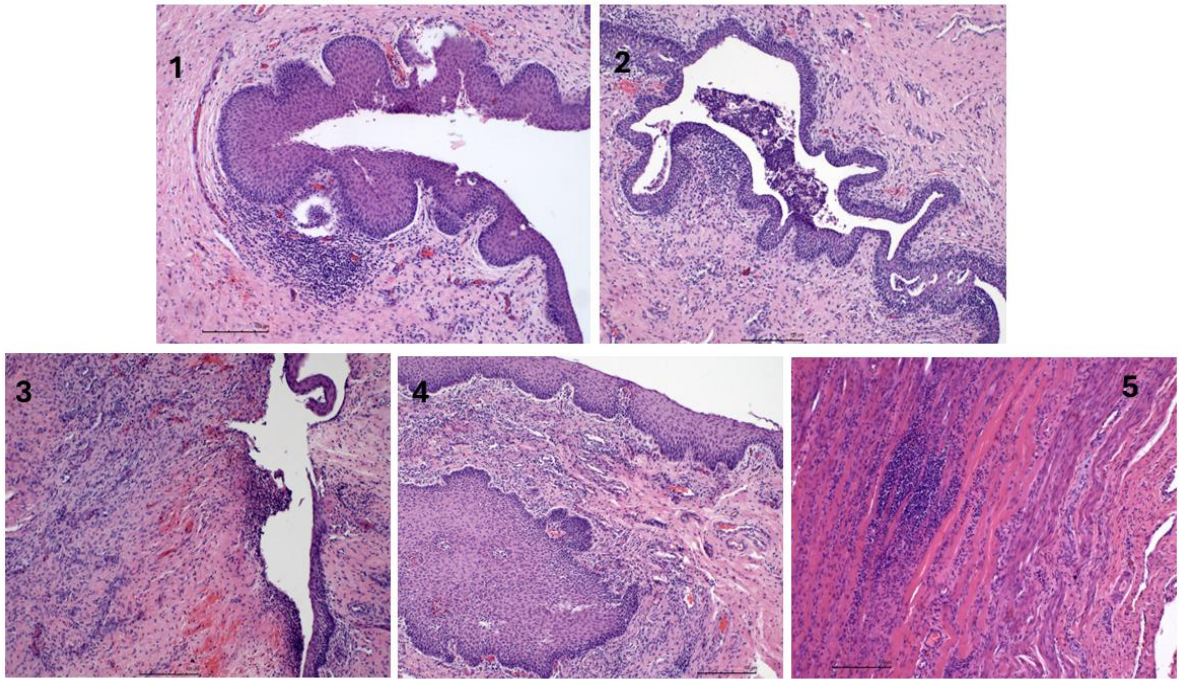


Figure 5.2: Histopathology images of the excised pig vaginal tissues showing; 1. normal vaginal tissue of a pig, 2. Focal vaginitis, 3. Focal ulcerative vaginitis, 4. Moderate neutrophil influx and 5. Muscular injury

5.4 Concluding remarks

In this chapter, a vaginal delivery system containing 60 mg of the TDF drug within alginate and ES100 nanoparticles embedded into the HPMC film matrix was successfully administered into the pig vagina. When this film delivery system was implanted for a duration of four days in pigs, histopathological examination revealed mild to moderate modifications. This indicates that it is possible to develop a non-toxic microbicide that could be administered for a prolonged period in the vagina for HIV patients.

5.5 References

Acarturk, F. (2009). Mucoadhesive vaginal drug delivery systems. Recent patents on drug delivery & formulation, 3(3), 193–205. https://doi.org/10.2174/187221109789105658

Alexander, N. J., Baker, E., Kaptein, M., Karck, U., Miller, L., & Zampaglione, E. (2004). Why consider vaginal drug administration? Fertil. Steril, 82(1), 1–12. https://doi.org/10.1016/j.fertnstert.2004.01.025

Choukaife, H., Doolaanea, A. A., & Alfatama, M. (2020). Alginate nanoformulation: Influence of process and selected variables. In Pharm 13 (11), 1–35. MDPI AG. https://doi.org/10.3390/ph13110335

De Clercq, E. (2016). Tenofovir alafenamide (TAF) as the successor of tenofovir disoproxil fumarate (TDF). Biochem. Pharmacol, 119, 1–7. https://doi.org/10.1016/j.bcp.2016.04.015

De Moura, M. R., Avena-Bustillos, R. J., McHugh, T. H., Krochta, J. M., & Mattoso, L. H. C. (2008). Properties of novel hydroxypropyl methylcellulose films containing chitosan nanoparticles. J. Food Sci, 73(7). https://doi.org/10.1111/j.1750-3841.2008.00872.x

Foster, C., Lyall, H., Olmscheid, B., Pearce, G., Zhang, S., & Gibb, D. M. (2009). Tenofovir disoproxil fumarate in pregnancy and prevention of mother-to-child transmission of HIV-1: Is it time to move on from zidovudine? In HIV Med 10(7), pp. 397–406. https://doi.org/10.1111/j.1468-1293.2009.00709.x

Ghadermazi, R., Hamdipour, S., Sadeghi, K., Ghadermazi, R., & Khosrowshahi Asl, A. (2019). Effect of various additives on the properties of the films and coatings derived from hydroxypropyl methylcellulose—A review. Food sci. nutr, 7(11), 3363–3377. https://doi.org/10.1002/fsn3.1206

Ghosal, K., Brata Bhowmik, B., & Ranjan, A. (2014). A novel vaginal drug delivery system: Anti-HIV bioadhesive film containing abacavir. J. Mater. Sci.: Mater. Med, 1-25.

Ghosal, K., Taran Hazra, B., Brata Bhowmik, B., & Thomas, S. (2016). Formulation development, physicochemical characterization and *In vitro-In vivo* drug release of vaginal films. Curr. HIV Res, 14(4), 295–306. https://doi.org/10.2174/1570162x14666151113123040

Joshy, K. S., George, A., Jose, J., Kalarikkal, N., Pothen, L. A., & Thomas, S. (2017). Novel dendritic structure of alginate hybrid nanoparticles for effective anti-viral drug delivery. Int. J. Biol. Macromol, 103, 1265–1275. https://doi.org/10.1016/j.ijbiomac.2017.05.094

Kalla, D., Kind, A., & Schnieke, A. (2020). Genetically engineered pigs to study cancer. Int. J. Mol. Sci, 21(2). https://doi.org/10.3390/ijms21020488

Marrazzo J.M., Ramjee G., Richardson B.A., Gomez K., Mgodi N., Nair G et al. (2015) Tenofovir-based preexposure prophylaxis for HIV infection among African women. N Engl J Med 372(6): 1-16.

Mumtaz, H., Asim Farooq, M., Batool, Z., Ahsan, A., & Syed, A. (2018). Significance of in-vitro and in-vivo correlation in drug delivery system. RPHS, 4(4), 523–531. https://doi.org/10.32463/rphs.2018.v04i04.23

Thakral, S., Thakral, N. K., & Majumdar, D. K. (2013). Eudragit®: A technology evaluation. In Expert Opin. Drug Deliv, 10(1), 131–149. https://doi.org/10.1517/17425247.2013.736962

Tyo K.M., Vuong H.R., Malik D.A., Sims L.B., Alatassi H., Duan J *et al*. (2017) Multipurpose tenofovir disoproxil fumarate electrospun fibers for the prevention of HIV-1 and HSV-2 infection. Int J Pharm, 531: 118-133.

Zimet, P., Mombrú, Á. W., Faccio, R., Brugnini, G., Miraballes, I., Rufo, C., & Pardo, H. (2018). Optimization and characterization of nisin-loaded alginate-chitosan nanoparticles with antimicrobial activity in lean beef. LWT, 91, 107–116. https://doi.org/10.1016/j.lwt.2018.01.015

CHAPTER 6

CONCLUSIONS AND RECOMMENDATIONS

6.1. Conclusions

LDCs show exciting potential for enhancing oral bioavailability, permeation, and absorption of poorly water-soluble ARV drugs. This is due to the fact that, LDCs, like TDF, can be well integrated into suitable nano delivery systems for administration through different routes. Thus, to overcome various biological barriers that hinder the delivery of ARV drugs through membranes by limiting their absorption and bioavailability. Although it is worth noting that only TDF and TAF have been approved by the FDA as lipidic prodrugs, among the ARV medications that have been developed to date. The LDC approach appears to possess significant potential for enhancing antiretroviral efficacy in the future.

On the other hand, this study describes the successful synthesis of the TDF drug loaded into alginate-ES100 nanoparticles and further incorporated into HPMC films. The presence of spherical and uniformly distributed nanoparticles was revealed in SEM and TEM nanoparticle images, whereas SEM images for films showed significant degrees of porosity and compactness. The FTIR spectrum showed that alginate and ES100 interacted via the ester C=O amide stretching, resulting in the formation of a novel and potent anhydride bond. This anhydride bond also held HPMC in place. The results obtained from XRD and DSC, on the other hand, revealed a favorable interaction between sodium alginate and ES100 polymers, as evidenced by the crystallization peaks observed. A successful capping of TDF-loaded nanoparticles with the HPMC polymer was confirmed by the DSC results.

The overall optimization results demonstrated that the DOE model was adequate. This was exemplified by the R^2 values, as well as the S and low F-statistics P values, which were found to be significant and within the desired ranges for nearly all models. The optimal nanoparticle formulation exhibited a maximum cumulative *in vitro* release of 72% (pH 4.2) for a duration of 96 h, whereas the 2.5% film released the highest amount (54%) of the TDF drug for a duration of 96 h. These results revealed that incorporating alginate-ES100 nanoparticles into the HPMC film during synthesis results in a sustained release, as polymer compositions can significantly impact properties of the film, such as mechanical strength and disintegration time. Consequently, this can affect the drug release rate. Thus, films based on 100% HPMC have previously been developed, and they had a high swelling index and disintegrated within 60 minutes. Therefore, they were considered unsuitable for the required long-time drug release purposes.

The cytotoxicity evaluation for both *in vitro* and *in vivo* studies demonstrated the safety of alginate, ES100 and HPMC polymers in the female genital tract. Lastly, histopathology analysis showed mild to moderate changes when the film delivery system containing 60 mg of the TDF drug was inserted for four days. When taken together, the *in vitro* findings indicate that alginate-ES100 nanoparticles possess the capability to preserve and sustain the release of the TDF drug in the FGT. On the contrary, *in vivo* studies suggest the possibility of developing a non-toxic microbicide that can be administered for a prolonged period in the vagina for HIV patients.

6.2. Limitations of the study

The histopathological results of alginate-eudragit S100 nanoparticles loaded with 60 mg of the TDF drug within the film matrix showed overall mild to moderate changes when inserted into the pig vagina for four days. More analyses could be required until no changes are observed. Thus, repeated use of the formulation could be done to see if it has an impact on the vaginal microbiota or epithelial integrity.

6.3. Recommendations

Regarding the development of the delivery system, it would be imperative to conduct a thorough investigation of the therapeutic implications to ensure the viability of the nanosystem. This may entail the creation of additional film formulations with varying concentrations and the expansion of the *in vivo* study to a full study. Other potential HIV drugs on the market with similar or close functionalities to the TDF drug could be tested in the same formulation for improved results. The dose or different concentrations of these drugs can also be compared to see if there is any change taking place when the formulation is inserted into the pig model.

Additionally, collecting blood and vaginal tissues after administration of the formulation and using techniques such as high-performance liquid chromatography (HPLC) or ultra-performance liquid chromatography (UPLC) for analyses can help determine the safety and long-term effects of the formulation. Moreover, as stated in chapter 3, section 3.1, there have been fewer studies reported regarding the use of alginate and ES100 polymers in the FGT. Subsequently, there is significantly less information available regarding clinical investigations. Future studies could explore the potential for clinical translation and scalability.

The long-term objective can be directed towards the development of a low-dose non-toxic microbicide that can be administered in the vagina for an extended period, catering to both pregnant and non-pregnant HIV patients. It is worth noting that pregnant women cannot be completely excluded from the utilization of vaginal films, as blood only commences flowing

from the maternal region to the placenta and fetus during the second trimester. Thus, at the beginning of the second trimester, the plug that encloses the maternal spiral arteries during differentiation is released.

APPENDIX A

Lipid–drug conjugates and associated carrier strategies for enhanced antiretroviral drug delivery

Funanani Takalani[1], Pradeep Kumar[1], Pierre P.D. Kondiah[1], Yahya E. Choonara[1] and Viness Pillay[1]*

Wits Advanced Drug Delivery Platform Research Unit, Department of Pharmacy and Pharmacology, School of Therapeutic Sciences, Faculty of Health Sciences, University of the Witwatersrand, Johannesburg, 7 York Road, Parktown 2193, South Africa.

*Corresponding Author: viness.pillay@wits.ac.za

Abstract

Mortality rate of patients infected with HIV-1 has been significantly reduced by using HAART. However, the virus to date has not been eradicated. Transmission of HIV-1 infection through sexual intercourse remains an ongoing challenge, with increased risk of infection occurring in women. Interestingly, ARV drugs can be chemically linked with lipids to produce lipid–drug conjugates (LDCs). This alters pharmacokinetic properties of ARV drugs and thereby resulting in improved effectiveness. Although LDCs can be administered without a delivery carrier, they are usually incorporated into suitable delivery systems such as lipid nanoparticles, polymeric nanoparticles, micelles, liposomes, emulsions, and carbon nanotubes. Given that LDCs have the potential to improve oral bioavailability, lipophilicity, toxicity, and drug targeting, it is of our great interest to review strategies of lipid–drug conjugation together with their delivery systems for enhanced antiretroviral efficacy.

Keywords: HIV-1; antiretrovirals; lipid–drug conjugates; drug delivery; nanoparticles

APPENDIX B

Co-emulsified Alginate-Eudragit Nanoparticles: Potential Carriers for Localized and Time-defined Release of Tenofovir in the Female Genital Tract

Funanani Takalani[1], Pradeep Kumar[1], Pierre P.D. Kondiah[1] and Yahya E. Choonara[1]*
Wits Advanced Drug Delivery Platform Research Unit, Department of Pharmacy and Pharmacology, School of Therapeutic Sciences, Faculty of Health Sciences, University of the Witwatersrand, Johannesburg, 7 York Road, Parktown 2193, South Africa.
*Corresponding Author: yahya.choonara@wits.ac.za

Abstract

This research aimed to explore the possibilities of Eudragit S100 (ES100) and sodium alginate as carriers for tenofovir disoproxil fumarate (TDF) in the female genital tract. Alginate and alginate-ES100 nanoparticles were prepared using the ionic gelation and emulsion/gelation complexation method, respectively. The nanocarriers were tested using morphological, physicochemical, *in vitro* drug release, and cytotoxicity analyses. In SEM and TEM images, the presence of spherical and uniformly distributed nanoparticles was revealed. The FTIR spectrum showed that alginate and calcium chloride interacted due to ionic bonds linking divalent calcium ions and the -COO- of alginate groups. Alginate and ES100 interacted via the ester C=O amide stretching. The results obtained from XRD and DSC, on the other hand, revealed a favorable interaction between sodium alginate and ES100 polymers, as evidenced by the crystallization peaks observed. Under experimental design analysis and optimization, overall size distribution profiles ranged from 134.9 to 228.0 nm, while zeta potential results showed stable nanoparticles (−17.8 to −38.4 MV). The optimal formulation exhibited a maximum cumulative in vitro release of 72% (pH 4.2) up to 96 h. The cytotoxicity tests revealed the safety of TDF-loaded nanoparticles on vaginal epithelial cells at concentrations of 0.025 mg/mL, 0.5 mg/mL, and 1 mg/mL for 72 h. These results indicated that alginate-ES100 nanoparticles have the potential to preserve and sustain the release of the TDF drug in the FGT. The future goal is to develop a low-dose non-toxic microbicide that can be administered long term in the vagina to cater to both pregnant and non-pregnant HIV patients.

Keywords: female genital tract · human immunodeficiency virus 1 · nanoparticles · sodium alginate · tenofovir disoproxil fumarate

ANIMALS RESEARCH ETHICS COMMITTEE (AREC)

UNIVERSITY OF THE WITWATERSRAND, JOHANNESBURG

STRICTLY CONFIDENTIAL

CLEARANCE CERTIFICATE NUMBER: AREC23-07-002C

APPLICANT: Ms F Takalani
School: School of Therapeutic Sciences; Department: N/A; Location: Wits Research Animal Facility (WRAF)

PROJECT TITLE: Assessment of a nano-enclatherated bioadhesive system (TDF-loaded nanoparticles-in-films) in large white female pigs for prolonged release and minimimal toxicity of the TDF drug for vaginal delivery.
Category: A; Species and Numbers involved: 5X Female, 35-40 Kg, Large white, pigs

Approval is hereby given for the use of animals for the research project named above and described in the application reviewed by a quorate meeting of the AREC held on 29 Aug 2023. This approval remains valid until 7 Dec 2025 and is conditional to the following (if blank there are no special conditions):

Condition 1	Condition 2	Condition 3	Condition 4

All material changes to the approved research must be reported to the AREC before they are implemented. Failure to do so will invalidate this clearance certificate.

An annual progress report must be provided to the AREC.

The use of these animals is subject to AREC guidelines on the use and care of laboratory animals, is limited to the procedures described in the application and is subject to additional conditions listed below:

I, the Chair of the AREC (or my designated representative) am satisfied that the proposed research is ethical as judged by local law, international standards and University policy.

Signed: _____ _____ Date: ___08/12/2023_____
(Chairperson of the AREC)

I am satisfied that the persons listed in this application are competent to perform the procedures described in the application, in the context of Section 23 (1) (c) of the veterinary and Para-veterinary Professions Act (19 of 1982).

Signed: ____ _____ Date: 8/12/2023
(Registered Veterinarian)

CC: Student supervisor: Prof Y Choonara
Acting Director Wits Research Animal Facility (WRAF): Sr Amelia Rammekwa